Investigating the role of SCAR-Arp2/3 dependent cortical remodelling in asymmetrically dividing *Drosophila* neuroblasts.

Giulia Cazzagon

University College London

Laboratory for Molecular and Cell Biology

PhD Supervisor:

Professor Buzz Baum

A thesis submitted for the degree of

Doctor of Philosophy

December 2022

Declaration

I, Giulia Cazzagon, confirm that the work presented in this thesis is my own. Where information has been derived from other sources, I confirm that this has been indicated in the thesis.

Abstract

Division is one of the most important events in the life of a cell, which ensures that the genetic material and the entire set of cellular components segregate in the correct way between the two daughter cells. To divide, cells have to undergo profound shape changes in a timely manner. While the actin cortex is known to control the changes in cell shape that accompany division, much remains to be discovered about the molecular and cellular mechanisms that control cortical remodelling and that coordinate asymmetric stem cell divisions.

In this work, I identify the SCAR-Arp2/3 pathway as a potential new regulator of the polarised shape changes in anaphase that help drive asymmetric stem cell divisions in *Drosophila melanogaster.* I show that filopodia-like membrane protrusions are found at the apical cortex in metaphase and their organization is dependent on Arp2/3. Interestingly, SCAR localizes preferentially at the apical cortex of neural stem cells, and both SCAR and the membrane protrusions disappear from the apical cortex as cells undergo cortical expansion when they enter anaphase. Finally, cells depleted of SCAR or the Arp2/3 complex show a disorganized microtubule spindle and cortical defects at the end of mitosis, suggesting a role for Arp2/3 in stabilizing cortical shape and tension at the metaphase-anaphase transition. This is surprising as the branched actin network nucleated by Arp2/3 is known for its role in trafficking, motility of organelles and cell migration, rather than in cell division, which depends on Formin-based actin nucleation.

Through this work I propose a role for the SCAR-Arp2/3 pathway in maintaining proper cortical organization in the dividing neuroblasts to aid proper asymmetric division, hence suggesting a new cellular mechanism that contributes to asymmetric cell division in the *Drosophila* neural stem cells.

Impact statement

In this work I provide new information about the role of different actin networks in neuronal stem cells division. Several mechanisms underlying the generation of physical asymmetry have been proposed, but it is not well understood how events are spatiotemporally coordinated and molecularly controlled. The data gathered here help to shed light on these mechanisms in the *Drosophila* neuroblast, and therefore contribute to a better understanding of this model system. A manuscript for publication is currently in preparation, which will make these data available for the researchers working in the field, providing a background for further research on polarity and the actin cytoskeleton.

Many important pathways and processes are controlled by evolutionary conserved proteins that are shared by flies and humans, making *Drosophila* an excellent model for the study of division. The discoveries made in this work can be applied to better understand stem cell division in other animals, including humans. Hopefully, in the future, this improved knowledge will help us elucidate fundamental biological processes to improve human health - such as in regenerative, stem cell medicine.

Acknowledgements

I only made it to this point thanks to the direct or indirect help and support of many people – so here we go.

First and foremost I would like to thank Buzz. You are a brilliant thinker and an extremely kind human being. I am a better scientist (and a better writer) thanks to you. You showed me how to always look at things with curiosity, and you make the lab the great place it is.

To all past and present members of the Baum lab, who makes it a rich and fun environment to do science: Chantal and Mateusz, for all things flies; Helen and Sushila, for your kindness; Vaibhav, for letting me give you cheap life advice that you never needed, I miss you; Gabriel, for the philosophical discussions; Agata, for making the flat feels like home (and sparing me having to live with some 18 yo); Diorge and Andre, for the Brazilian vibe; Joe, for the lemon sherbets; Jovan, for the drama and the gossip; Kris, for your energy and positivity; Baukje, for all the liquorice; Alice and Fred, for making the lab feel like home, and for the chats about food, the pictures of food, and the real food we've shared, for the board games and the pub nights. I love you guys!

To all the people back at the LMCB, that made it a very special place. To the office pals Henry, Alejandra, Gabriel and Agathe for quickly updating me with the important gossip. Neza, for the long walks and warm coffees. To Koshiro, Laure and Ffion, for the highlight of the week, the Friday pub. To all the LMCB PhD students, who science hard, but party harder.

To the LMB student community, that made me feel less lonely during hard times. To Aly, for the conversations about movies and the Egyptian sweets. To Ilaria, your friendship was like a warm hug when is most needed: grazie per Propaganda live, coping con il mio OCD e per avermi insegnato come fare bene la pasta, ti voglio bene baffetta.

To the Fish Floor, that showed me first that science should be fun and interesting: to Gaia and Steve, who welcomed me to the lab; to all the people that make the

floor special, and to Nicco, my first PhD parent: your young padawan is about to become a jedi (not the more wise I'm afraid).

To all my friends, far and close: to Marta and Lisa, for the comfort you've been giving me the longest. To the Pizza Gang, for reminding me what Italy sounds like and for sharing with me the joys and miseries of the PhD. Betta, I'd have gone back to Italy crying a long time ago without you; Giulini you made the quarantine somehow special; Stefano, what would I do without the Trivia Engineering and the cat love; Raffo, for the awkward hugs and controversial statements.

To Thomas, who especially supported me during the long and challenging last months of writing. For always telling me that I could do it, and much more.

To my parents, who made possible for me something that was not possible for them. Sono arrivata dove sono oggi specialmente grazie a voi.

To all of you,

a big, warm, smiling Thank You.

Table of contents

Abbreviations

Arp2/3 – Actin-related protein 2 and 3

ATP/ADP – Adenosine tri-phosphate/di-phosphate

dsRNA – double strand RNA

GFP – Green fluorescent protein

GMC/GMCs – Ganglion mother cell/s

NB/NBs – Neuroblast/s

PH – Pleckstrin Homology

PIP_2 – Phosphatidylinositol 4,5-bisphosphate

PLCΔ1 – Phospholipase CΔ1

RFP – Red fluorescent protein

RNAi – RNA interference

SCAR – Suppressor of cyclic AMP repressor

SOP – Sensory organ precursor

Sqh – Spaghetti squash

Wor – Worniu

Chapter 1.

Introduction

1.1 Actin

Actin is one of the most abundant proteins in eukaryotic cells (Dominguez and Holmes 2011). It is highly conserved (Dominguez and Holmes 2011; Joseph et al. 2008) and contributes to complex biological processes such as cell motility, maintenance of cell shape, and cell division (Pollard and Cooper 2009).

In cells, actin can be found as either a free monomer called G-actin (globular) or as part of a polymer microfilament called F-actin (filamentous). Actin filaments are formed by two intertwined helical strands (Hanson and Lowy 1963). Actin monomers are enzymes that can catalyse the hydrolysis of an ATP molecule, and in free subunits this process is very slow (Carlier et al. 1988).

The subunits assemble head-to-tail to generate actin filaments, and since they all point towards the same end of the filaments, these acquire a distinct structural polarity. The end that possesses an actin subunit that has its ATP binding site exposed is called, by convention, the “minus end”, while the opposite end where the ATP cleft faces the adjacent monomer is called the “plus end”. Nucleotide hydrolysis within the filament is one of the main factors regulating actin polymer dynamics. Actin monomers join the fast-growing plus end (also called barbed end) bound to ATP, undergo changes in conformation that lead to increased efficiency in hydrolysing ATP, and so as the filament ages, actin-associated ATP is converted to ADP. ADP F-actin is less stable than ADP G-actin, so near the pointed end depolymerisation occurs releasing ADP G-actin back into the cellular actin pool (Dominguez and Holmes 2011; Sept and McCammon 2001; Wegner and Isenberg 1983) (Fig. 1.1A).

The rates at which monomers are added or lost are influenced by actin-binding proteins, which can stabilize the filaments or induce depolymerisation (Dominguez and Holmes 2011). Through regulation of these proteins, the cell controls actin cytoskeleton dynamics and functions (Pollard and Cooper 2009).

1.2 Arp2/3

The nucleation of filaments by pure actin monomers is unfavourable owing to the extreme instability of small actin oligomers (Sept and McCammon 2001). To overcome this obstacle, and to tune the organization of the actin cytoskeleton, cells use factors that directly nucleate actin, such as formin family proteins, the actin-related protein-2/3 (Arp2/3) complex, and Spire.

Formins can bind plus end of a filament to promote growth, providing an anchor and protection against capping (Pring et al. 2003), or they can bind actin monomers and enhance nucleation in the presence of Profilin (Heimsath and Higgs 2012). On the other hand, the Arp2/3 complex associates with the side of an existing filament and initiates the formation of a new filament from the minus end at a characteristic ~70° angle (Amann and Pollard 2001; Mullins, Heuser, and Pollard 1998) .As a result, the type of actin network generated by these two nucleators is different: bundles of long actin filaments in the case of Formins, and branched networks for Arp2/3 (Campellone and Welch 2010) (Fig. 1.1B).

The intact Arp2/3 complex was first purified from the *Acanthamoeba* (Machesky et al. 1994), but it is found in most eukaryotic cells (Muller et al. 2005). It consists of a stable assembly of seven polypeptides, two of which are the actin-related proteins Arp2 and Arp3. These are stabilized in an inactive state by five other subunits: ARPC1, ARPC2, ARPC3, ARPC4, and ARPC5 (actin-related protein complex-1 to 5) (Goley and Welch 2006) (Fig. 1.2A).

Arp2 and Arp3 initiate the actin daughter filament by mimicking an actin dimer that is then extended by the addition of monomers to the free plus end. ARPC2 and ARPC4 form the structural core of the complex, with the remaining subunits organized around them. ARPC1 is a seven-bladed β-propeller protein, whereas ARPC3 and ARPC5 are primarily α-helical and are the most peripheral of the subunits (Gournier et al. 2001).

The Arp2/3 complex coordinated nucleation and branching has an important role in several cellular processes. The complex has been shown by genetic studies to be essential for viability of both unicellular and multicellular organisms. For

example, in yeast, inactivation of specific subunits of the Arp2/3 complex leads to severe growth defects or lethality (Winter et al. 1997). In *Drosophila* the disruption of Arp2/3 function causes lethality before adulthood, defects in cytoplasmic organization in the blastoderm, axon development and eye morphology (Hudson and Cooley 2002a; Zallen et al. 2002). The severity of the phenotypes induced by loss of function of the Arp2/3 complex in diverse species reflects its role in fundamental and conserved cellular processes.

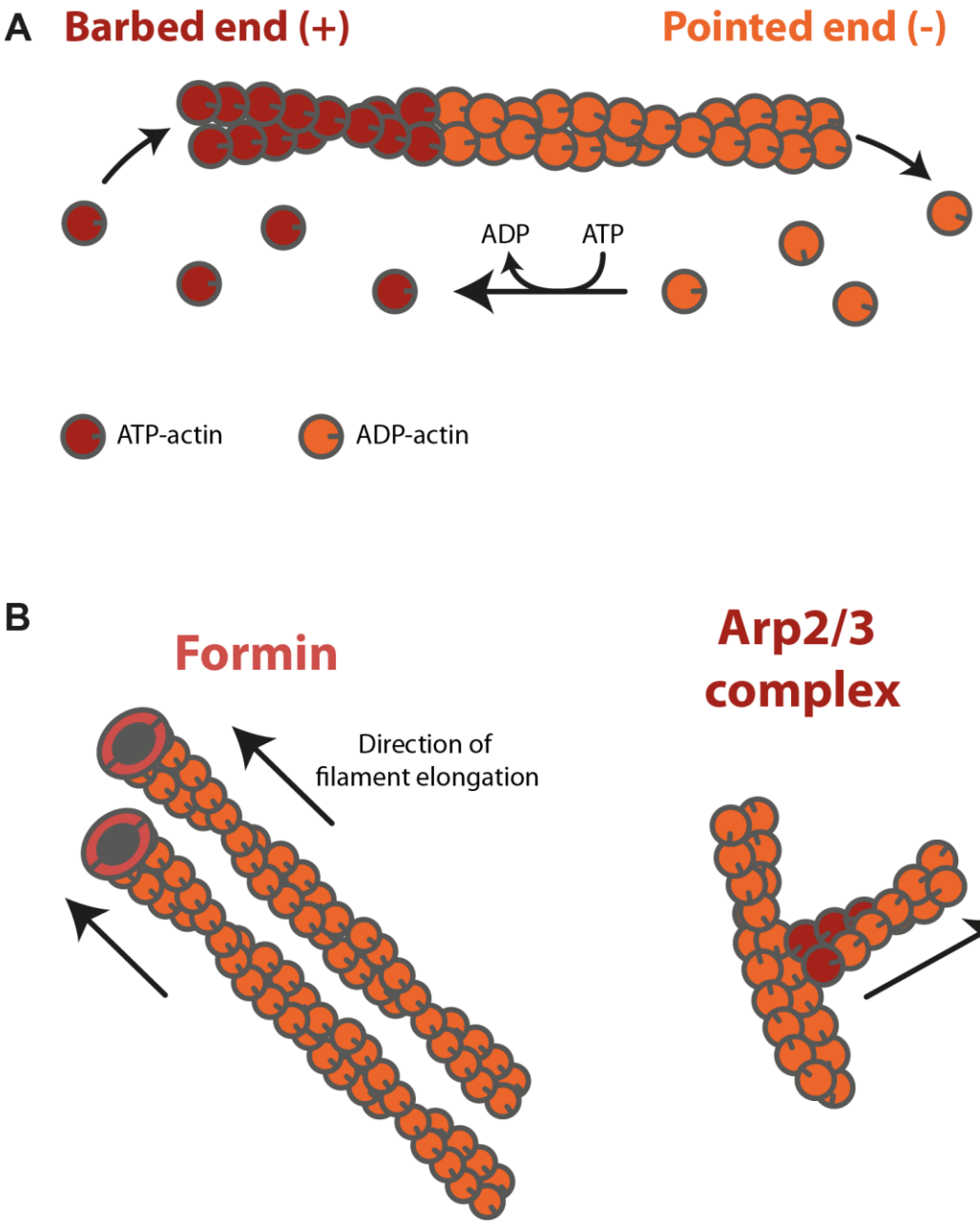

Figure 1.1. F-actin nucleation process and nucleation factors. A. Schematics showing how new G-actin is added to a growing filament. **B.** Schematic representation of main two actin nucleator in forming filaments and the resulting different shape of actin networks.

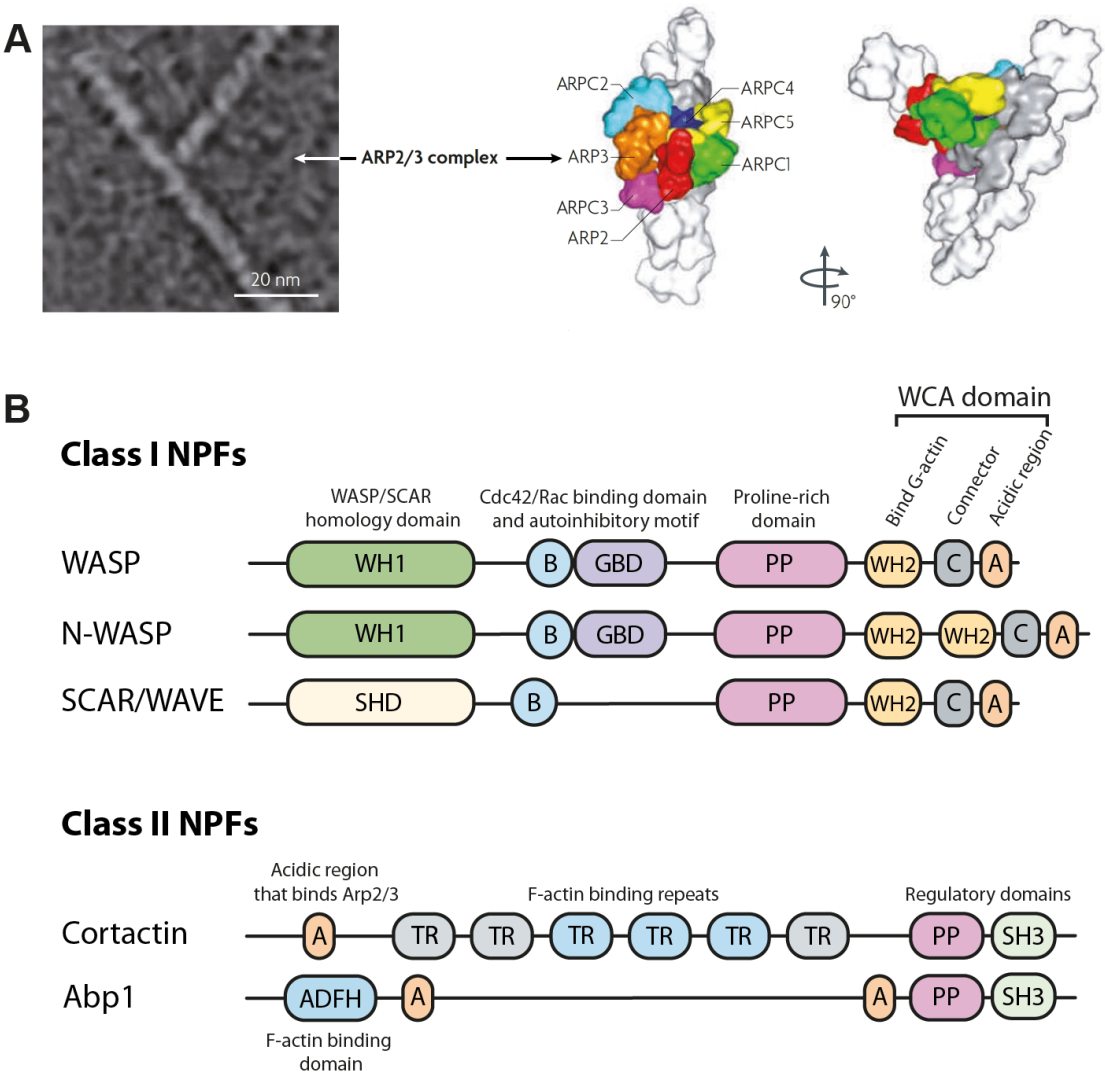

Figure 1.2. Structure of Arp2/3 complex and its nucleator promoting factors. **A.** Electron micrograph shows the morphology of a y-branched actin filament and the Arp2/3 complex. On the right the model for the Arp2/3 complex is based on electron tomography. **B.** Domain organization of representative call I and II NPFs. A, acidic; ADFH, actin-depolymerizing factor homology; B, basic; C, central; GBD, GTPase-binding domain; PP, poly-proline; SDH, SCAR-homology domain; SH3, Src-homology-3; TR, tandem repeat; WH1 & 2, WASP-homology 1 & 2. Adapted from Campellone and Welch 2010, and Goley and Welch 2006b.

1.3 Arp2/3 nucleation promoting factors

By itself, the Arp2/3 complex is an inefficient nucleator, and needs to be activated by the so-called nucleation promoting factors (NPFs). NPFs are classified in two main groups, class I and II, based on the mechanism of activation and their effect on the y-branching reaction (Goley and Welch 2006). Class I NPFs possess a WCA domain, which is comprised of one or more WASp homology 2 (WH2) domains that bind actin monomers (Chereau et al. 2005; Marchand et al. 2001), an amphipathic connector region and an acidic peptide that mediate binding to Arp2/3 (Panchal et al. 2003) (Fig. 1.2B). Class I NPFs function by delivering an actin monomer to the complex, facilitating the formation of a nucleus for the polymerization of the daughter filament. After the initiation of a Y-branch, the NPF dissociates from the Arp2/3 complex and can participate in multiple rounds of Arp2/3 activation (Egile et al. 2005). Part of this class are Wiskott-Aldrich syndrome protein (WASP), suppressor of cyclic AMP repressor (SCAR, also called WASP-family verprolin-homologue protein (WAVE)), and WASP and SCAR homologue (WASH).

Class II NPFs include yeast actin-binding protein-1 (Abp1) (Goode et al. 2001) and Cortactin (Weed et al. 2000). These proteins have an Arp2/3-binding acidic region, but lack WH2 domains for binding G-actin. Instead, they contain an F-actin-binding region that is required for Arp2/3 activation (Fig. 1.2B). Compared to Class I, class II NPFs are far less potent activators of the Arp2/3 complex *in vitro* (Campellone and Welch 2010; Goley and Welch 2006).

WASP was the first NPF to be discovered, and now is one of the best characterized. It is found in mammals, fungi and protists. Mammals usually have two WASPs: N-WASP is expressed in most cell type while WASP is expressed specifically in hematopoietic cells (Bosticardo et al. 2009; Snapper et al. 2001). WASP has a modular domain organization consisting of a N-terminal WASP homology 1 (WH1) domain, a domain that interacts with activators Cdc42 and Rac, and an autoinhibitory motif. WASP is predominantly found in an autoinhibited conformation, in which the C-terminus of the protein is occluded through its interaction with the N-terminus. This state is released by the

competitive binding of the small GTPase Cdc42 and the phospholipid PIP_2 (Campellone and Welch 2010; Kim et al. 2000).

The highly conserved SCAR/WAVE lacks a GTPase binding domain, and its N-terminal SCAR homology domains (SHDs) are distinct from the regulatory portions of WASP. The SHD associates with a regulatory complex consisting of PIR121/CYFIP/Sra1, Nap1/Kette, Abi and HSPC300 (Gautreau et al. 2004). Furthermore, like WASPs, WAVEs are basically inactive when purified as recombinant proteins (Lebensohn and Kirschner 2009). Mammals have three isoforms, WAVE1, 2 and 3, that are expressed in numerous cell types, with WAVE1 and 2 distributed most broadly, although all are enriched in brain tissue (Campellone and Welch 2010; Soderling et al. 2003). Activation of the WAVE complex requires simultaneous interaction with the small GTPase Rac1 and acid phospholipids, like phosphatidylinositol (3, 4, 5)-triphosphate (PIP_3), as well as a specific state of phosphorylation (Kobayashi et al. 1998; Lebensohn and Kirschner 2009).

WASH is a type I NPF that is found on endosomes (Derivery et al. 2009). WASH contains 2 WASH homology domains (WHD1 and 2), a proline-rich region and a C-terminal acid connecting domain. WASH is intrinsically inactive and exists in a macromolecular complex including FAM21, Strumpellin, KIAA1033 and CCDC53 (Derivery et al. 2009). It is not entirely clear which proteins are needed for WASH activation. While studies in *Drosophila* melanogaster have revealed a role for Rho1 in its activity (Liu et al. 2009), mammalian RhoA did not activate the WASH regulatory complex *in vitro* (Jia et al. 2010). At the same time, phosphorylation appears to be a general mechanism for regulating WASH-mediated actin polymerization and endosomal transport (Tsarouhas et al. 2019).

1.3.1 Biological functions of WASP-family proteins.

Numerous biological processes that involve the reorganisation of the actin cytoskeleton require the activity of the WASP family of proteins. One of their main roles is the formation of actin-based structures, like lamellipodia, filopodia and podosomes.

Lamellipodia are sheet-like structures at the leading edge of the cell, and the SCAR/WAVE complex is required for their formation (Kunda et al. 2003; Ridley

et al. 1992; Yan et al. 2003). In these processes, WAVE1 and 2 have partially overlapping functions, as deficient cells exhibit severe defects in peripheral membrane ruffling, lamellipodia formation, and cell mobility (Steffen et al. 2006; Suetsugu et al. 2003). WAVE2 might also help organize and maintain cell-cell contacts (Yamazaki, Oikawa, and Takenawa 2007).

By contrast, the role of the WASP family in the formation of filopodia – long, finger-like cell-membrane protrusions that contain bundles of straight actin filament – is less clear. Formins localize to filopodial tips, and their genetic requirement for filopodial assembly is undisputed, but WASP family proteins have been suggested to play a role in their formation (Biyasheva et al. 2004; Schirenbeck et al. 2005). In addition, the Arp2/3 complex and WASP have been found to associate with proteins involved in filopodia formation (Ideses et al. 2008). Thus, the “convergent elongation” model has been put forward, which proposes that Arp2/3-nucleated filaments can be brought together and elongated by Formins to generate the bundles of parallel filaments that underlie filopodial formation (Chesarone and Goode 2009).

In addition to these structural roles, WASP-family proteins have central roles in membrane trafficking, and are manipulated during infection by intracellular pathogens, like *Shigella* and *E. coli* (Stevens, Galyov, and Stevens 2006). WASP and N-WASP are recruited, along with Arp2/3, to sites of phagocytosis, and have been implicated in the final steps of clathrin-mediated endocytosis, a process in which F-actin facilitates membrane fission and drives endosome movement (Jin et al. 2022; Qualmann and Kelly 2000).

Finally, another role for WASP-family proteins is to regulate the architecture of the endo-lysosomal system. WASH localizes to early and recycling endosomes, where it stimulates Arp2/3 activity to nucleate actin filaments to control the shape of these membranes and to influence retromer-mediated trafficking to the trans-Golgi network, recycling to the plasma membrane and trafficking to late endosomes (Derivery et al. 2009; Gomez and Billadeau 2009).

1.3.2 Functions in *Drosophila*

Flies have one homolog for each of the WASP-family proteins, called respectively WASp, SCAR and WASH. Genetic analysis indicates that SCAR is the primary NPF in *Drosophila*, since the loss of both Arp2/3 and SCAR activity leads to similar developmental and cellular defects (Zallen et al. 2002). Indeed, SCAR activity is involved in axon development, egg chamber structure and adult eye morphology (Rodriguez-Mesa et al. 2012; Zallen et al. 2002). Both WASp and SCAR are essential for myoblast fusion, during the formation of muscles in both embryos and adults (Berger et al. 2008a). SCAR is also responsible for cell-cell contact expansion between the two sensory organ precursor (SOP) daughters, and Rac-dependent Arp2/3 regulates the timing of adherens junction formation upon cell division in the epithelial tissue (Herszterg et al. 2013; Trylinski and Schweisguth 2019). *Drosophila* epithelial cells possess dynamic filopodia and lamellipodia, whose morphology depends on Cdc42, aPKC and Par-6. The actin network responsible for the formation of these protrusions is nucleated by Rac-dependent SCAR and Arp2/3 complexes (Georgiou and Baum 2010).

WASp is also required for specific Notch-mediated fate decisions following asymmetric cell divisions in developing central nervous system, microvilli formation, and bristle development (Ben-Yaacov et al. 2001a; Bogdan et al. 2004; Trylinski, Mazouni, and Schweisguth 2017; Trylinski and Schweisguth 2019; Zelhof and Hardy 2004). These functions of WASp are mediated by the Arp2/3 complex, since the loss of the Arp3 and Arpc1 subunits leads to cell fate defects like the ones caused by loss of WASp activity (Rajan et al. 2009).

WASH has a non-essential function during oogenesis, where it regulates actin and microtubule dynamics downstream of Rho GTPase (Liu et al. 2009; Nagel et al. 2017). WASH was also shown to be important for regulating nuclear architecture, integrin receptor trafficking and lysosome acidification (Nagel et al. 2017; Verboon et al. 2015).

Consistent with WASP family proteins carrying out their effects through activation of the Arp2/3 complex, *Drosophila* Arp2/3 mutants have similar defects in cytoplasmic organization and cytoskeleton dynamics in many morphogenetic

events taking place during oogenesis and early embryogenesis (Hudson and Cooley 2002b).

1.4 Role of different actin networks in mitosis.

The NPFs and Arp2/3 play numerous roles in actin regulation during interphase. However, the mitotic actin cortex is, for the most part, thought to be nucleated by Formins. This is due to a shift in dominance of actin nucleators as cells enter mitosis (Bovellan et al. 2014; Rosa et al. 2015). Mitotic entry is accompanied by loss of Arp2/3-dependent lamellipodia and the assembly of a mitotic cortical actin network nucleated instead by the formin Dia (Davidson et al. 2013; Ibarra, Pollitt, and Insall 2005; Rosa et al. 2015; Zhuang et al. 2011). The non-branched Dia-nucleated actin cortex provides an ideal substrate for Myosin motors to walk on (Skau, Neidt, and Kovar 2009). The resulting cortical tension generated causes cells entering mitosis to round up and adopt a near spherical form (Stewart et al. 2011). At anaphase, this Dia-dependent actomyosin network is then rearranged to generate a contractile actomyosin ring at the cell furrow which, along with polar relaxation, drives constriction and cell division (Ramkumar and Baum 2016). (D'Avino, Giansanti, and Petronczki 2015). While the loss of Formins compromises cytokinesis, making clear their role in this process, in some cell types, the Arp2/3 complex has been shown to contribute a significant amount of F-actin to the cortex. In addition, actin and Arp2/3 have been proposed to play additional roles in mitosis (Bovellan et al. 2014).

Some of the first clear evidence for a mitotic role for branched actin networks came from the study of cytoplasmic actin filaments and their functions in large oocytes, egg and embryo cells (Field 2011). Mouse oocytes lack centrosomes, and the asymmetric localization of the spindle within the enormous ooplasm is regulated by actin in place of microtubules. Inhibiting Arp2/3 in this system disrupts migration of the spindle and the completion of cytokinesis (Sun et al. 2011; Yi et al. 2011). Furthermore, an M-phase-specific increase in cytoplasmic Arp2/3-dependent F-actin has been observed by live imaging in *C. elegans* and *Xenopus* embryos (Field et al. 2011; Velarde, Gunsalus, and Piano 2007).

Novel actin structures have also been observed in somatic cells in mitosis. In HeLa cells, a cluster of actin filaments appears during prometaphase and revolves along the cell cortex at constant speed, before fusing into the contractile ring after a few revolutions as cells exit mitosis. This was shown to depend on the Arp2/3 complex (Fink et al. 2011; Mitsushima et al. 2010). Arp2/3-dependent actin has also been observed forming close to centrosomes at mitotic exit, and WASH was identified as the NPF involved in its generation (Farina et al. 2019). However, the functions of both these actin pools remains to be determined.

Another relatively unexplored role for the Arp2/3 complex in mitosis is the prevention of excessive Formin activity. In the *C. elegans* one-cell embryo, treatment with Arp2/3 complex inhibitor delays contractile ring formation and constriction. The authors of the study present evidence that the delays are due to an excess in Formin-nucleated cortical F-actin, since the Arp2/3 complex negatively regulates Formin activity (Chan et al. 2019), even though the Arp2/3 complex does not localize in the contractile cytokinetic ring. Furthermore, an excess of Arp2/3-dependent F-actin in the cytoplasm can indirectly disrupt dynamic events during mitosis. Thus, in patients affected by X-linked neutropenia, dysregulated activation of Arp2/3 in mitosis leads to defects in cell division, and consequently cell death (Moulding et al. 2007, 2012).

These observations show that overcoming technical challenges in visualizing actin enables one to define new structures missed in earlier studies. In addition, it shows that different cells and organisms use different mechanisms to achieve the same objectives. These data also emphasize the need to further explore the role of the Arp2/3 complex in mitosis.

1.5 The neuroblasts as a model system.

The focus of this work will be on *Drosophila* neural stem cells or “neuroblasts” (NBs), which divide to give rise to both neurons and glia. *Drosophila* neurogenesis begins during embryonic stages of development, when NBs delaminate from the neuroectoderm and start dividing shortly thereafter (Fig. 1.3A-B). NBs from the ventral neuroectoderm go on to form the ventral nerve cord, and NBs from neural placodes at the head of the embryo form the larval brain (Harding and White 2018; Udolph et al. 1995). Delamination and acquisition of NB identity depends on Delta/Notch signalling, which refines the expression of pro-neural genes to individual cells (Artavanis-Tsakonas, Rand, and Lake 1999; Skeath and Carroll 1992).

At the end of embryogenesis, most NBs in the abdominal region of the embryo undergo apoptosis. However, in the cephalic and thoracic regions, a fraction becomes quiescent and re-enters the cell cycle during the late 1st instar larval stage (Truman and Bate 1988; Tsuji, Hasegawa, and Isshiki 2008). This second wave of neurogenesis generates 90% of adult neurons, and continues throughout larval stages into pupal stages, at which point the NBs exit from the cell cycle and disappear (Homem and Knoblich 2012) (Fig. 1.3A).

The proliferation patterns of NBs differ between populations. Most NB divisions are asymmetric, producing a new stem cell and a smaller ganglion mother cell (GMC). In abdominal and thoracic NBs in the ventral nerve cord and type I NBs in the larval brain, GMCs divide to produce two daughter cells, which terminally differentiate into neurons or glia. A subset of NBs in the larval brain then undergo type II divisions, in which the NB divides asymmetrically to generate an intermediate neural progenitor (Fig. 1.3C). This progenitor first maturates and then divides asymmetrically to produce another progenitor and a GMC (Bello et al. 2008; Boone and Doe 2008; Homem and Knoblich 2012).

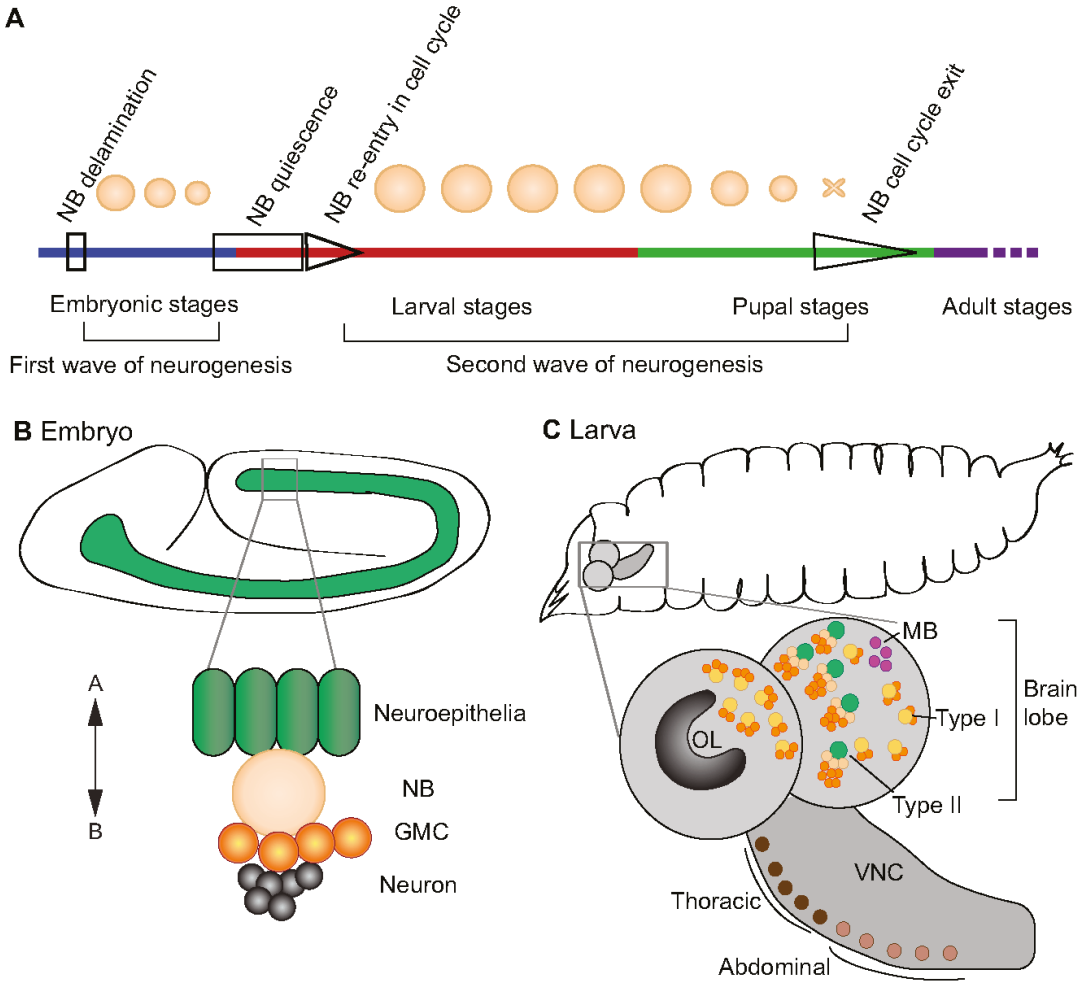

Figure 1.3. Neuroblasts development in *Drosophila* embryo and larvae. A. Timeline of the two waves of neurogenesis occurring during fly development. **B.** Schematics of NB delamination from neuroectoderm (in green). NB progeny is represented by GMC (orange) and neurons (black). **C.** 3rd instar larvae and its brain, with representation of the different parts of the brain and the various NB types. Adapted from Homem and Knoblich 2012.

1.5.1 Establishment of asymmetry and segregation of cell fate determinants.

All *Drosophila* NBs exploit the same mechanism to divide asymmetrically. Four major steps are necessary for proper asymmetric division: establishment of the polarity axis; alignment of the mitotic spindle along the apico-basal polarity axis; asymmetric localization of cell fate determinats; and finally, segregation of these determinants into the dividing NB (Homem and Knoblich 2012) (Fig. 1.4).

Apico-basal polarity is established during early prophase with the formation of the apical Par complex, which is composed by Bazooka in flies (Baz; Partitioning defective 3, Par-3 in vertebrates), Partitioning defective 6 (Par-6) and atypical Protein Kinase C (aPKC) (Gallaud, Pham, and Cabernard 2017; Petronczki and Knoblich 2000; Schober, Schaefer, and Knoblich 1999a; Wodarz et al. 1999a, 2000). When a NB delaminates from the epithelium, it maintains contact with the surrounding epithelial cells, and the Par complex localization is inherited from this contact (Schober et al. 1999a; Wodarz et al. 1999a; Yoshiura, Ohta, and Matsuzaki 2012). Polarity axis orientation is then maintained through sequential divisions by intrinsic cues like the apically localized centrosome, microtubules and the last-born daughter cell (Loyer and Januschke 2018; Rebollo et al. 2007; Rebollo, Roldán, and Gonzalez 2009; Rusan and Peifer 2007).

Once Baz localization has been established and restricted to the apical side of the NB, it serves as a platform to recruit other polarity proteins: Par-6 and aPKC (Schober et al. 1999a; Wodarz et al. 1999a). Several studies have shown that Baz is likely to be the most upstream component of the complex. However there is co-dependency between proteins of the Par complex for proper apical localization and activity (Rodriguez et al. 2017; Rolls et al. 2003). The Rho GTPase Cdc42 also plays a key role, since it is required for the cortical localization of both aPKC and Par-6 (Atwood et al. 2007; Loyer and Januschke 2020).

Once Baz is localized to the NB apical pole, it triggers the recruitment of the machinery that aligns the mitotic spindle with the polarity axis. The conserved key players for spindle orientation are Inscuteable (Insc), Partner of Inscuteable (Pins; LGN in vertebrates), the heterotrimeric G-protein alpha subunit (Gαi), and

Mushroom body defect (Mud; NuMa in vertebrates) (Kraut et al. 1996; Parmentier et al. 2000; Schaefer, A. Shevchenko, et al. 2000a; Schaefer et al. 2001; Schober et al. 1999a; Siller, Cabernard, and Doe 2006; Yu et al. 2000a). Insc expression starts during neuroblast delamination and in NBs, the protein localizes to the apical cell cortex. In the absence of Insc, mitotic spindles in NBs are misoriented (Kraut et al. 1996). Insc colocalizes with the Par complex, and its apical localization is dependent on binding to both Baz and Pins (Schaefer, A. Shevchenko, et al. 2000b; Schober, Schaefer, and Knoblich 1999b; Wodarz et al. 1999b; Yu et al. 2000b). Pins is recruited to the apical cortex upon binding of Gαi, which induces a conformational change in Pins and allows for further binding of Gαi. Pins also recruits Mud to the apical NB cortex (Bowman et al. 2006a; Nipper et al. 2007; Siller et al. 2006), and is essential for proper alignment of the spindle to the polarity axis, as *pins* mutant cells fail to correctly orient the mitotic spindle (Schaefer, A. Shevchenko, et al. 2000b; Yu et al. 2000b). Furthermore, heterotrimeric G-proteins are involved in directing asymmetric cell division in the NB. The G-protein alpha subunit Gαi localizes asymmetrically and it was shown that overexpression or depletion in delaminating NBs causes defects in both spindle orientation and determinant localization. This suggests that G-proteins establish a positional cue at the apical cell cortex during NBs delamination which is needed for maintaining apical protein localization and ultimately, for orienting asymmetric cell division (Schaefer, A. A. Shevchenko, et al. 2000; Schaefer et al. 2001).

Another important component for spindle orientation is Mud, which binds to Pins and acts downstream of Insc/Pins/Gαi. In contrast to *pins* or *Gαi*, *mud* mutant NBs show a compromised spindle orientation but correct Par complex localization (Bowman et al. 2006b; Izumi et al. 2006; Siller et al. 2006). In the end, the forces exerted on astral microtubules to position the spindle are thought to be generated by cortical Dynein - a microtubule-based motor (Merdes et al. 1996; Wang et al. 2011). However, a second pathway implicated in spindle orientation involves the protein Disc Large 1 (Dlg1), which links Pins to kinesin Khc-73, providing a further anchor between the Insc/Pins/Gαi complex and microtubules (Januschke and Gonzalez 2010; Johnston et al. 2009; Siegrist and Doe 2005).

The activity of the Par complex also controls the basal localization of molecules involved in cell fate determination. These include Numb and its binding partner, Partner of Numb (Pon), the adaptor protein Miranda (Mira), which binds the fate determinants Prospero (Pros; Prox1 in vertebrates) and Brain tumor (Brat; Trim in vertebrates) and transports them into the GMC (Doe et al. 1991; Lee et al. 2006; Lu et al. 1998; Rhyu, Jan, and Jan 1994; Shen, Jan, and Jan 1997). These proteins form a crescent at the basal NB cortex at metaphase, and segregate asymmetrically into the GMC in telophase. Prospero is a transcription factor that induces activation of genes involved in neural differentiation, Numb represses Notch signalling, further inhibiting self-renewal in the GMC, while Brat acts as a post-transcriptional regulator during embryogenesis (Bello, Reichert, and Hirth 2006; Choksi et al. 2006; Homem and Knoblich 2012; Lee et al. 2006; Schweisguth 2004). Although not essential, Pon assists in the asymmetric localization and segregation of Numb (Lu et al. 1998; Wang et al. 2007). Mira prevents the fate determinants from entering the NB nucleus by tethering them to the basal membrane in mitosis. The mechanism for restricted basal Mira localization is not completely clear. It is well established that aPKC inhibits Mira from binding the apical plasma membrane via phosphorylation (Atwood and Prehoda 2009). Experiments have shown that when aPKC is still inactive in interphase, Mira localizes uniformly around the cortex. Mira is then removed from the apical cortex as soon as aPKC is recruited and its removal continues in an apico-basal direction (Hannaford et al. 2018; Ikeshima-Kataoka et al. 1997; Shen et al. 1997). However, aPKC inhibition in metaphase results in only partial loss of Mira asymmetry, and Mira keeps being enriched at the basal cortex even after prolonged periods of aPKC inhibition (Hannaford et al. 2019). These results suggest that while aPKC likely contributes to increased Mira asymmetric localization, other mechanisms are required for Mira patterning, possibly involving actomyosin networks (Barros, Phelps, and Brand 2003; Loyer and Januschke 2020). Once segregated into the GMC, Mira is then degraded and the transcription factors it has sequestered at the cortex are then free to enter the nucleus (Ikeshima-Kataoka et al. 1997; Shen et al. 1997).

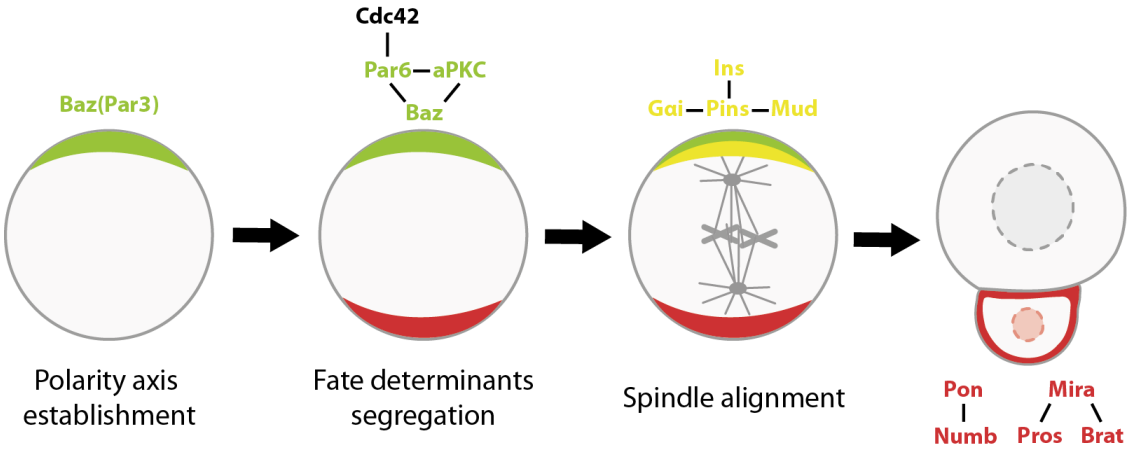

Figure 1.4. Polarity establishment and mechanisms in the dividing NB. Baz (Par-3 in vertebrates, green) localizes first and defines the NB apical pole. Other proteins of the Par complex are recruited via Baz and Cdc42, and restrict fate determinants (red) on the basal side of the NB. Baz also recruits the spindle orientation machinery (yellow). Adapted from Loyer and Januschke 2020.

1.5.2 Mechanisms of asymmetric division.

Asymmetric cell divisions lead to the formation of daughter cells with distinct fates in development. This kind of division has been extensively studied in the first embryonic cell division in *C. elegans*, where asymmetry is established by dynein-dependent pulling of the spindle towards one of the embryo poles. In this case, the spindle displacement leads to unequally sized daughter cells (Gönczy et al. 1999; Schneider and Bowerman 2003). A different mechanism of asymmetric cell division is observed in drosophila sensory organ precursors (SOPs), where segregation of proteins in the mother cell can enable directional Delta-Notch signalling between daughter cells to establish different fates (Gönczy 2008). Finally, other cell types, like *C. elegans* Q neuroblast lineage and *Drosophila* neuroblasts use Myosin II polarization to establish asymmetry, therefore exploiting the generation of asymmetric contractile forces (Ou et al. 2010; Pham et al. 2019).

The first evidence that Myosin plays an important role in *Drosophila* NBs was observed by Barros et al., who showed that Myosin is required for the localization of basal fate determinants and that it is asymmetrically localizing in the dividing NB (Barros et al. 2003). At metaphase, non-muscle Myosin II (hereafter called Myosin) appears uniformly localized around the NB cortex, as it is in mammalian cells in mitosis (Chugh and Paluch 2018). However, at the onset of anaphase it is cleared asymmetrically from the apical and basal poles of the NB. The molecular mechanisms leading to this symmetry-breaking are not completely understood. It is known that Myosin localization is not dependent on the spindle, since spindle chemical ablation does not compromise apical Myosin relocalization. On the contrary, Myosin clears from both poles at the same time in *dlg;;pins* double mutants, leading to NBs dividing symmetrically, indicating that Myosin asymmetrical clearance depends on Pins and Dlg (Barros et al. 2003; Cabernard, Prehoda, and Doe 2010). Furthermore, a role for Rho kinase (Rok) and Protein Kinase N (Pkn) has been proposed in linking Pins to Myosin regulation, since Pins enriches Rok and Pkn at the apical NB cortex after nuclear envelope breakdown, and these proteins in turn affect Myosin activity through phosphorylation (Tsankova et al. 2017).

Shortly after anaphase onset, Myosin asymmetry is immediately visible when one images the actomyosin cortex since Myosin clears from the apical cortex, before it clears from the basal cortex. As it flows away from cell poles, Myosin becomes enriched at the lateral side of the NB cortex, where it pulls on anti-parallel actin filaments to induce constriction of the cytokinetic furrow (Roubinet et al. 2017). The fact that Myosin is cleared first from the apical side leads to an apical cortical expansion, which contributes to the basal positioning of the cleavage furrow (Fig. 1.5). At mitotic exit, the recruitment of Pebble (Plb; Ect2 in vertebrates), a RhoGEF, to the spindle midzone leads to the activation of the small GTPase Rho1 (RhoA in vertebrates). This active pool of Rho1 at the plasma membrane triggers a cascade of events that leads to the assembly and contraction of a cytokinetic actomyosin ring (Basant and Glotzer 2018; D'Avino et al. 2015). The contractile ring is connected to both the cell membrane and the central spindle, via proteins like Anillin and citron kinase (CIT-K) (Bassi et al. 2011; D'Avino et al. 2015; Piekny and Glotzer 2008). Anillin in turn recruits cytoskeletal proteins septins to the cleavage site (Field et al. 2005; Liu et al. 2012). NB cleavage furrow is also enriched in microtubules, Myosin, actin, Plb, and Rho1.

Even though Myosin asymmetrical clearance is only dependant on polarity cues, spindle cues are necessary for proper constriction of the cytokinetic furrow and division completion. Indeed, in experiments where these cues are removed, the furrow does not close completely, and division is never completed (Cabernard et al. 2010; D'Avino et al. 2015). Therefore, proper NB asymmetric division that leads to the formation of a big NB and a small GMC can only be carried out when polarity and spindle cues are temporarily and spatially coordinated (Connell et al. 2011; Roubinet et al. 2017).

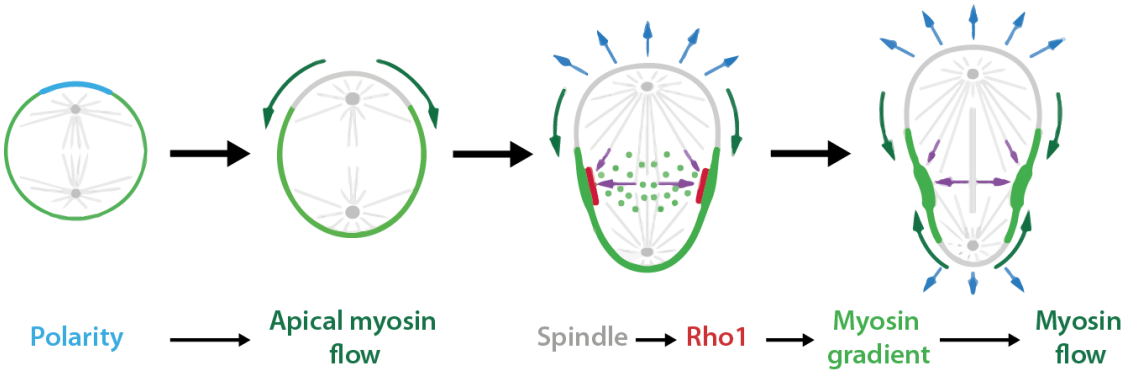

Figure 1.5. Mechanism of Myosin flow during NB division. Polarity cues induce Myosin clearance from the apical NB pole at anaphase onset. This leads to a flow of Myosin towards the basal side of the NB. Spindle cues activate Rho1 which induces Myosin accumulation at the sides of the NB, where the cytokinetic furrow starts to form. Cytoplasm is pushed towards the apical side because of the asymmetric Myosin flow, and this leads to an apical cortical expansion (blue arrows). Lateral Myosin enrichment induces Myosin clearance from the basal side, which leads to further accumulation of lateral Myosin. Adapted from Roubinet 2017.

1.5.3 Relationship between polarity, actin and plasma membrane.

Recently a more direct link between polarity proteins and the actin cortex of dividing NBs has been discovered. Experiments in which NBs were treated with Latrunculin show that actin filaments are important for both the initiation and maintenance of apical polarity (Hannaford et al. 2018; Oon and Prehoda 2019). Furthermore, the actin cytoskeleton is required for Baz polarization, but not for its polarity maintenance in early mitosis, while mutations in the actin-binding protein Moesin lead to defects in apical polarity maintenance (Abeysundara, Simmonds, and Hughes 2018; Oon and Prehoda 2019). Similar results are seen with aPKC. In prophase NBs, aPKC appears cytoplasmic (Hannaford et al. 2018). However, aPKC appears to accumulate at the apical cortex through cortical flow, which is coordinated by an actomyosin network (Oon and Prehoda 2019, 2021). As a result, by metaphase aPKC accumulates at the apical pole, where it directs the polarization of cell fate determinants, like Miranda, to the basal cortex.

In some ways, this process appears similar to what is known about cortical directional transport of polarity proteins in the *C. elegans* embryo, where isotropic cortical Par complex is polarised as it is transported by a cortical actomyosin flow that is triggered by sperm entry. The symmetry is therefore broken, and the Par complex accumulates at the anterior pole (Illukkumbura, Bland, and Goehring 2020; Lang and Munro 2017; Munro, Nance, and Priess 2004). In NBs, however, while Myosin II has been implicated in polarization of the basal cortex, it appears dispensable for apical polarity (Barros et al. 2003; Hannaford et al. 2018).

Membrane flows also seem to play a role in cortical polarization of the dividing NB. The NB membrane undergoes several phases of movements that may explain the movement of aPKC, and that depend on the actomyosin cytoskeleton (LaFoya and Prehoda 2021). Again this is similar to polarisation of the *C. elegans* zygote where the polarized distribution of the plasma membrane lipid phosphatidylinositol 4,5-bisphosphate (PIP_2) is regulated by antero-posterior polarity cues. Furthermore, PIP_2 and F-actin cortical movements are coupled, and PIP_2 cortical structure formation and movement is actin-dependent (Scholze et al. 2018).

These studies outline a new and interesting relationship between the actin cytoskeleton, the membrane and cell polarity, showing that more work is needed in this area to elucidate the mechanisms that allow recruitment and maintenance of polarity in the NB.

1.5 Aim of the thesis

The actin nucleator Arp2/3 complex has mostly been studied in interphase cellular processes, even though recent studies show a variety of possible roles for the complex in different systems. However, it remains to be tested whether or not Arp2/3-dependent actin filament formation plays important roles during mitosis in asymmetric cell divisions. *Drosophila* neuroblasts, like other stem cell types, are likely to face particular challenges as they divide, due to the necessity to repartition different fate determinants to the two daughter cells. Recent studies have shown a link between membrane flows, polarity and the actin cytoskeleton, but more work is needed to specifically understand the role of the branched actin network in this system.

To do so, in this thesis I aim to:

1. Explore the consequences of Arp2/3 complex inhibition on the NB cortex and membrane.
2. To determine the mechanisms that polarise Arp2/3 in the dividing neuroblast.
3. To understand the role of Arp2/3 in asymmetric NB division.

Chapter 2.

Materials and methods

2.1 *Drosophila* techniques

Flies were raised in vials containing standard cornmeal-agar medium (yeast 148 g/l, sugar 740 g/l, agar 88g/l, Flour/cornmeal 848 g/l, Nipagin 0.0124 % (v/v)) supplemented with baker's yeast. Stocks were maintained at 18°C, 22°C or 25°C, while crosses were incubated at 25°C and larvae were grown for 3 days before being dissected for live imaging.

2.1.1 Marking subsets of cells

Expression of fluorescent proteins and dsRNA were driven using the UAS/GAL4 system, that derives from yeast and has been adapted for genetic manipulation in *Drosophila* (Brand, Manoukian, and Perrimon 1994). GAL4 is a transcriptional activator which specifically recognizes the target UAS motifs. GAL4 expression is usually directed by a promoter or enhancer, and GAL4 in turn induces expression of genes downstream of UAS sites. GAL4 expression can be tuned by coupling it with promoters active in specific tissues or during specific developmental phases, allowing the selective expression of downstream targets in a wide variety of cell and tissue specific patterns (Brand et al. 1994).

The model system used in this thesis is the neuroblast, hence most perturbations relied on expression driven by the *worniu* promoter (e.g. worGAL4) which starts to be expressed in the neuroectoderm during embryogenesis and is then expressed in neuroblasts (Albertson and Doe 2003; Ashraf et al. 1999). In some instances the promoter *neuralized* was also used, which is expressed throughout neuroectoderm and then in neuroblasts too (Boulianne et al. 1991; Trylinski and Schweisguth 2019).

An additional approach to fine-tune the system is to use the temporal and regional gene expression targeting (TARGET) technique. This technique exploits the protein GAL80, which is a repressor of GAL4 and hence binds and prevents GAL4 from activating transcription (Caygill and Brand 2016). For this work GAL80 was expressed ubiquitously under the *α-tubulin* promoter.

2.1.2 Genetic techniques

In the case of mutations like Arp3^{EP3640} and Sas4^{s2214}, one line carrying the mutation was crossed with a line carrying a chromosomal deletion including the gene of interest. Mutant genes or deletions on the second chromosome were balanced with Cyo::ActGFP chromosome and the ones on the third chromosome were balanced with TM6B, *tubby* chromosome. Thus, homozygous mutant larvae were selected discriminating against GFP fluorescence at the midgut.

For essential genes, different methods were used to generate mutant tissue or to reduce gene function using RNAi in clones in an otherwise wild type animal.

For RNAi experiments, males from each UAS-dsRNA were crossed with virgin females carrying either worGal4, Sqh::GFP, UAS-cherry::Jupiter or worGal4, Jupiter::GFP, neur-PLCΔPH::RFP. Crosses were kept at 25°C and dissected for live imaging after 4 days.

To knock-down expression of the Arp2/3 subunit Arp3, I tested two different dsRNA by expressing them in the notum using pannier-Gal4, but only one was efficient in inhibiting bristle formation (Rajan et al. 2009), therefore all data shown in chapter 3 was collected only using this one line (VDRC35260) (Fig. 2.1).

To generate homozygous mutant *scar* clones in an otherwise wild type animal, the TARGET system was used in combination with the flippase-FRT system. This system exploits the activity of the yeast flippase to carry on mitotic recombination between chromosomes within a single dividing cell. The mutant allele to be recombined must be on a chromosome arm that carries an FRT site close to the centromere. This mutant line is then crossed with a line carrying a wild type chromosome arm marked by GAL80 carrying the same centromeric FRT site. Expression of the flippase in G2 cells induces recombination at the FRT site so that, at mitosis, one daughter cell inherits two mutant alleles while its sister inherits two copies of the corresponding wildtype alleles together with two copies of GAL80. The mutant cells in the clone can be recognized because, lacking GAL80, GAL4 leads to expression of a reporter – in this case, UAS-cherry::Jupiter (Xu and Rubin 1993).

To generate *scar* somatic clones, the flippase (FLP) was expressed under the heat shock promoter Hsp70 (hs), and was activated when putting the vials with larvae at 37°C for 1h in a water bath. The heat shock was performed 2 days after the cross had been set up. The cross was the following:

$hsFLP^{X}$; Gal80, FRT^{II} / CyoActGFP ; worGal4, Sqh::GFP, UAS-cherry::$Jupiter^{III}$

x

$scar^{\Delta 37}$, FRT^{II} / CyoActGFP

The second chromosome of both lines was balanced over Cyo::ActGFP. As a result, wild type clones express Sqh::GFP, while *scar* mutant clones express both Sqh::GFP and UAS-cherry::Jupiter (Fig. 2.2). To verify that the $scar^{\Delta 37}$ allele was producing mutant clones, I let some heat shocked larvae grow into adults and analyzing their eyes I could observe patches of defective ommatidia, as expected (Zallen et al. 2002) in a tissue carrying $scar^{\Delta 37}$ mutant clones (Fig. 2.3).

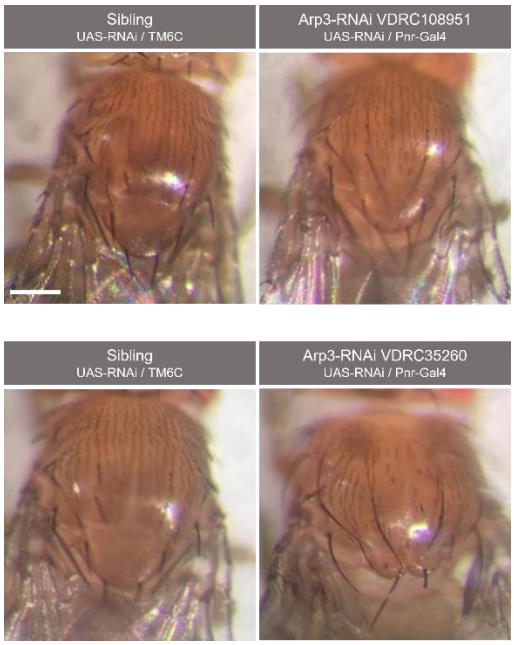

Figure 2.1. Expression of arp3 dsRNAs in the notum shows knock-down effectiveness. UAS-Arp3-RNAi(III) x pnr-Gal4/TM6C. dsRNA against arp3 were tested by expression in the notum via pnr-Gal4, and only VDRC35260 showed efficiency in perturbing bristle development. Scale bar: 0.25 mm

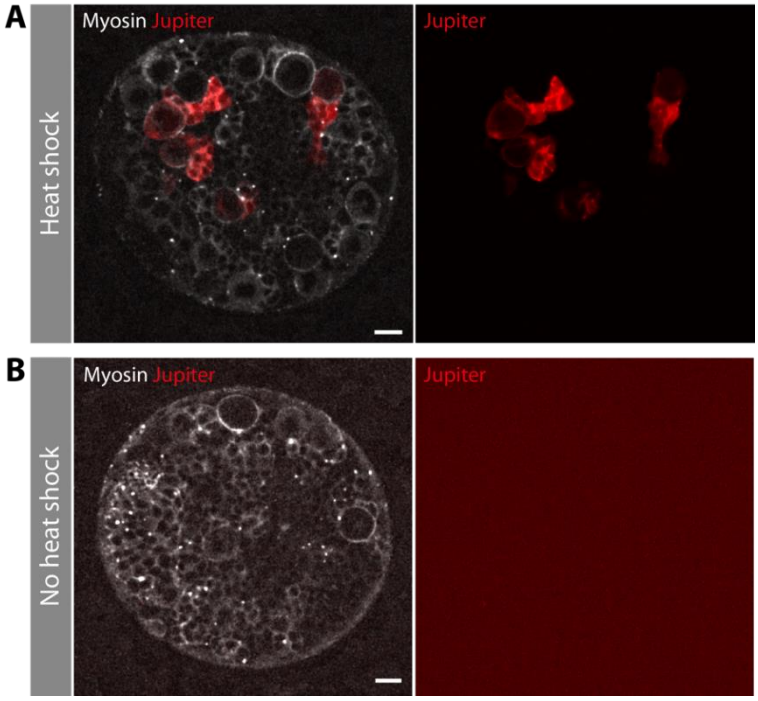

Figure 2.2. Heat shock leads to expression of the flippase and to the formation of *scar* somatic clones marked in red. The genotype of both brains is hsFLP; FRT, scar$^{\Delta 37}$ / FRT, GAL80; worGal4, Sqh::GFP, UAS-cherry::Jupiter. **A.** Brain has undergone heat shock and shows *scar*$^{\Delta 37}$ somatic clones. **B.** Control in the absence of heat shock to verify that there is no leakage of flippase expression, hence no clones. In white, non-muscle Myosin II expression in neuroblasts can be seen due to the Sqh::GFP.
N brains = 6. Scale bar: 10 µm.

Figure 2.3. Expression of the scar$^{\Delta 37}$ allele leads to defective ommatidia in the adult fly. Expression of the scar$^{\Delta 37}$ allele through hsFLP and heat shock determines the formation of somatic clones in the adult fly, and results in patches of defective ommatidia (arrowheads). No defects were exhibited in wild type siblings, which carry Cyo::ActGFP and therefore should not undergo recombination following heat shock. Scale bar: 100 µm.

2.3 Fly stocks

Transgenes	Description	Source	Identifier/origin
wor-Gal4	*worniu*: neuroblasts specific promoter	(Albertson and Doe 2003)	FBti0161165
Sqh::GFP	*Drosophila* non-muscle Myosin II. Knock-in	(Royou, Sullivan, and Karess 2002)	FBti0073027
UAS-cherry::Jupiter	Microtubule reporter	(Cabernard and Doe 2009)	FBtp0040573
Jupiter::GFP	Knock-in	(Karpova et al. 2006)	BDSC6836
UAS-Arp3::GFP	Arp3 reporter	(Hudson and Cooley 2002c)	BDSC39722
UAS-Arpc1::GFP	Arpc1 reporter	(Hudson and Cooley 2002c)	BDSC26692
UAS-SCAR::GFP	SCAR reporter		González-Gaitán M.
UAS-WASp::GFP	WASp reporter	(Schäfer et al. 2007)	FBtp0055473
UAS-WASH::GFP	Wash reporter		BDSC81640
tub-Gal80, FRT40A	GAL4 inhibitor expressed under *α-tubulin* promoter		BDSC5192
Ubi-mCherry::Abi	Abi reporter expressed under *ubiquitin* promoter		BDSC58729
neur-PLCΔPH::RFP	Membrane marker expressed under *neuralized* promoter	(Trylinski and Schweisguth 2019)	FBtp0140211
UAS-PLCΔPH::GFP	Membrane marker	(Verstreken et al. 2009)	BDSC39693
UAS-LifeAct::GFP	Actin marker		BDSC58718
sqh-mCherry::GAP43	Membrane marker expressed under *squash* promoter	(Martin et al. 2010)	FBtp0087760

Mutants and deletions	Description	Source	Identifier/origin
Df(3L)Exel6112	*arp3* deficiency		BDSC7591
$Arp3^{EP3640}$	*arp3* mutant. Insertion of transposable element	(Rørth 1996)	BDSC17149
$Sas4^{s2214}$	*sas4* mutant. Insertion of transposable element	(Basto et al. 2006)	BDSC12119
$Wash^{\Delta 185}$	*wash* mutant. Deletion by P-element excision.	(Linardopoulou et al. 2007)	BDSC79220
$Wasp^{3}$	*wasp* mutant. Single site mutation.	(Ben-Yaacov et al. 2001b)	BDSC39725
$Rod^{H4.8}$	*rough deal* mutant	(Basto, Gomes, and Karess 2000)	Roubinet C.
$SCAR^{\Delta 37}$, FRT40A	*scar* mutant for somatic clones. Excision allele.	(Zallen et al. 2002)	BDSC8754
$Pins^{P62}$ & $Pins^{P89}$	*pins* mutants	(Yu et al. 2000c)	Roubinet C.

dsRNA target	Line	Origin
Arp3	GD12273	VDRC35260
WASH	GD7950	VDRC24642
SCAR	HMS01536	BDSC36121
WASp	GD1559	VDRC13757

2.4 Live imaging

Larvae were dissected with forceps to extract the brains in imaging medium (Schneider's insect medium mixed with 10% FBS (Sigma), 2% PenStrepNeo (Sigma), 0.02 mg/mL insulin (Sigma), 20mM L-glutamine (Sigma), 0.04 mg/mL L-glutathione reduced (Sigma) and 5 µg/mL 20-hydroxyecdysone (Sigma)). Brains were then transferred with the medium onto 15µ-slide angiogenesis (Ibidi) and imaged.

When brain dissociation was performed, 20-25 larvae were dissected in Chan & Gehring solution 2% FBS (CG-FBS) to extract the brain (Chan and Gehring 1971). GC-FBS composes as follow: NaCL 3.2 g/l, KCl 3 g/l, $CaCl_2$-$2H_2O$ 0.69 g/l, $MgSO_4$-$7H_2O$ 3.7 g/l, Tricine buffer Ph7 1.79 g/l, glucose 3.6 g/l, sucrose 17.1 g/l, BSA 1g/l and FBS 2%. Papain (Sigma, #P4762-50MG, 10 mg/ml) and collagenase (Sigma, #C2674-1G, 10 mg/ml) were added to the brains in CG-FBS solutions and they were incubated at 29°C for 45 minutes, to activate the enzymes. After incubation, brains were washed with imaging medium and finally dissociated through vigorous pipetting. The cells were then transferred with the medium onto 15µ-slide 8 well (Ibidi) and imaged.

For experiments in Chapter 3 and 4, live cell imaging was performed on a UltraView Vox spinning disk confocal microscope (Perkin Elmer Nikon TiE; Yokogawa CSU-X1 spinning disc scan head) with 60×/1.40 N.A oil objective and equipped with a Hamamatsu C9100-13 EMCCD camera, or a 3i spinning disk confocal microscope (Zeiss AxioObserver Z1; Yokogawa CSU-W1 spinning disk scan head) with 63×/1.40 N.A objective and equipped with a photometrics prime 95B scientific CMOS camera.

For most experiments in Chapter 5 or where high-resolution imaging was necessary, live imaging was performed on a CSU-W1 SoRa spinning disk confocal microscope (Nikon Ti Eclipse 2; Yokogawa CSU-W1 SoRa spinning disk scan head) with 60×/1.40 N.A oil objective and equipped with a photometrics prime 95B scientific CMOS camera. The SoRa system exploits microlensing the emission pinhole to achieve an improved resolution without compromising the signal brightness. Furthermore, the sample does not need special preparation

like in other super-resolution techniques and the imaging is carried on in the same way of any other confocal system (Nikon n.d.).

Whole brain imaging has been acquired with a z-stack spacing of 1 µm, while single cell imaging with a spacing of 0.7 µm. Time resolution was 60 seconds per frame, unless specified otherwise. All microscopes are equipped with a temperature-controlled environment chamber set at 26° C for the experiments.

2.5 Drug treatments

For chemical treatments to inhibit the Arp2/3 complex, the inhibitor CK-666 (Sigma #SML0006, final concentration 400 µM) or the inactive equivalent compound, CK-689 (Sigma #182517, final concentration 400 µM), were added before live imaging. To induce actin or microtubules depolymerization, respectively Latrunculin B (Sigma #L5288-1MG) at a final concentration of 10 µM or colcemid (Sigma #234109-5MG-M) to a final concentration of 0.1 mM were added to the media.

2.6 Image processing and analysis

All image analysis was carried out on unprocessed raw images. For clarity, images displayed in this thesis were processed using ImageJ software (Schindelin et al. 2012). Background was removed (rolling ball radius 50 pixel) and a Gaussian Blur applied (radius 1). All neuroblasts represented in montages come from whole mount brains, unless otherwise stated. As stated in figure legends, images represent a single confocal z-stack section or a maximum z-projection. In all figures, the time point 0 is anaphase onset, defined in this work as the first frame where the spindle starts to separate. Figures were assembled using Adobe Illustrator CS6.

To compare the size of NBs and GMCs before and after CK-666 treatment, the diameter was chosen as representative measure. Only cells dividing along the axis parallel to the field of view, and hence fully visible for the whole division, were measured, and a line was drawn from the apical pole (for NBs) or basal pole (for

GMCs) membrane to the intersection between the two daughter cells at the time of cytokinetic completion.

Experiments in which cortical PH or Myosin intensity were measured, a line of a specific width and length was drawn on the area of interest and the mean pixel value was calculated. The data were normalized by subtracting the background and were centred at the time 0.

To calculate the movement of the membrane during cortical expansion, a maximum projection of 3 z-slices from the centre of cells dividing along the axis parallel to the field of view was generated. A line was drawn from the centre of the spindle to the apical membrane, starting two time-frames before anaphase onset. A kymograph was generated from this line, the movement of the membrane was traced and the set of coordinates was used to generate the curves in the graphs. Coordinates were centred to start at (x=0, y=0). To plot the mean, the curves were interpolated in Excel using linear interpolation.

2.7 Statistical analysis

For experiments with quantification, the data were collected from at least 2 independent experiments , and, for each independent experiment, at least 2 brain lobes were imaged. For the analysis, “n” refers to the number of cells analysed (biological replicates) and “$N_{replicas}$” refers to the amount of time the experiment was performed (technical replicates). Both numbers are represented on the graphs or mentioned in figure legends.

Statistical significance was determined with Student’s t test where two groups were compared and 2-way ANOVA where more than two groups were compared, using GraphPad Prism 9 software. The two variables analysed when the 2-was ANOVA was performed were within the following:

- NB/GMC diameters and condition (like control/treatment) (Fig. 3.3, 3.6D),
- mitotic intervals and condition (Fig. 3.4, 3.5, 3.6E, 4.1-4.3)
- Apical/basal cortex and condition (mutant/control) (Fig. 5.13)

In all of these cases, a post hoc Tukey's test was also performed, and single p-values are reported in figures. The p-values resulted from the 2-way ANOVA are not reported, since they are not relevant for the hypothesis testing in place in the above cases. In all figures the Prism convention is used: ns ($P > 0.05$), *($P \leq 0.05$), **($P \leq 0.01$), ***($P \leq 0.001$) and ****($P \leq 0.0001$). In all graphs showing mean, the error bars correspond to standard deviation (SD).

Chapter 3.

Arp2/3 inhibition in the dividing neuroblast leads to formation of a membrane protrusion after cytokinesis.

3.1 Introduction

While the actin cortex is known to control the changes in cell shape that accompany division, much remains to be discovered about the molecular and cellular mechanisms that control cortical remodelling during mitosis. In this first chapter I exploit different techniques to inhibit the Arp2/3 complex to explore its role in neuroblast divisions. I describe the phenotype induced by Arp2/3 inhibition, and investigate a potential role for microtubules in generating the Arp2/3-loss of function phenotype.

3.2 Chemical inhibition of the Arp2/3 complex in the dividing neuroblast determines delayed anaphase and cytokinesis and cortical defects at cytokinesis.

In previous work in the lab, Chantal Roubinet observed an effect of the Arp2/3 inhibitor CK-666 on *Drosophila* neuroblast (NB) division. CK-666 is a small molecule that acts by stabilizing the inactive state of the Arp2/3 complex, preventing it from nucleating actin (Hetrick et al. 2013). I decided to use a non-muscle Myosin II reporter, Sqh::GFP (Myosin from now on) to observe eventual defects induced by Arp2/3 inhibition, because this reporter would allow me to see if Myosin flows are affected and therefore if establishment of asymmetry is affected. Myosin behavior and localization have been previously well characterized, making it a good marker to observe changes in NB division. I decided to not look at Actin markers first, as I suspected the actin cortex, nucleated by Formin, might overshadow any subtle changes in the Arp2/3-nucleated actin network.

I therefore used live imaging of larval NBs expressing Sqh::GFP, and a microtubule marker, cherry::Jupiter (Fig. 3.1A). In control experiments, untreated NBs divide asymmetrically (Fig. 3.1D). This is driven by a basally-directed cortical Myosin flow, as Myosin accumulates isotropically around the metaphase cortex, is cleared apically in early anaphase, and then cleared from the basal cortex, before becoming concentrated at the furrow at cytokinesis (Fig. 3.1A).

Since CK-666 is dissolved in DMSO, I used DMSO and an inactive version of the small molecule that does not bind the Arp2/3 complex, CK-689 (Nolen et al. 2009), as additional controls. In both cases, most NB divisions appeared normal, and a small percentage of cells exhibited a mild phenotype in which ectopic Myosin accumulated after cytokinesis (Fig. 3.1D). In these cases, Myosin spots were visible at the basal side of the cell and were associated with a mild contraction of the membrane (Fig. 3.1B arrowheads).

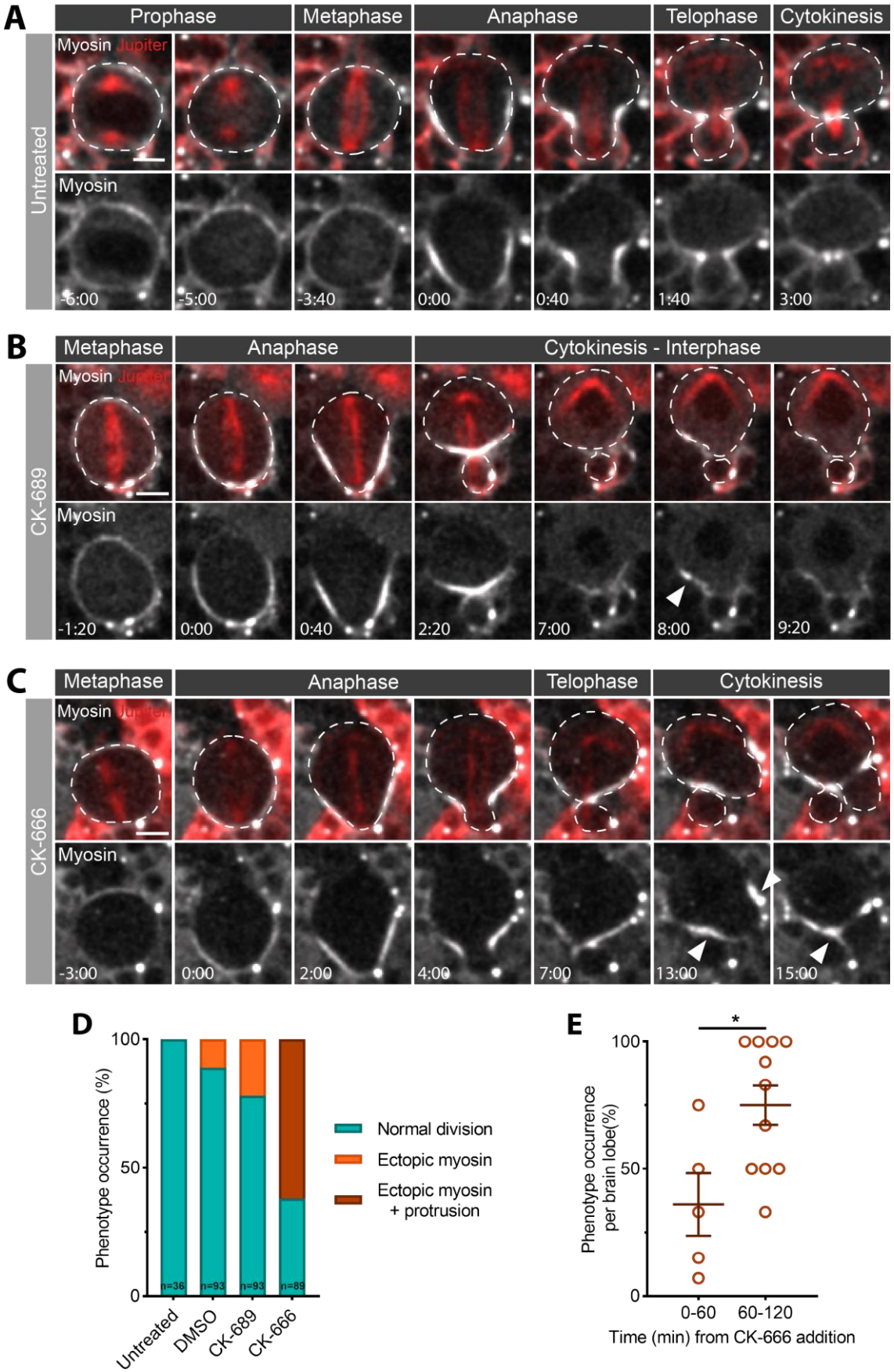
A
Prophase
Metaphase
Anaphase
Telophase
Cytokinesis
Untreated
Myosin Jupiter
Myosin
-6:00
-5:00
-3:40
0:00
0:40
1:40
3:00
B
Metaphase
Anaphase
Cytokinesis - Interphase
CK-689
Myosin Jupiter
Myosin
-1:20
0:00
0:40
2:20
7:00
8:00
9:20
C
Metaphase
Anaphase
Telophase
Cytokinesis
CK-666
Myosin Jupiter
Myosin
-3:00
0:00
2:00
4:00
7:00
13:00
15:00
D
Phenotype occurrence (%)
100
50
0
n=36
n=93
n=93
n=89
Untreated
DMSO
CK-689
CK-666
Normal division
Ectopic myosin
Ectopic myosin + protrusion
E
*
Phenotype occurrence per brain lobe(%)
100
50
0
0-60
60-120
Time (min) from CK-666 addition

Figure 3.1. The Arp2/3 complex inhibitor CK-666 induces ectopic Myosin accumulation and formation of a cell protrusion after cytokinesis in *Drosophila* NBs. A-C. Genotype: Wor-Gal4, UAS-cherry::Jupiter, Sqh::GFP / Cyo. Time-lapse images of dividing larval NBs expressing a non-muscle Myosin II reporter Sqh::GFP (grey) and a microtubule marker cherry::Jupiter (red). **A.** Untreated representative NB going through a normal asymmetric division. **B.** Example of a NB in a brain treated with CK-689 400 µM (inactive version of CK-666). Arrowheads point to ectopic Myosin accumulation. **C.** Representative NB in a brain treated with the Arp2/3 complex inhibitor CK-666 400 µM. Arrowheads point to ectopic Myosin accumulation and membrane protrusion. **D.** Bar graph showing total percentage of NBs with specific phenotype divided by condition. $N_{replicates}$=3. ****P<0.0001 (Chi-square test). **E.** Plot showing phenotype occurrence per brain lobe, of brains treated with CK-666 for different amounts of time. $N_{replicates}$=3, n_{brains}=16. Asterisk (*) denotes statistical significance. $P \leq 0.05$ (unpaired t-test).
Scale bar: 5 µm. Central and error bars: mean and SD.

In brains treated with CK-666, however, I observed a range of more severe phenotypes. In 60% of dividing cells (Fig 3.1D) Myosin was observed ectopically accumulating at the cell cortex after the completion of cytokinesis. This led to an aberrant late constriction of the plasma membrane, which generated a large rounded ectopic protrusion (Fig. 1C arrowheads). In all cases, however, the neck of the protrusion was never seen closing. Furthermore, the protrusion was always forming after abscission had been completed completed (n_{cells}= 20/20). Since the drug needs time to penetrate into the brain, I measured the phenotype occurrence per brain lobe in brains kept in the drug for different amounts of time (Fig. 3.1E). Unsurprisingly, a higher percentage of cells with a phenotype was observed in brains imaged 60-120 minutes following exposure to CK-666.

The initial shape of the protrusion induced by CK-666 treatment appeared very similar to that of the nascent GMC at cytokinesis in an untreated NB. This observation led me to generate maximum Myosin intensity z-projections of control NB (CK-689) and NB treated with CK-666. In these movies, the Myosin ring induced by the treatment (Fig. 3.2B) appeared very similar to the cytokinetic ring observed at the cleavage furrow in terms of shape, size and dynamics (Fig. 3.2A). For this reason, hereafter I refer to the phenotype as “ectopic cleavage furrow”.

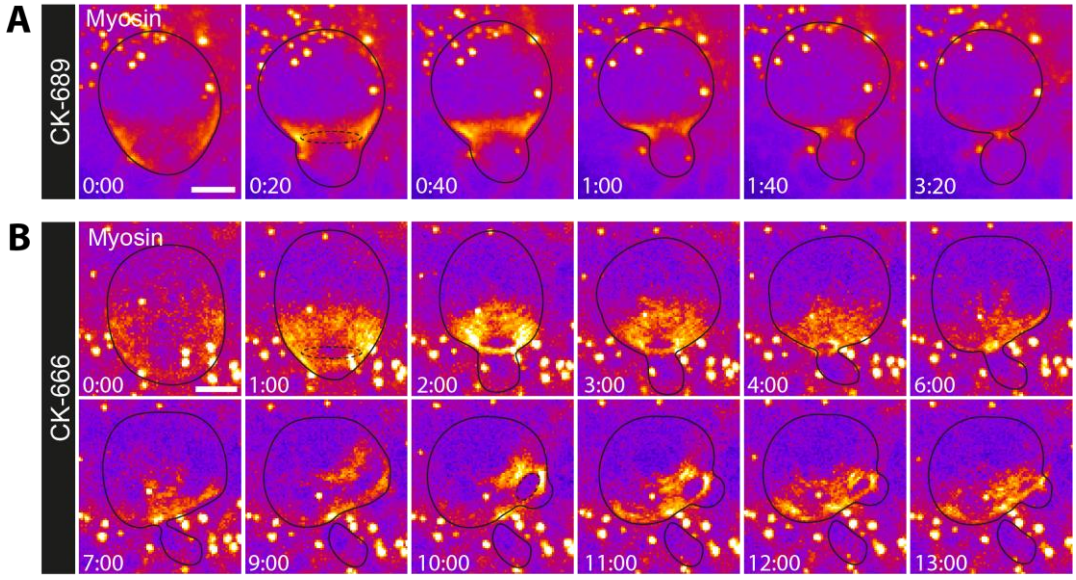

Figure 3.2. CK-666-induced membrane protrusion at cytokinesis resembles a cleavage furrow. Genotype: Wor-Gal4, UAS-cherry::Jupiter, Sqh::GFP / Cyo. **A.** Maximum Myosin intensity projection of a control cell (CK-689, 400 µM) undergoing division. The cytokinetic furrow starts forming at 20 seconds and is highlighted by a dotted ellipse. **B.** Maximum Myosin intensity projection of NB treated with CK-666 400 µM. The normal furrow is visible at 1 minute and the second furrow induced by the treatment is visible at 10 minutes.
Scale bar: 5 µm.

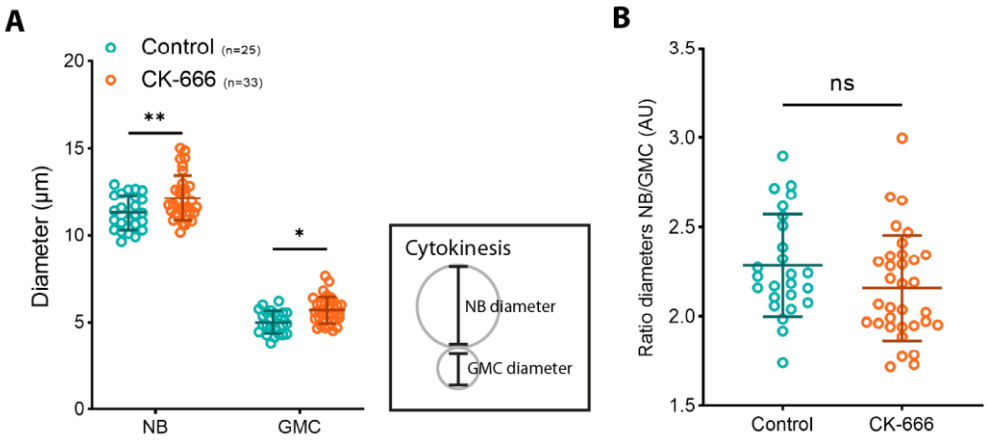

Figure 3.3. Dividing NBs treated with CK-666 show a slight increase in size at cytokinesis, but not significant change in division asymmetry. A. Plot comparing diameters, measured at cytokinesis, of NB and GMC between control (DMSO, 1 µl in 250 µl) condition and treatment (CK-666, 400 µM). Schematics shows how diameters were measured. $N_{replicates}$ = 3. Asterisks denote statistical significance. *P ≤ 0.05, **P ≤ 0.01 (Tukey's multiple comparison test). **B.** Plot comparing NB and GMC diameters' ratio between control and treatment conditions. ns, not significant. P > 0.05 (unpaired t-test).
Central and error bars: mean and SD.

Since CK-666 treatment seems to affect cell shape, I decided to examine the relative sizes of NB and GMC pairs following the inhibition of the Arp2/3 complex. To do so, I measured the diameter of NBs and GMCs and calculated the ratio between the two at the time of cytokinesis. I found that the size of both NBs and GMCs significantly increases in treated cells relative to the control (Fig. 3.3A), while NB/GMC ratio does not change significantly (Fig. 3.3B).

Furthermore, I noticed that the time to complete division was longer in CK-666 treated cells, so I decided to measure the timing of specific phases of mitotic progression to asses if this delay was limited to a specific interval or was consistent throughout division. The schematic in figure 3.4A shows how mitosis was divided up into distinct time periods: nuclear envelope breakdown (NEB); elongation of the spindle; the constriction of the cleavage furrow; and nuclear envelope reformation (NER).

Since I acquired some of the time-lapse movies with a temporal resolution of a frame every 20s (frame/sec) and others with a frame/60s interval, I first verified that the different imaging protocols did not alter the results. By comparing untreated cells imaged every 20 seconds, with ones imaged every 60 seconds, I found no significant difference in the timing of events even though the mean value for the A-B interval was slightly longer in the frame/60sec group, possibly due to the fact that lower temporal resolution leads to time overestimation (Fig. 3.4B). I then proceeded to compare the timing of different mitotic phases between control (CK-689) and CK-666 treated cells using imaging with resolution of a frame/60sec. The analysis reveals that inhibiting Arp2/3 induces a significant delay between NEB and cytokinesis, that is in time intervals A-B and B-C, but does not affect the length of the interval C-D (Fig. 3.4C). The fact that not all mitotic intervals were delayed in the same way suggests that inhibiting Arp2/3 has a specific effect on some processes at metaphase and/or cytokinesis and that the delay measured is unlikely to result from generalized stress in dividing NBs.

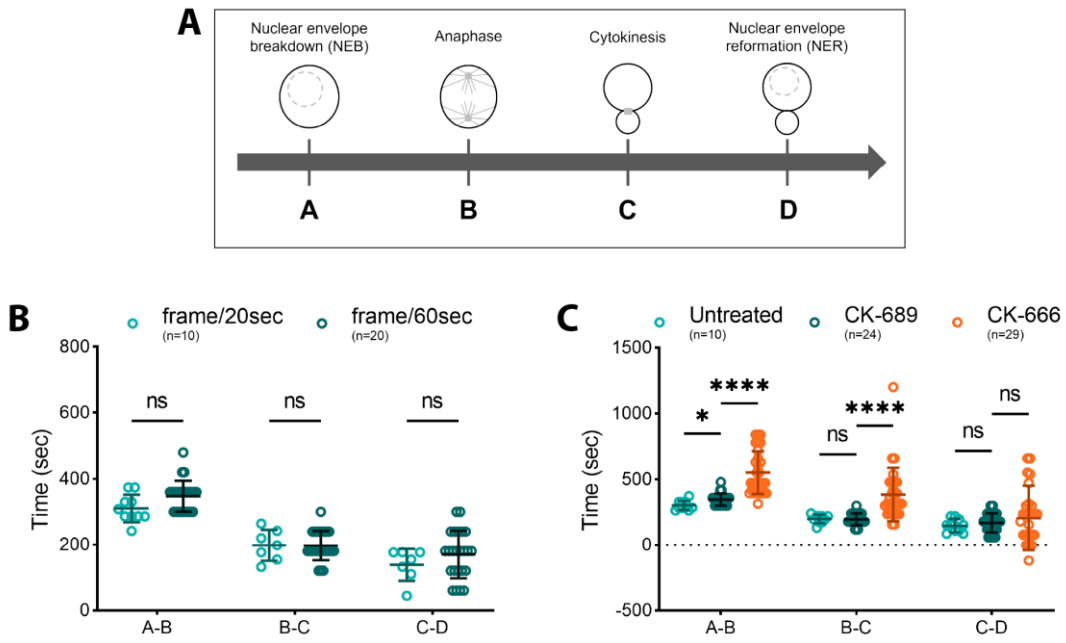

Figure 3.4. CK-666 treatment affects the length of mitotic phases in dividing NBs. A. Schematics showing how mitosis was divided up to calculate time intervals: nuclear envelope breakdown (A), elongation of the spindle (B), constriction of the cleavage furrow (C), and nuclear envelope reformation (D). **B.** Graph comparing imaging temporal resolutions of one frame every 20 seconds (frame/20sec) or every 60 seconds (frame/60sec) in untreated cells. $N_{replicates}$ = 2. **C.** Plot comparing length of mitotic intervals between different conditions with a temporal resolution of frame/60sec. Both CK-689 and CK-666 were used at a concentration of 400 µM. $N_{replicates}$ = 3. Asterisks denote statistical significance. ns, not significant P > 0.05, *P ≤ 0.05, and ****P ≤ 0.0001 (Tukey's multiple comparison test).
Central and error bars: mean and SD.

3.3 Genetic loss of function experiments confirm ectopic cleavage furrow and mitotic delay in dividing NBs lacking Arp2/3 complex activity.

To confirm the specificity of the ectopic cleavage furrow and other phenotypes seen following chemical inhibition of the Arp2/3 complex, I next exploited RNA interference (RNAi) to test the effects of knocking-down expression of the Arp3 subunit of the complex. To express the dsRNA I used the UAS/GAL4 system. GAL4 was expressed from the *worniu* promoter to restrict it to NB cells in the embryo and larval brain. 37% (13/35 cells) of NBs where arp3 knock-down was performed exhibited a phenotype resembling an ectopic cleavage furrow similar to that observed after CK-666 treatment (Fig. 3.5A, arrowheads). As before, ectopic Myosin accumulation was found to precede membrane contraction (Fig. 3.5A, top panel, arrowheads). However, the protrusion phenotype was less severe than that observed after CK-666 treatment, and was not accompanied by formation of a clear Myosin ring. Furthermore, some cells exhibited an apical bleb (6/35 cells, Fig. 3.5A, bottom panel). In these cases, ectopic Myosin was not observed prior to the formation of the apical protrusion, and the temporal dynamics of this cortical defect were different in that the protrusion both appeared and disappeared before the formation of the ectopic cleavage furrow (Fig. 3.5A, bottom panel).

I also measured the time interval between mitotic phases in wild type (WT) and Arp3 knock-down (*arp3* RNAi) NBs. As observed following CK-666 treatment, there was a significant difference in the duration of A-B and B-C, but not the interval C-D (Fig. 3.5B), when comparing control and knock-down conditions. These data confirm the hypothesis that inhibition of the Arp2/3 complex both induces an ectopic cleavage furrow in dividing NBs, and delays earlier mitotic phases.

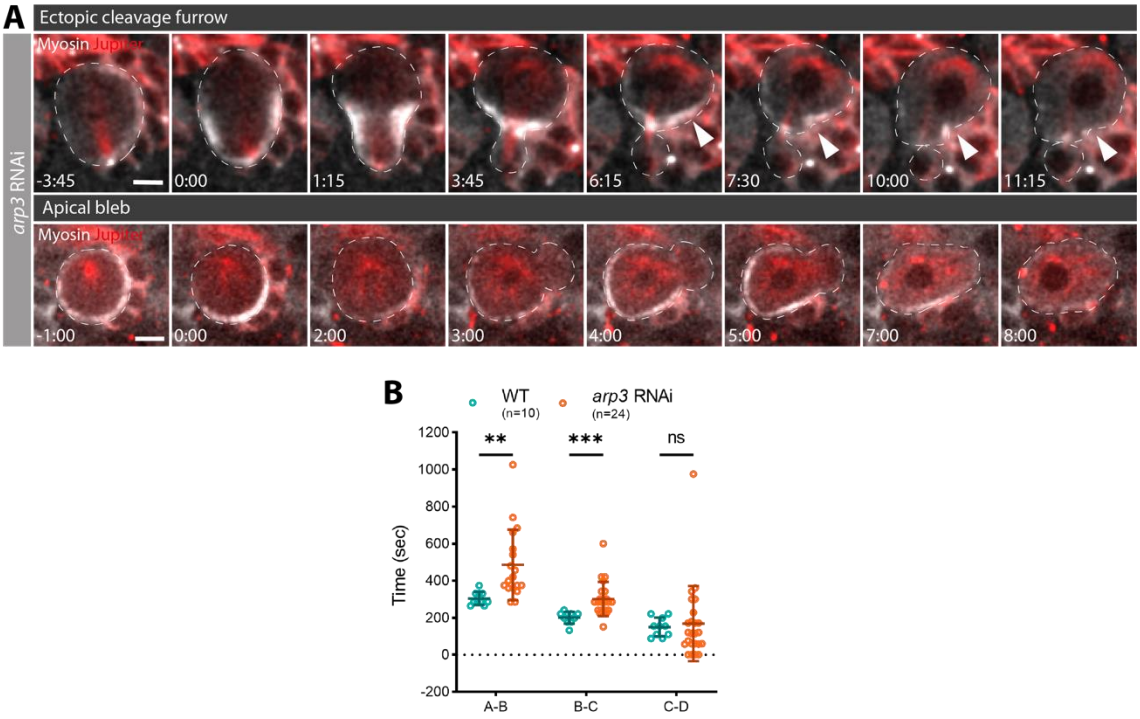

Figure 3.5. Arp3 inhibition through RNAi leads to the formation of an ectopic cleavage furrow at cytokinesis in dividing NBs. A. Genotype: Wor-Gal4, UAS-cherry::Jupiter, Sqh::GFP / Cyo x UAS-RNAi. Time-lapse images of a dividing NB in which Arp3 was silenced using RNAi, expressing the Myosin marker, Sqh::GFP (grey) and the microtubule marker, cherry::Jupiter (red). Panel on top shows example of a NB with ectopic cleavage furrow. Ectopic Myosin (6:15, arrowheads) precedes membrane contraction (7:30, arrowheads). Bottom panel shows the formation of an apical bleb following Arp3 knock-down. The GMC is not visible in the bottom panel because of the plane of division relative to the imaging plane. **B.** Plot comparing mitotic intervals between wild type cells (WT) and Arp3 knock-down cells (*arp3* RNAi). Intervals are: NEB-anaphase (A-B), anaphase-cytokinesis (B-C), cytokinesis-NER (C-D). $N_{replicates}$ = 2. Asterisks denote statistical significance. ns, not significant $P > 0.05$, $^{**}P \leq 0.01$, $^{***}P \leq 0.001$ (Tukey's multiple comparison test).
Scale bar: 5 µm. Central and error bars: mean and SD.

In the absence of a working antibody against Arp3, it is hard to know if the dsRNA is effective at reducing expression. To overcome these problems and further validate the phenotype, I decided to use the *arp3*^{EP3640} mutant. This allele was generated by transposable element insertion (Rørth 1996) and was previously mapped and used to generate an amorphic phenotype in homozygous mutant embryos (Hudson and Cooley 2002d; Zallen et al. 2002). I crossed this mutant line with a line carrying the deficiency Df(3L)Exel6112 and I imaged control (*arp3/*TM6B) and mutant (*arp3/*Def) cells. Around 50% of mutant cells exhibited an ectopic cleavage furrow at cytokinesis (Fig. 3.6A, arrowheads; Fig. 3.6B). High resolution imaging of mutant cells showed a less severe ectopic cleavage furrow (Fig. 3.6C, arrowheads) compared to the one observed with chemical inhibition of Arp2/3. The phenotype overall was more similar to that observed using dsRNA mediated Arp3 knock-down (Fig. 3.5A).

Confusingly, *arp3* mutant cells were smaller than the heterozygous control cells (Fig. 3.6D), instead of bigger, as seen after CK-666 treatment (Fig. 3.3A). This suggests that cell size might be influenced by other factors, e.g. the surrounding tissue, not just Arp2/3. Finally, the change in the timing of mitotic phases observed in the mutant was consistent with previous results: both NEB-anaphase and anaphase-cytokinesis intervals took longer in *arp3* mutant cells compared to control cells, even though only NEB-anaphase delay was statistically significant (Fig. 3.6E).

These experiments confirm that inhibiting the Arp2/3 complex in NBs leads to cortical defects at cytokinesis, affects cell size, and delays metaphase-anaphase. Together they strongly suggest that the Arp2/3 complex has a role in regulating proper cell division in the NB.

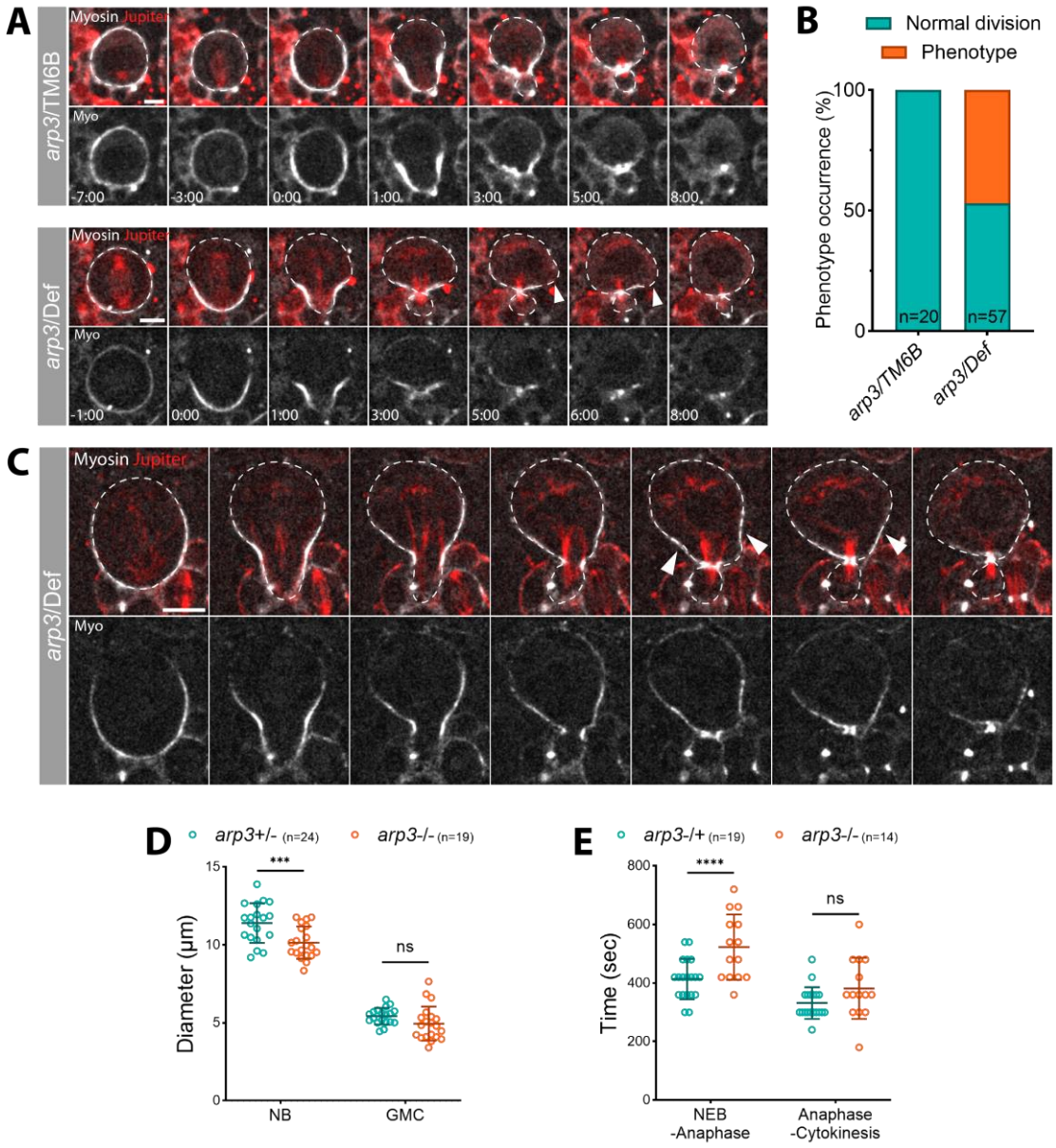

Figure 3.6. *arp3* mutant cells display an ectopic cleavage furrow at cytokinesis, altered cell sizes and delayed mitosis. A. Genotype: Wor-Gal4, UAS-cherry::Jupiter, Sqh::GFP / Cyo; *arp3*^{EP3640} /TM6B x Df(3L)Exel6112/TM6B. Time-lapse images of control (heterozygous *arp3*/TM6B) and *arp3* mutant (*arp3* mutant over deficiency Df(3L)Exel6112, *arp3*/Def) cells expressing a Myosin marker (Sqh::GFP, grey) and a microtubule marker (cherry::Jupiter, red). Arrowheads point to membrane constriction during ectopic cleavage furrow formation at cytokinesis in mutant cells. **B.** Plot showing percentage of cells with phenotype in control and mutant. **C.** High resolution imaging shows ectopic Myosin localization and cortical defects (arrowheads) in an *arp3* mutant cell. **D.** Plot showing diameter length of NB and GMC in the two conditions. $N_{replicates}$ = 2. **E.** Graph showing time of mitotic intervals between the two conditions. $N_{replicates}$ = 2. Asterisks denote statistical significance. ns, not significant $P > 0.05$, ***$P \leq 0.001$ and ****$P \leq 0.0001$ (Tukey's multiple comparison test). Scale bar: 5 µm. Central and error bars: mean and SD.

3.4 Microtubules are not involved in the formation of the ectopic cleavage furrow.

The spindle assembly checkpoint monitors defects and delays progress through division when there are problems with the spindle (Lara-Gonzalez, Westhorpe, and Taylor 2012). Since I observed a delay in mitosis starting from anaphase following the Arp2/3 inhibition and noticed an abnormal spindle in some CK-666 treated cells, I wanted to better observe spindle dynamics in cells with reduced levels of Arp2/3 activity. To do so, I used a line that expresses endogenous Jupiter tagged to GFP to image microtubules, in place of the transgene used in previous movies. I then carried on high resolution imaging of single NBs after CK-666 treatment. These time-lapses revealed significant spindle defects long before ectopic cleavage furrow (Fig. 3.7A-B). Microtubules were seen outside of the spindle in anaphase (Fig. 3.7B, 1:00-3:00, arrowheads), where they contacted the part of the cell cortex where the ectopic cleavage furrow later formed (Fig. 3.7B, 7:00-11:00, arrowheads). This accumulation of cortical microtubules at telophase was seen in around 70% of the cells treated with CK-666 imaged and analysed for this experiment (Fig. 3.7C). Of this group, 64% exhibited clear spindle defects at metaphase/anaphase (Fig. 3.7B, C), while 100% of control cells appeared normal throughout. These data suggest that spindle defects at metaphase/anaphase precede the mislocalization of microtubules at telophase, which are at the right place and time to contribute to the formation of the ectopic cleavage furrow.

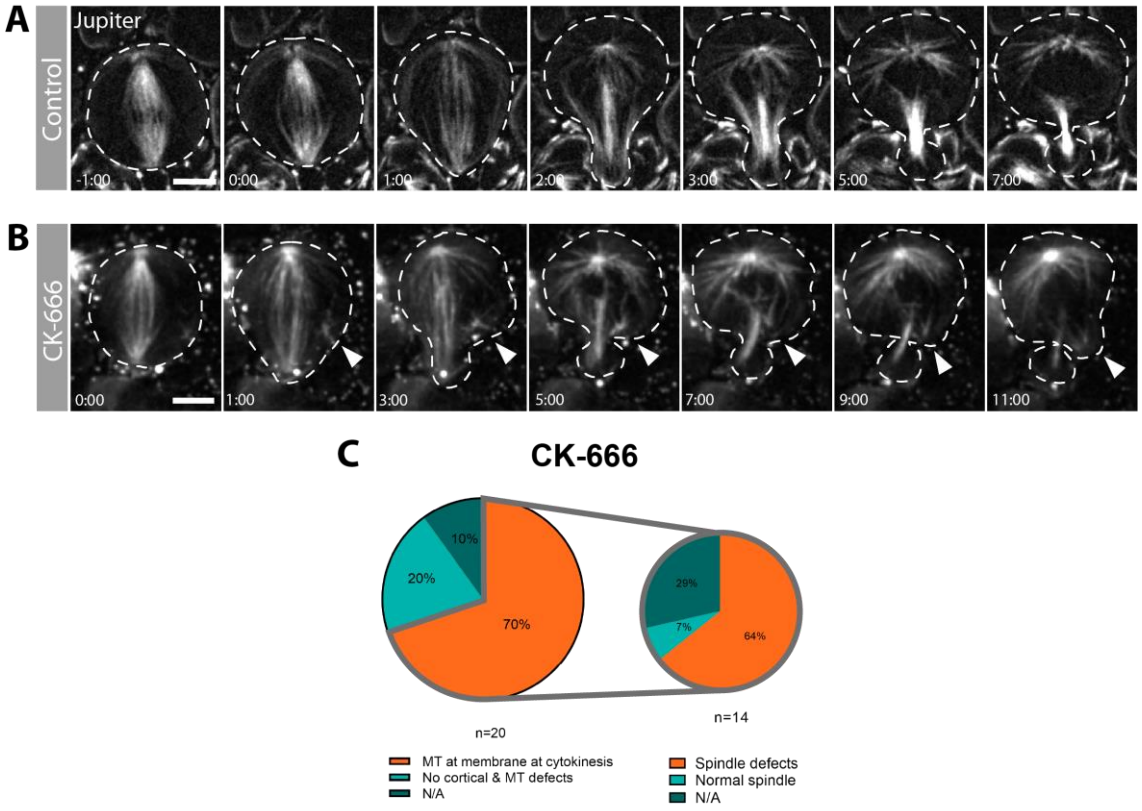

Figure 3.7. Arp2/3 inhibition by CK-666 leads to early spindle defects and microtubules mislocalizing at the cell cortex. A-B. Genotype: Jupiter::GFP(III). High resolution imaging of control (CK-689, 400 µM) (**A**) and CK-666 treated (400 µM) (**B**) NBs, expressing microtubule marker Jupiter::GFP, where endogenous Jupiter is tagged with fluorescent protein. This allows higher resolution microtubule imaging. **C.** Graph showing percentages of CK-666 treated cells that present both displaced microtubules (MT) at metaphase and at the membrane at telophase. Pie on the left shows the percentage of NBs showing microtubules at the cortex at cytokinesis, and pie on the right shows the percentage of cells within this group that also shows spindle defects. N/A (not applicable) means cells in which was not clear if misplaced microtubules were present or not. No control cells (n=15) show microtubules or spindle defects. $N_{replicates}$ = 2. Scale bar: 5 µm.

At this point, to better understand the potential role of microtubules in the formation of the ectopic cleavage furrow, I decided to test whether the centrosomal microtubules were responsible for the observed cortical defects by seeing if removing the centrosomes would rescue the phenotype. To do so, I decided to exploit the *sas4*^{s2214} mutant (Basto et al. 2006). Sas4 protein is essential for centrioles replication, even though most *sas4* mutant cells still divide asymmetrically (Basto et al. 2006). In line with the published data, in my hands ≈70% of *sas4* mutant cells divided asymmetrically (Fig. 3.8A, D), ≈20% divided symmetrically (Fig. 3.8B, D) and 10% did not complete cytokinesis (Fig. 3.8D). The subset of NBs that divided symmetrically did so because of a misalignment of the spindle and the polarity axis. In these cells it was possible to see from the montage that Myosin starts to be cleared from the bottom right of the cell in metaphase (Fig. 3.8B, arrowhead), while the plane of division was determined by the apico-basal direction of the spindle.

To test if removing the centrosomes would rescue the ectopic cleavage furrow in cells where Arp2/3 is inhibited, I treated *sas4* mutant brains with CK-666. Strikingly, the *sas4* mutation enhanced the incidence of ectopic cleavage furrow formation. About 90% of treated *sas4*$^{-/-}$ cells exhibited a cortical phenotype (Fig. 3.8D) in which ectopic Myosin accumulated at cytokinesis leading to the formation of an ectopic cleavage furrow soon after (Fig 3.8C arrowheads). Therefore, contrary to my initial expectations, this experiment indicated that centrosomes are not required for the formation of the ectopic cleavage furrow in NBs where Arp2/3 is inhibited.

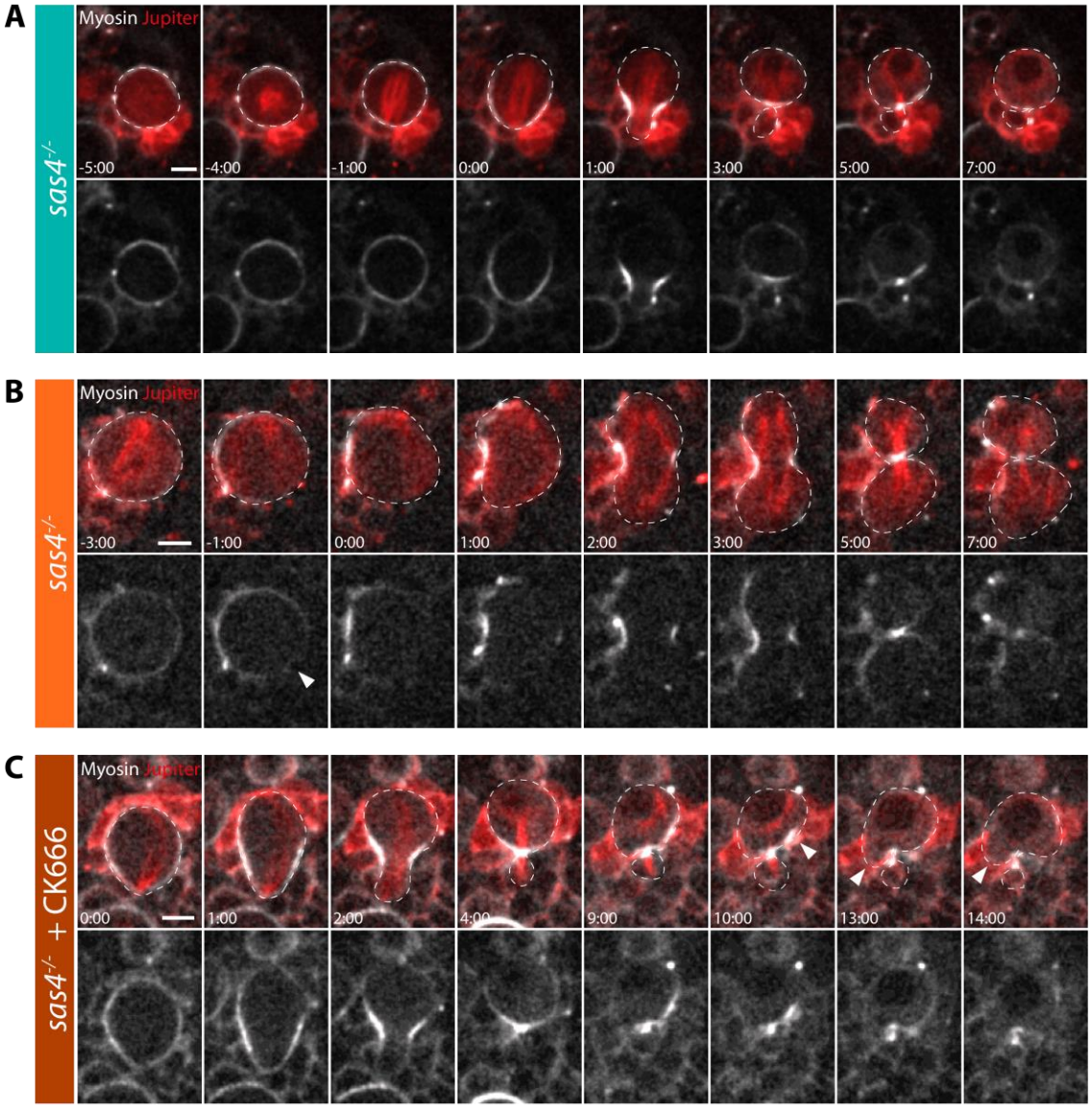
A
sas4-/-
Myosin Jupiter
-5:00
-4:00
-1:00
0:00
1:00
3:00
5:00
7:00
B
sas4-/-
Myosin Jupiter
-3:00
-1:00
0:00
1:00
2:00
3:00
5:00
7:00
C
sas4-/- + CK666
Myosin Jupiter
0:00
1:00
2:00
4:00
9:00
10:00
13:00
14:00

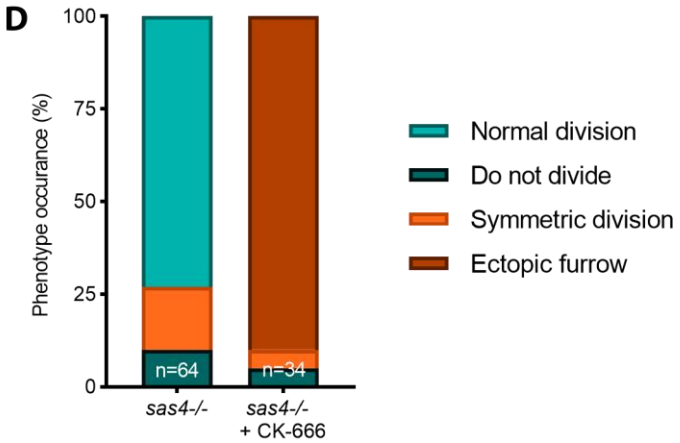
D
Phenotype occurance (%)
100
75
50
25
0
n=64
n=34
sas4-/-
sas4-/-
+ CK-666
Normal division
Do not divide
Symmetric division
Ectopic furrow

Figure 3.8. The absence of centrosomes in CK-666 treated NBs increases the occurrence of the ectopic cleavage furrow. A-C. Genotype: Wor-Gal4, UAS-cherry::Jupiter, Sqh::GFP / Cyo; *sas4*^{s2214}/TM6B. Live imaging of *sas4*^{s2214} mutant cells, expressing Myosin marker (Sqh::GFP, grey) and microtubule marker (cherry::Jupiter, red). **A.** Example of *sas4* mutant cell that divides asymmetrically. **B.** Example of *sas4* mutant cell that divides symmetrically. Arrowhead points to Myosin clearance being mis-aligned from spindle axis. **C.** Example of *sas4* mutant cell treated with CK-666 (400 µM). Arrowheads point to ectopic cleavage furrow. **D.** Graph showing percentages of cells with various phenotypes, between *sas4*$^{-/-}$ and *sas4*$^{-/-}$ + CK-666 treatment. $N_{replicates}$ = 2. ****P<0.0001 (Chi-sqaure test).
Scale bar: 5µm.

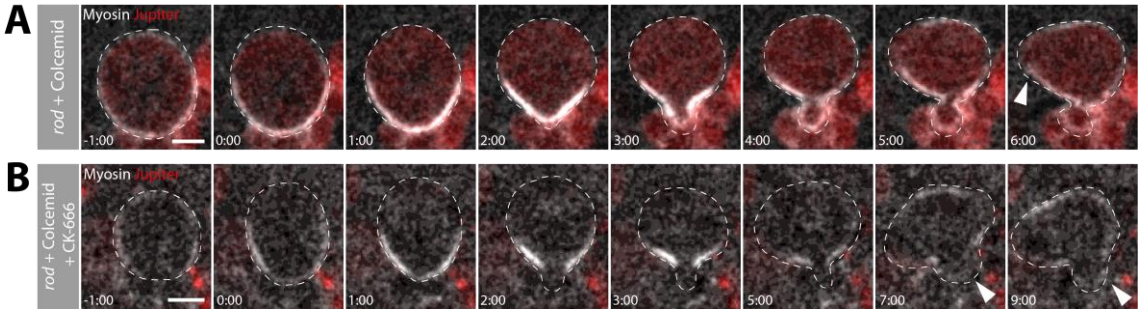

Figure 3.9. Colcemid inhibition of all microtubules does not rescue the ectopic cleavage furrow in CK-666 treated NBs. A-B. Genotype: Wor-Gal4, UAS-cherry::Jupiter, Sqh::GFP / Cyo; *rod*/TM6B Live imaging of *rod* mutant cells treated with colcemid, and expressing Myosin marker (Sqh::GFP, grey) and microtubule marker (cherry::Jupiter, red). Colcemid treatment (0.1 mM) leads to inhibition of all microtubules, and *rod* mutation allows to bypass the spindle-assembly checkpoint. **A.** Arrowhead shows example of cortical defects in control cells. (5/10 cells show cortical defects). **B.** CK-666 treatment (400 µM) on cells where microtubules are inhibited (6/6 cells show phenotype). Arrowheads point to ectopic cleavage furrow. $N_{replicates}$ = 2.
Scale bar: 5 µm.

Finally, to test if microtubules are required for the formation of the ectopic cleavage furrow in NBs where Arp2/3 is inhibited, I decided to see if the phenotype would be rescued by the removal of all microtubules. To do so, I performed live imaging of NBs in which microtubules were depolymerised using colcemid in flies carrying a mutation in *rough deal* (rod) to bypass the spindle-assembly checkpoint (Basto et al. 2000; Brinkley, Stubblefield, and Hsu 1967; Cabernard et al. 2010). Mutant *rod* cells treated with colcemid completely lack microtubules, but still enter anaphase. However, cytokinesis is never completed, since the spindle is required for proper constriction of the acto-myosin ring, and some of these cells exhibited cortical defects at various phases of division (Fig. 3.9A, arrowhead). When these cells were treated with CK-666 they showed severe membrane deformations at cytokinesis (Fig. 3.9B, arrowheads). Thus, the ectopic cleavage furrow is not rescued by complete ablation of microtubules. This implies that the microtubule defects observed at metaphase in cells compromised for Arp2/3 function are not the cause of the ectopic cleavage furrow, but are another consequence of the Arp2/3 complex inhibition.

3.5 Conclusion

With this work I have shown that both chemical and genetical inhibition of the Arp2/3 complex lead to the formation of an ectopic cleavage furrow after cytokinesis, to abnormal cell size and to a delay of metpahse-anaphase. These data suggest that even though the most obvious loss of function Arp2/3 phenotype arises at the end of cell division, Arp2/3 might function much earlier in mitosis.

In the second part of this Chapter I showed that in cells treated with the Arp2/3 inhibitor, spindle microtubules are mislocalized in metaphase and are found at the cortex at cytokinesis. While this suggested that defects in the spindle might cause ectopic cleavage furrow formation, removing the centrosomes or all microtubules did not rescue the phenotype. Instead, it only increased the occurrence of the ectopic cleavage furrow. These results strongly indicates that the ectopic cleavage furrow might be a secondary consequence of defects that arise when Arp2/3 is compromised earlier in mitosis.

Chapter 4.

SCAR is the main Arp2/3 activator during NB division.

4.1 Introduction

To clarify the role of the Arp2/3 complex in dividing NBs and to try to understand the cause of the phenotypes induced by Arp2/3 inhibition, I decided to carry on a screen for the nucleation promoting factors (NPFs) of Arp2/3. Different NPFs are active in different pathways and in different subcellular localizations. Finding the right NPF would allow to understand more clearly the context of Arp2/3 localization and activity.

In this chapter, focusing on WASH, SCAR and WASp, I present a screen that exploited RNA interference (RNAi), mutants and protein localization.

4.2 RNAi and mutants screen points to SCAR as best candidate for Arp2/3 activation in dividing NBs.

For the RNAi screen, I crossed virgin females of the wor-GAL4 driver line, that was also carrying the Myosin marker Sqh::GFP and the microtubule marker cherry::Jupiter, with males carrying the dsRNAs for each of the NPFs: WASH, SCAR and WASp. Since the microtubule marker is also expressed via the UAS/GAL4 system, it can be used as a control for GAL4-induced expression: only cells showing red signal will be expressing dsRNAs.

The RNAi screen showed that both WASH and SCAR are good candidates as Arp2/3 activators in the dividing NB, as in both experiments knock-down (KD) cells presented an ectopic cleavage furrow. In particular, when WASH was knocked-down, 47% of NBs (13/38 cells) had an ectopic cleavage furrow (Fig. 4.1 top panel, arrowheads) and 13% (4/38) exhibited an apical bleb (Fig. 4.1, bottom panel, arrowheads). In cells in which SCAR expression was silenced, 44% (8/18 cells) exhibited an ectopic cleavage furrow (Fig. 4.2 top panel, arrowheads) and 11% (2/18 cells) had an apical bleb (Fig. 4.2 bottom panel, arrowheads). Importantly, both phenotypes had features like those seen in CK-666 treated and Arp3-KD cells (Fig. 3.1C, 3.5A). Mitotic interval length also appears similar to previous experiments where Arp2/3 was inhibited. Indeed, in both WASH (Fig. 4.1B) and SCAR (Fig. 4.2B) knock-down cells, intervals A-B and B-C are significantly longer compared to control, while interval C-D is unaffected.

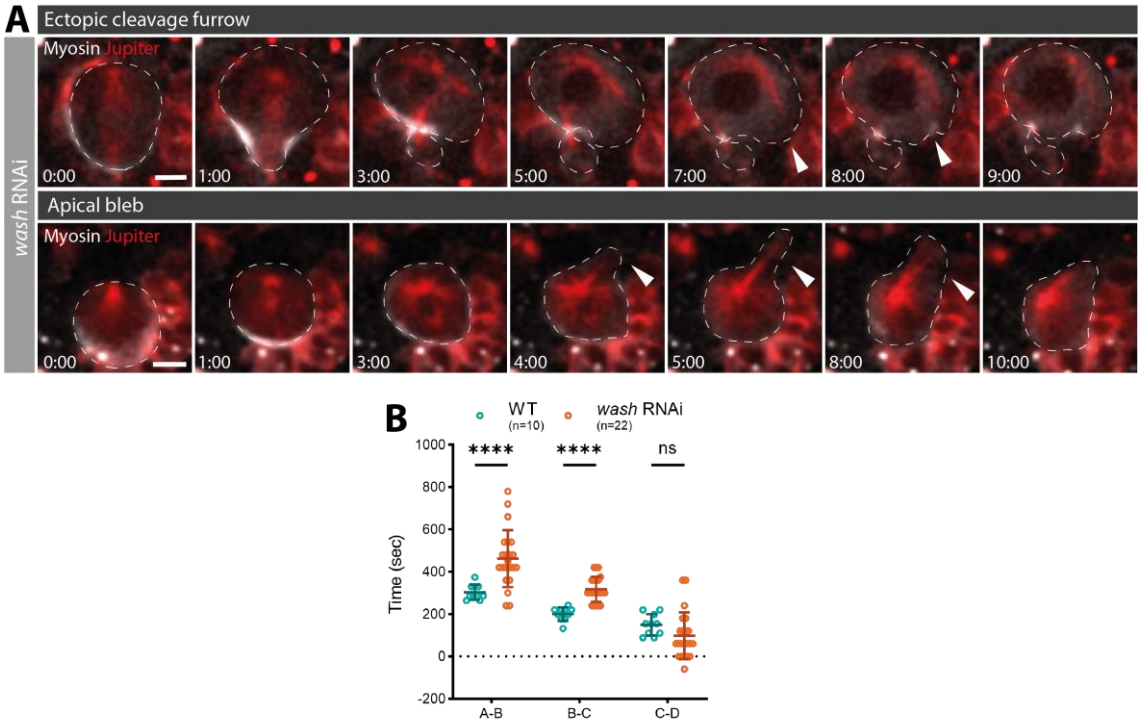

Figure 4.1. Inhibition of WASH activity through RNAi leads to ectopic cleavage furrow formation, and to a delay in mitotic progression in dividing NBs. A. Wor-Gal4, UAS-cherry::Jupiter, Sqh::GFP / Cyo x UAS-RNAi. Representative time-lapse images of dividing WASH-KD NB, expressing the Myosin marker Sqh::GFP in grey, and the microtubule marker cherry::Jupiter in red. Panel on top shows example of ectopic cleavage furrow (arrowheads). Bottom panel shows example of an apical bleb (arrowheads). GMC is not visible in bottom panel because of cell inclination. **B.** Plot showing time interval between mitotic phases in wild type (WT) cells and WASH RNAi cells. Intervals are: NEB-anaphase (A-B), anaphase-cytokinesis (B-C), cytokinesis-NER (C-D). $N_{replicates}$ = 2. Asterisks denote statistical significance. ns, not significant $P > 0.05$, and ****$P \leq 0.0001$ (Tukey's multiple comparison test).
Scale bars: 5 µm. Central and error bars: mean and SD.

By contrast, when WASp was inhibited by RNAi in NBs a different kind of phenotype was observed in 19.5% of cells (16/82 cells). Ectopic Myosin and membrane contraction appeared after cytokinesis on the basal side of the newly formed NB and then moved towards the apical pole (Fig. 4.4A, arrowheads). In this case, I did not observe apical blebs. When measuring the time interval between mitotic phases, only B-C was found to be significantly delayed compared to control conditions, while there was no significant difference in the duration of A-B or C-D (Fig. 4.3B).

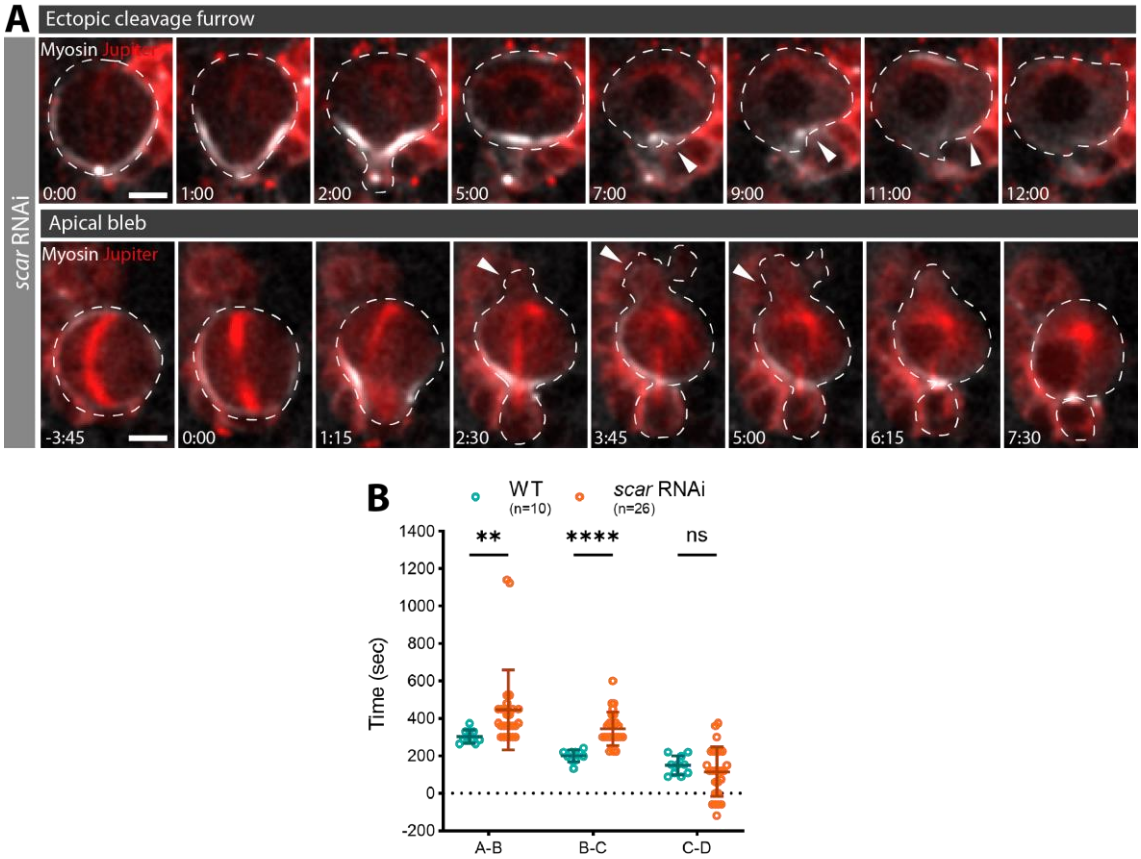

Figure 4.2. Inhibition of SCAR activity through RNAi leads to ectopic cleavage furrow formation, and to delayed passage through mitosis in dividing NBs. A. Wor-Gal4, UAS-cherry::Jupiter, Sqh::GFP / Cyo x UAS-RNAi. Representative time-lapse images of dividing SCAR-KD NB, expressing Myosin marker Sqh::GFP in grey, and microtubule marker cherry::Jupiter in red. Panel on top shows example of ectopic cleavage furrow (arrowheads). Bottom panel shows example of an apical bleb (arrowheads). **B.** Plot showing time interval between mitotic phases in wild type (WT) cells and SCAR knock down cells (scar RNAi). Intervals are: NEB-anaphase (A-B), anaphase-cytokinesis (B-C), cytokinesis-NER (C-D). $N_{replicates}$ = 2. Asterisks denote statistical significance. ns, not significant P > 0.05, **P ≤ 0.01 and ****P ≤ 0.0001 (Tukey's multiple comparison test).
Scale bars: 5 µm. Central and error bars: mean and SD.

The RNAi screen shows that inhibiting WASp determines a very different phenotype than what observed after CK-666 inhibition of Arp2/3 and *arp3* mutant and RNAi experiment, while both SCAR and WASH seems to be good candidates as Arp2/3 activators in the context of NB mitosis. Given the problems that can arise with RNAi, which include off-target RNA silencing and other non-specific effects, it was important to retest the role of the NPFs using mutants.

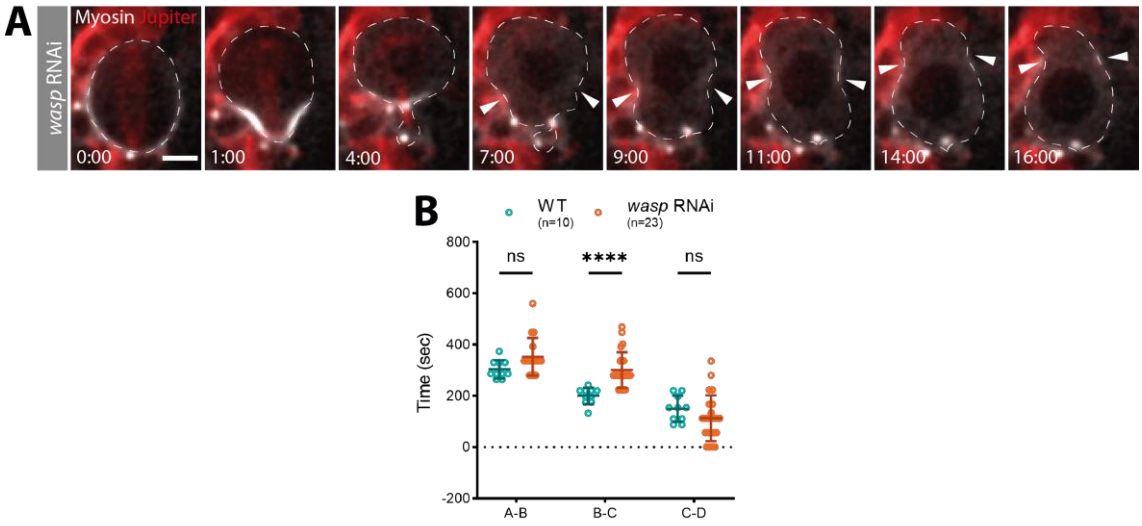

Figure 4.3. Inhibiting WASp through RNAi leads to the formation of a ring of Myosin that slides from the basal side of the cell to the apical side of the newly formed NB. A. Wor-Gal4, UAS-cherry::Jupiter, Sqh::GFP / Cyo x UAS-RNAi. Representative time-lapse images of a dividing WASp-KD NB, expressing a Myosin marker, Sqh::GFP, in grey, and a microtubules marker, cherry::Jupiter, in red. Panel shows an example of a cell with phenotype induced by KD of WASp: ectopic Myosin and membrane contraction appears at the same time (7:00, arrowheads), and "slide" from the basal to the apical side of the NB (9:00-16:00). **B.** Plot showing time interval between mitotic phases in wild type (WT) cells and WASp knock down cells (wasp RNAi). Intervals are: NEB-anaphase (A-B), anaphase-cytokinesis (B-C), cytokinesis-NER (C-D). $N_{replicates}$ = 2. Asterisks denote statistical significance. ns, not significant $P > 0.05$, and ****$P \leq 0.0001$ (Tukey's multiple comparison test).
Scale bars: 5 µm. Central and error bars: mean and SD.

Since *wash*$^{\Delta 185}$ and *wasp*^{3} mutations are not lethal, mutant lines could be crossed with lines carrying chromosomal deletions and larvae grown up until the time of imaging. Neither of these mutants exhibited a phenotype similar to the one observed in cells with reduced Arp2/3 activity (data not shown). This implies that the RNAi phenotype was not specific.

By contrast, the *scar*$^{\Delta 37}$ null mutant is lethal. Therefore, to image mutant *scar* cells I had to exploit mitotic recombination in the formation of somatic clones. With this technique, it is possible to induce the formation of mutant clones surrounded by wild type cells, where the clones are marked by fluorescent protein expression and so become distinguishable from wild type tissue. For this work, recombination was induced by heat shock, and clones containing two copies of the mutant

chromosome were marked by the expression of UAS-cherry::Jupiter, as a consequence of the loss of GAL80. Wild type cells instead expressed a copy of *scar* mutation and the GAL80, which inhibits UAS-cherry::Jupiter. When the time-lapses were analysed, it was possible to see that a small percentage of control cells were affected by cortical defects, possibly due to the heat shock toxicity, but most of them divided normally (Fig. 4.4A-B). On the other hand, homozygous *scar* mutant clones exhibited penetrant cortical defects and blebs during cytokinesis (Fig. 4.4A-B, arrowheads). High resolution imaging with the SoRa microscope of *scar* clones revealed that these cells form ectopic protrusions that are less severe than the ones observed with Arp2/3 chemical inhibition (Fig. 4.4C, arrowheads); perhaps because there is some redundancy with WASP and WASH. Nevertheless, the phenotype was similar to that observed in cells depleted for Arp3 and in the SCAR RNAi experiment.

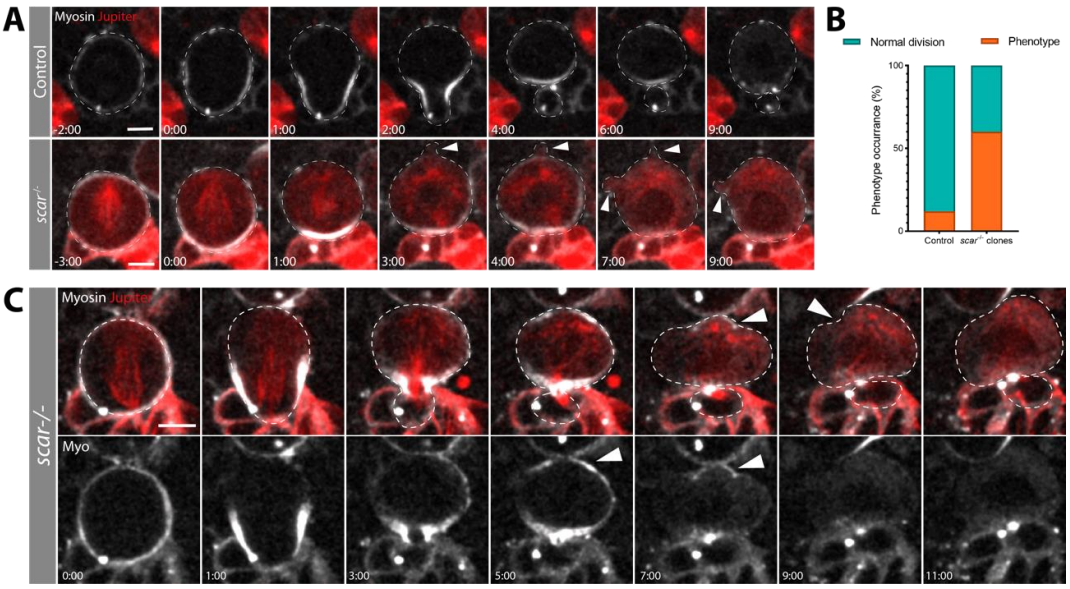

Figure 4.4. *scar* mutant clones exhibit cortical defects at cytokinesis. A. Genotype: see Methods. Live imaging of heat shocked larval brains. Control cells only express Myosin marker Sqh::GFP in grey, and are therefore wild type. *scar*$^{\Delta 37}$ somatic clones are recognizable because of expression of microtubule marker UAS-cherry::Jupiter, in red, on top of a Myosin marker. Representative images show control and mutant cells over time. Arrowheads point to blebbing and cortical defects in the mutant. **B.** Plot showing percentage of phenotype occurrence in representative control and *scar*$^{-/-}$ somatic clones. $N_{replicates}$ = 3. $n_{control}$ = 41, $n_{scar\ clones}$ = 15. **C.** High resolution imaging of *scar* mutant cell from a clone, where arrowheads show ectopic Myosin and membrane contraction at cytokinesis in dividing NB. Scale bar: 5 µm.

4.3 SCAR localises preferentially at the apical side of mitotic NBs.

To better understand which of the NPFs is regulating Arp2/3 in the dividing NB, I decided to look at protein localization, beginning with the Arp2/3 complex itself. I first looked at two subunits of the Arp2/3 complex, Arp3 and ArpC1, both labelled with GFP and expressed under the UAS promoter. I therefore used the UAS/GAL4 system to drive the expression of the transgenes in NBs.

Movies were then taken in intact brains. In both instances, a similar dynamic localisation was observed. As expected for an abundant complex, there was a high cytoplasmic signal. This made it hard to observe any local cortical signals in either case.

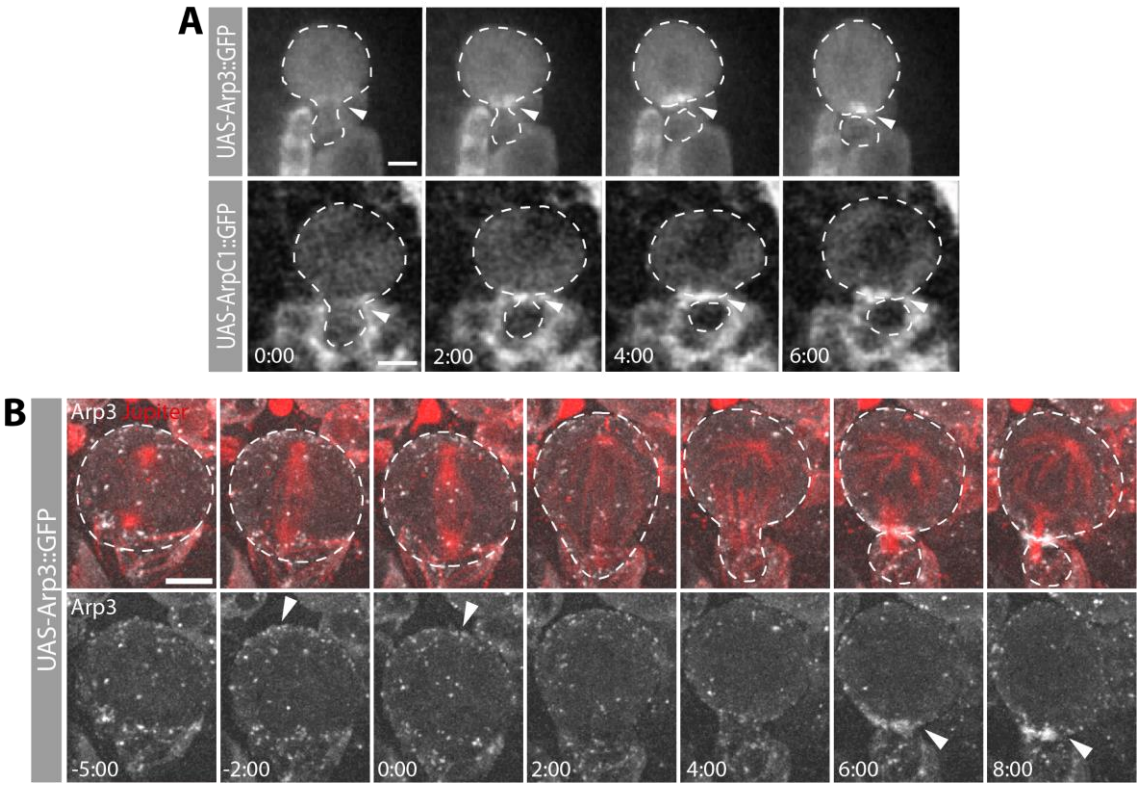

Figure 4.5. Fluorescently tagged Arp2/3 subunits Arp3 and ArpC1 localize at the cortex, and at the cytokinetic furrow of dividing NBs. A. Genotype: Wor-Gal4, UAS-cherry::Jupiter/Cyo x UAS-Arp3/C1::GFP. Confocal imaging of lines expressing UAS-Arp3::GFP and UAS-ArpC1::GFP. Expression is driven by wor-GAL4. Arrowheads point to fluorescent signal at the cytokinetic furrow. **B.** High resolution imaging of line expressing Arp3::GFP and microtubule marker cherry::Jupiter. Arrowheads reveal Arp3 puncta at the cortex in metaphase and at the furrow at cytokinesis. Scale bar: 5 µm.

Nevertheless, montages from this experiment show that for both subunits of the complex, there was a strong accumulation of fluorescent signal at telophase at the cytokinetic furrow, which peaked as cells divided (Fig. 4.5A, arrowheads). Later, I confirmed these results using the SoRa spinning disc confocal microscope for imaging at a higher spatial resolution of Arp3::GFP. In this case, Arp2/3 puncta were visible. Again, while some signal was visible at the cortex in metaphase, the most intense signal was observed at the furrow at cytokinesis (Figure 4.5B).

To assess the relationship between the NPFs and the Arp2/3 complex I then looked at the localization of WASH, SCAR and WASp. Interestingly, SCAR localized to the furrow starting from telophase until the end of cytokinesis, like the Arp2/3 complex (Fig. 4.6A, arrowheads). WASp did not seem enriched at any particular region of dividing NBs (Fig. 4.6C), and WASH was visible in cytoplasmic spots in interphase, which are likely to be endosomal (Derivery et al. 2009), but otherwise did not seem to localize in any specific region during mitosis (Fig. 4.6B, arrowhead).

These experiments show that SCAR and Arp2/3 both localize at the cytokinetic furrow during NB division, suggesting that SCAR is likely to be the dominant Arp2/3 activator during mitosis. Since SoRa high resolution imaging revealed details of Arp2/3 localization that could not be seen on a regular confocal, I decided to perform the same experiment on SCAR too.

Using this approach, SCAR appeared to localize asymmetrically at the apical side of the cell in metaphase in larval brains. However, because of the signal coming from surrounding cells, I could not be sure that this represented an asymmetric localization (data not shown). I therefore dissociated brains to look at isolated NBs. This experiment revealed that indeed SCAR was asymmetrically localized at the apical side of the NB in metaphase (Fig. 4.7, arrowheads). Interestingly the protein formed a cap on one side of the NB (Fig. 4.8). When the NB entered anaphase, SCAR signal started to disappear from the apical side, and the protein pool accumulated at the basal side of the cell, becoming concentrated at the cytokinetic furrow, as observed above (Fig. 4.7).

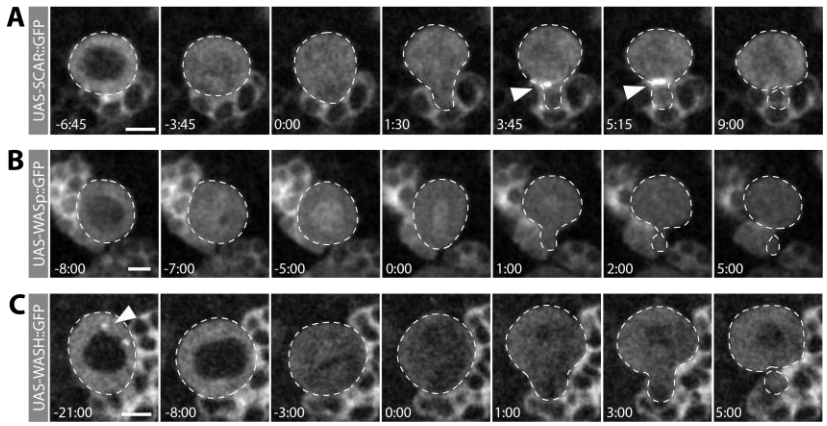

Figure 4.6. SCAR localizes at the cytokinetic furrow, while WASH and WASp do not show specific localization in dividing NBs. Genotype: Wor-Gal4, UAS-cherry::Jupiter/Cyo x UAS-NPF::GFP. NBs expressing different NPFs transgenes through wor-GAL4/UAS system. **A.** Representative images of a NB expressing SCAR::GFP. Arrowheads point to SCAR localization at the cytokinetic furrow. **B.** Representative images of a NB expressing WASp::GFP. **C.** Representative images of a NB expressing WASH::GFP. Arrowhead shows dots of signal in the cytoplasm of cell in interphase.
Scale bar: 5 µm.

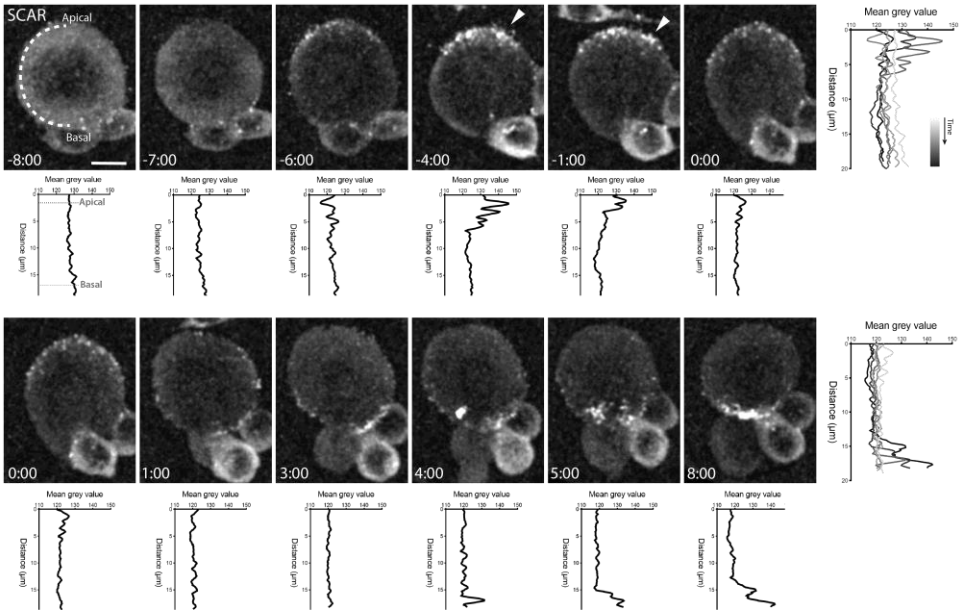

Figure 4.7. SCAR has a dynamic and polarised pattern of cortical localisation in dividing NBs. Genotype: Wor-Gal4, UAS-cherry::Jupiter/Cyo x UAS-SCAR::GFP(III). Representative high resolution maximum projections of dissociated NB imaging using the SoRa spinning disk, expressing SCAR::GFP driven by UAS/wor-GAL4 system. Arrowheads point to SCAR signal at the apical side of the NB in metaphase. Mean SCAR signal intensity was acquired by drawing a line from apical to basal side of the cortex, like depicted at time -8:00. Graphs on the bottom are shown together in graph on the right, where grey gradient represents different time points. Scale bar: 5 µm.

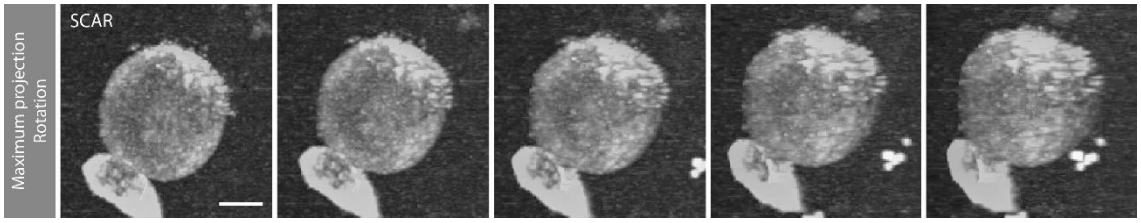

Figure 4.8. SCAR forms a cap on the apical side of the NB at metaphase. Genotype: Wor-Gal4, UAS-cherry::Jupiter/Cyo x UAS-SCAR::GFP(III). Frames show rotation of maximum intensity z-projection of isolated NB expressing wor-GAL4 and UAS-SCAR::GFP imaging using the SoRa spinning disk.
Scale bar: 5 µm.

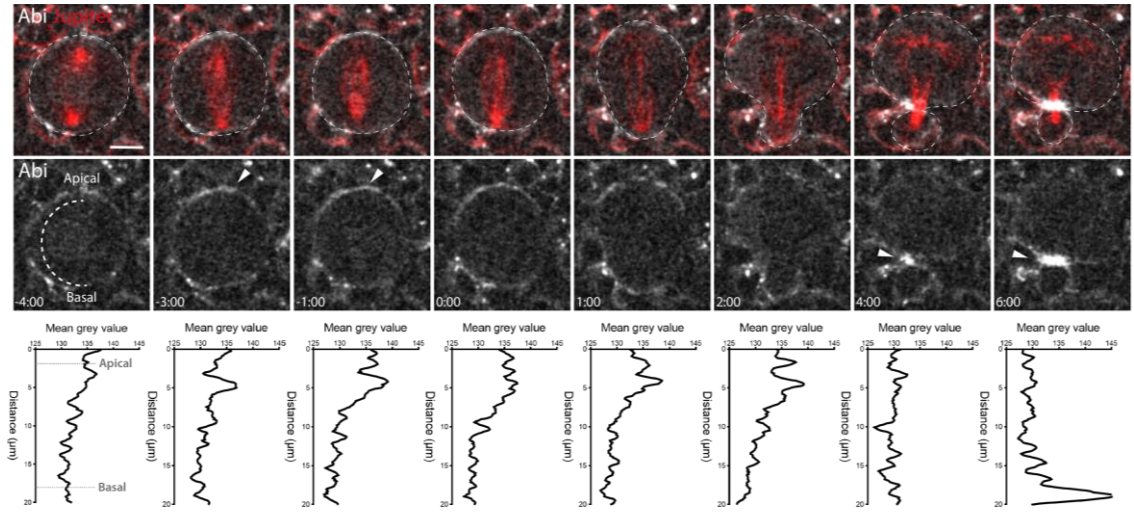

Figure 4.9. A second component of the SCAR complex, Abi, localizes at the apical side of the NB at metaphase and the furrow at cytokinesis. Genotype: Jupiter::GFP x ubi-mCherry::Abi/TM6B. Representative images of NB expressing ubi-mCherry::Abi imaged using the SoRa spinning disk. Arrowheads point to Abi localization at the apical cortex in metaphase and at the furrow at cytokinesis. Mean Abi signal intensity was acquired by drawing a line from apical to basal side of the cortex, like depicted at time -4:00, and was plotted in graphs on the bottom.
Scale bar: 5 µm.

SCAR is part of a multiprotein complex. Thus, to validate these findings I verified the localization of the complex using a second component, Abi (Eden et al. 2002; Kunda et al. 2003) expressed from the *ubi* promoter. Again using this line, I was able to observe the accumulation of a fluorescent signal at the apical side of the NB in metaphase, and at the furrow in cytokinesis (Fig. 4.9, arrowheads). Thus, both Abi and SCAR appear to have a very similar dynamic pattern of localisation in mitosis (Fig. 4.7).

4.4 Conclusion

In this chapter I have used a combination of RNAi, mutants and GFP-tagged protein localisation to test the roles of SCAR, WASH and WASP in the formation of cortical defects observed following Arp2/3 complex inhibition. While RNAi of both SCAR and WASH led to cortical instability and to a delay in mitosis in dividing NBs, only *scar* mutant cells had a similar range of cortical defects, resembling those observed following treatment with CK-666, in the Arp3 knock-down and the *arp3* mutant. Interestingly SCAR also exhibited an asymmetric apical localization in NBs in metaphase, suggesting a role for the Arp2/3/SCAR pathway in regulating mitosis at this stage.

Chapter 5.

SCAR/Arp2/3 regulates polar Myosin and plasma membrane organization in dividing neuroblasts.

5.1 Introduction

The metaphase-anaphase transition is a critical moment in the division of a NB. At this time the cortical expansion of the apical pole and the accompanying basal shift in division plane positioning lead to the pronounced asymmetry in cell size that characterizes these divisions. In this chapter I describe the temporal dynamics of these events, all of which take place in a narrow time-frame, as non-muscle Myosin II and SCAR are cleared from the apical side, the plasma membrane is remodeled, and the cortex deforms.

Furthermore, I explore the membrane morphology to understand if Arp2/3 and SCAR have a role in forming protrusions. This is because usually these proteins are found at the cortex and are involved in the formation of filopodia and lamellipodia.

Building on the work presented in earlier chapters of the thesis, I then explore what happens during metaphase-anaphase transition when the SCAR/Arp2/3 pathway is inhibited.

5.2 Characterization of apical membrane behaviour in NBs during passage through mitosis.

To image changes in membrane organisation during NB mitosis, I began by using the Pleckstrin Homology (PH) domain from the phospholipase CΔ1 (PLCΔ1) that interacts with the headgroup of the phosphatidylinositol 4,5-bisphosphate (PIP_2) (Verstreken et al. 2009) as a probe. This was chosen because it labels the plasma membrane, membrane protrusions, but not internal membranes. As previously reported (LaFoya and Prehoda 2021; Oon and Prehoda 2019), in prophase cells the PH probe labelled small membrane domains that moved slowly towards the apical side of the cell (Fig. 5.1A, B), leading to accumulation of PH-rich membrane structures in the apical hemisphere. At onset of anaphase, these membrane structures reversed their direction of motion, and moved rapidly towards the basal side of the cell (Fig. 5.1). Thus, the polarity of membrane flows depends on cell cycle stages.

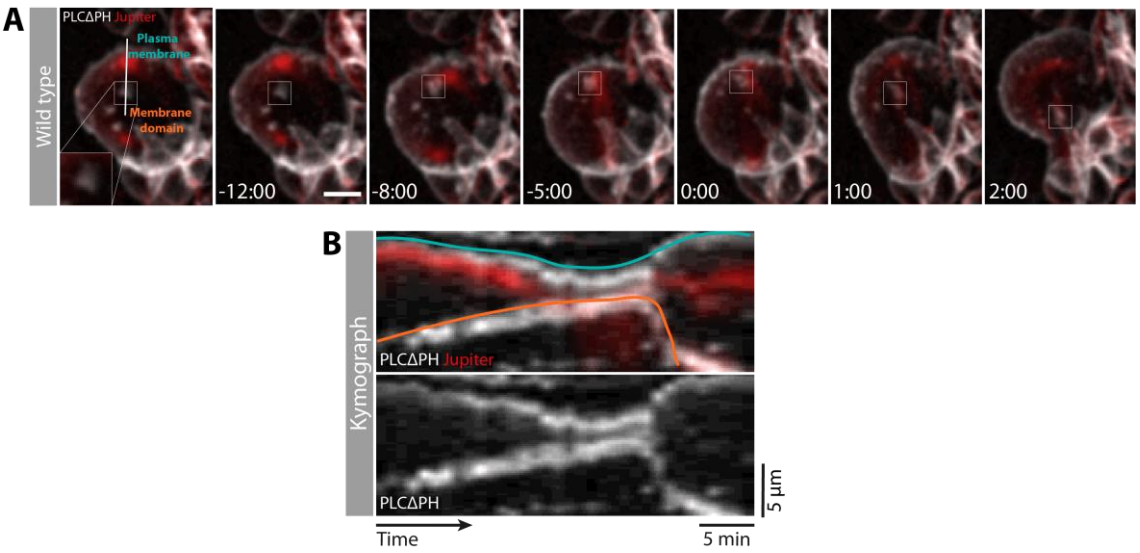

Figure 5.1. NBs possess membrane domains that move in a polarised direction along the apical-basal cell axis at different stages of mitosis. A. Genotype: Wor-Gal4, UAS-cherry::Jupiter/Cyo x L/Cyo ; UAS-PLCΔPH::GFP/TM6B. Maximum intensity projection of dividing NB expressing a membrane marker, PLCΔPH::GFP and a microtubule marker cherry::Jupiter, both expressed via UAS/wor-GAL4. The white line indicates the position used to generate the kymograph. Insert shows an example of a membrane domain. **B.** Kymograph showing the movement of the plasma membrane (blue) and of a more basal PLCΔPH::GFP-rich membrane domain (orange).
Scale bar: 5 µm.

The intensity of the PH marker also changed with mitotic progression (Fig. 5.2A, B). To see if these changes in the signal were global or local, I decided to measure PH intensity at both the apical domain and the lateral membrane of cells progressing through mitosis. This analysis revealed a consistent and sustained reduction in the intensity of the reporter at the apical membrane as cells transited from metaphase into anaphase, while the intensity of the signal in the lateral membrane remained unchanged (Fig.5.2C-D). These data suggest that the apical flow of PH-rich membranes early in mitosis generates a pool of excess membrane present at the apical side of the NB in metaphase, which is removed and/or redistributed basally during anaphase.

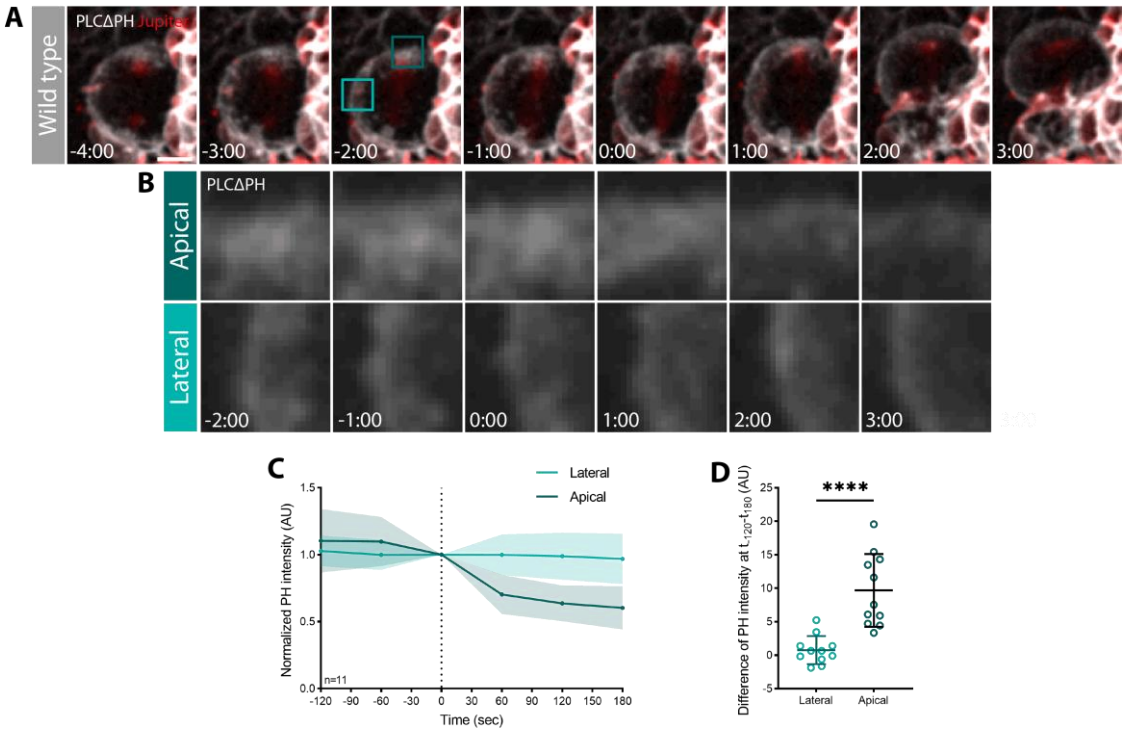

Figure 5.2. Apical levels of PH marker fall following the transition from metaphase into anaphase. A. Wor-Gal4, UAS-cherry::Jupiter/Cyo x L/Cyo ; UAS-PLCΔPH::GFP/TM6B. Membrane dynamics across a full NB division cycle shown as a maximum intensity projection of PH::GFP. Progression though mitosis is indicated by microtubule marker cherry::Jupiter. **B.** Zoom of apical and lateral membrane from A. **C.** Plot that shows PH intensity changes during metaphase-anaphase transition in apical and lateral membrane. **D.** Plot showing PH intensity difference between $t_{-120sec}$ and t_{180sec}. $N_{replicates}$ = 2. Asterisks (****) denote statistical significance. P ≤ 0.0001 (paired t-test).
Scale bar: 5 µm. Central and error bars: mean and SD.

To validate these dynamics, I used a different confocal spinning disk system, called the SoRa, that allows super-resolution imaging without special preparation of the sample. For this analysis I imaged dividing NBs expressing the PH::GFP reporter and a microtubule marker at higher temporal resolution (20 sec/frame). In these movies, when the apical surface of cells was not in contact with overlying tissue, filopodia-like membrane structures could be seen forming at the apical cell surface at metaphase (Fig. 5.3, Apical insert, -2:00 to 0:40 minutes), which were not present instead at the basal side of the cell (Fig. 5.3, Basal inserts). These protrusions were 0.7-1 µm in length, started to disappear 1 minute after anaphase onset and were completely gone by the end of telophase (Fig. 5.3, 1:00 to 2:20 minutes), suggesting that they might be absorbed when the apical cell increases its size during cortical expansion.

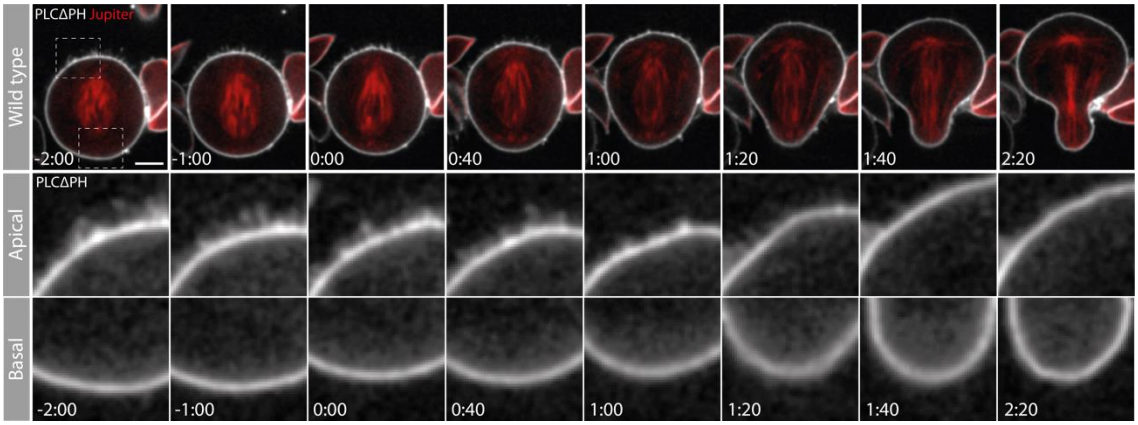

Figure 5.3. Dividing NBs exhibit polarized membrane protrusions at metaphase, that disappear with cortical expansion following anaphase onset. Wor-Gal4, UAS-cherry::Jupiter/Cyo x L/Cyo ; UAS-PLCΔPH::GFP/TM6B. Higher resolution imaging of a NB expressing PH::GFP and microtubule marker cherry::Jupiter. Apical inserts show portion of apical membrane with filopodia-like protrusions in metaphase (-2:00 to 0:40 minutes) and no protrusions in anaphase (1:20 to 2:20 minutes). Basal inserts show that the basal side of the NB is devoid of membrane protrusions.
Scale bar: 5 µm.

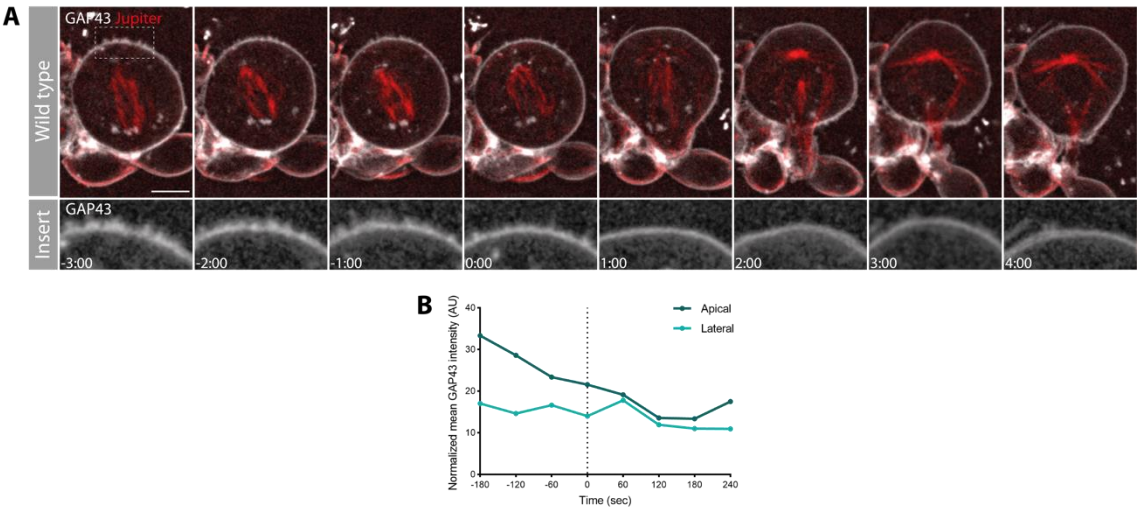

Figure 5.4. Membrane marker GAP43 confirms presence of polarized membrane protrusions at metaphase. A. Genotype: Wor-Gal4/Cyo ; Jupiter::GFP/TM6B x sqh-mCherry::GAP43/TM6B. High resolution imaging of NB expressing membrane marker, mCherry::GAP43, driven by *sqh* promoter. Insert shows membrane protrusions at the apical side of the cell in metaphase (-3:00 to -1:00). Apical protrusions begin to disappear as cells enter anaphase. **B.** Graph showing GAP43 signal intensity measured in depicted cell.
Scale bar: 5 µm.

To confirm that these observations were not specific to the PH reporter used, I imaged NBs expressing another membrane marker, mCherry::GAP43, at high spatial resolution (Fig. 5.4A). GAP43 associates with the plasma membrane through a fatty acid chain that is added to the protein via palmitoylation (Liu, Fisher, and Storm 1994). Once again, I observed membrane protrusions (0.6-0.9 µm long) on the apical side of the NB at metaphase, that disappear in anaphase (Fig. 5.4A, Insert). Furthermore, the apical membrane intensity was seen decreasing following the same dynamics as for the PH reporter, while the lateral membrane signal remained unchanged (Fig. 5.4B). These data confirm previous observations (Fig. 5.2) and show that the polarized protrusions are a characteristic feature of the apical membrane independently of the reporter used.

To test the idea that SCAR nucleates the apical actin-based protrusions, I first looked for the presence of actin filaments in apical membrane protrusions. As a first approach, I used a construct based on the calponin homology domain (CH) of Utrophin, an actin filament binding protein, fused to GFP, which has been shown to faithfully report the distribution of F-actin in some tissues (Burkel, Von Dassow, and Bement 2007). In this case, however, I was unable to observe apical structures, perhaps due to the high brightness of the cortex (data not shown). By contrast, I was able to observe apical protrusions at the cortex of metaphase NBs (Fig. 5.5, arrowheads) using the LifeAct probe - a small peptide generated from another actin binding domain fused to GFP (Riedl et al. 2008). Even though the protrusions were more evident when using the PH reporter, there was partial co-localization of membrane and actin signals. This supports the hypothesis that the membrane protrusions are generated by an underlying actin network.

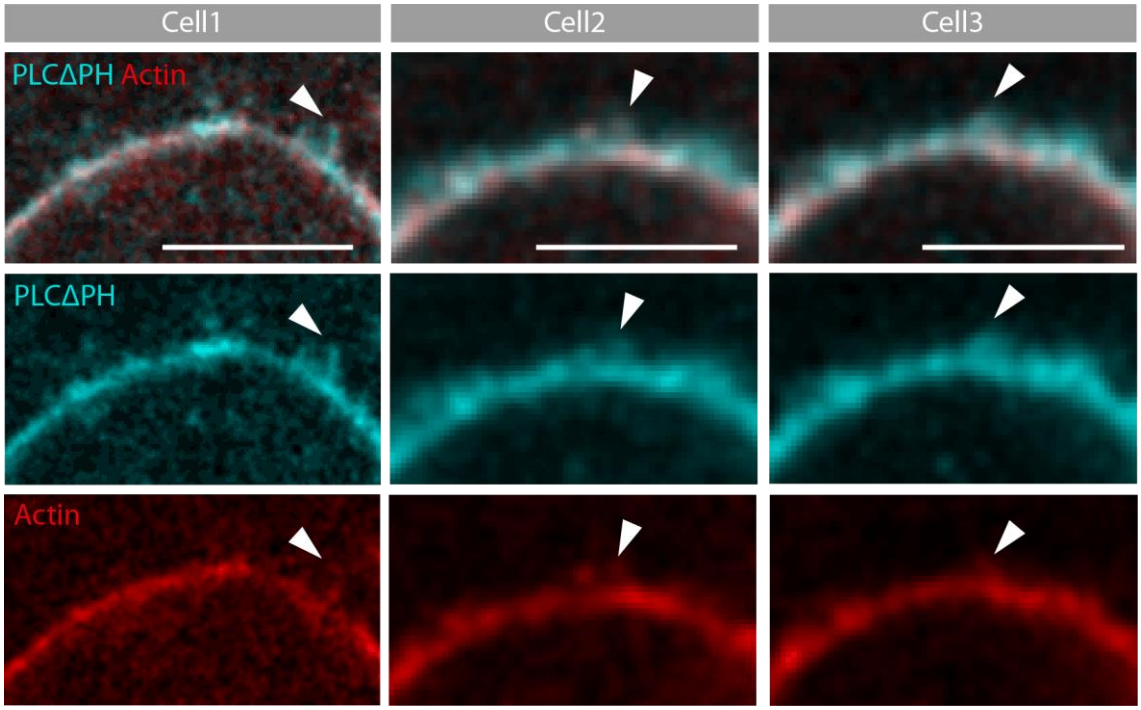

Figure 5.5. Actin filaments are visible inside membrane protrusions in NB at metaphase. Genotype: Wor-Gal4/Cyo::ActGFP, UAS-PLCΔPH::RFP x UAS-LifeAct::GFP/Cyo ;; MKRS/TM6B. High resolution live imaging of cells in metaphase expressing PH::RFP and LifeAct::GFP, both driven by wor-GAL4/UAS system. Arrowheads point to membrane protrusions that appear to be positive for actin filaments in 3 different cells.
Scale bar: 5 µm.

Next, to investigate the relationship between SCAR and membrane protrusions, I imaged on the SoRa cells expressing PH::RFP and SCAR::GFP, both driven by the wor-GAL4/UAS system. Figure 5.6 shows a representative example of a NB in which SCAR and the PH probe colocalize during mitosis. At prophase (-8:00 minutes), the fluorescent signal was low, and there were few protrusions. At metaphase (-2:00 min), numerous SCAR-positive membrane rich protrusions were visible decorating the apical surface of NBs. When this was quantified by measuring intensity along a line drawn along the apical cell surface, it was clear that the peaks of SCAR and PH overlap. At anaphase (1:00 minute), PH signal appeared to smooth out, while the SCAR::GFP signal was still visible at puncta on the cortex in places that lack protrusions, which could represent inactive complexes. These data suggest there is a relatively tight correlation between the presence of SCAR::GFP signal and membrane protrusions in metaphase cells.

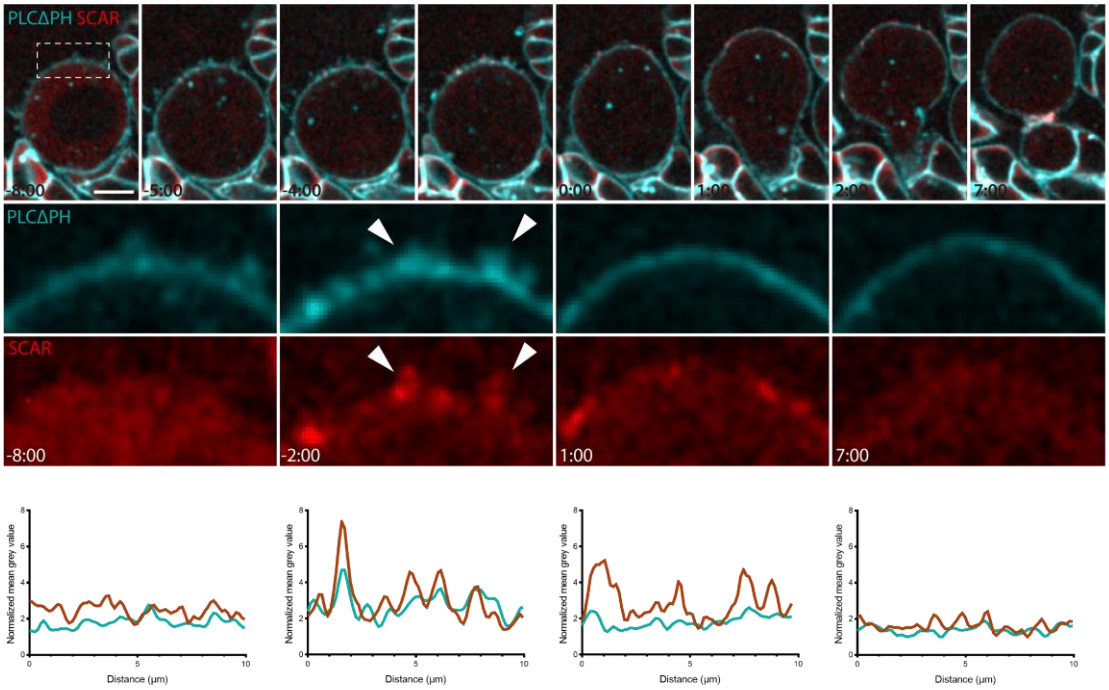

Figure 5.6. SCAR and PH signals colocalise at the apical side of the dividing NB. Genotype: Wor-Gal4/Cyo::ActGFP, UAS-PLCΔPH::RFP x UAS-SCAR::GFP. High resolution imaging of a representative NB, showing co-localization of membrane protrusions and peaks of SCAR signal. The graphs were obtained by drawing a line in the portion of cortex included in the inserts and averaging PH or SCAR signals. Data was normalized by subtracting background. Scale bar: 5 µm.

5.3 The SCAR/Arp2/3 pathway regulates the organization of the apical membrane protrusions.

After having characterized membrane dynamics and organization in wild type NBs, I started looking at how cortical remodelling is affected by SCAR and Arp2/3 inhibition. First, to determine if SCAR is necessary to organize the apical membrane in NBs at metaphase-anaphase transition, I measured the PH reporter intensity in cells where SCAR was inhibited through RNAi (Fig. 5.7A). The analysis shows that in control cells PH intensity is high before anaphase onset and it decreases fast during cortical expansion (Fig. 5.7B), in the same way as previously observed in wild type cells (Fig. 5.2). In cells where SCAR is inhibited instead, the signal is lower at -120 seconds and decreases less than control. As a result, the curve is more similar to a straight line than a sigmoid (Fig. 5.7B). This indeed suggests that SCAR is involved in regulating membrane organization at the apical side of the NB.

Next, to test if the Arp2/3 complex contributes to cortical dynamics, I treated cells expressing the apical membrane marker (PH::GFP) and a microtubule marker (cherry::Jupiter) with the Arp2/3 inhibitor, CK-666. I generated kymographs to better visualise changes in apical membrane organisation during the metaphase-anaphase transition. I then extracted coordinates of the membrane to measure cortical expansion (Fig. 5.8A), which I plotted and averaged (Fig. 5.8B). In control cells, the resulting curve had a clear sigmoid shape, due to a sudden expansion that quickly came to a stop (Fig. 5.8B, Control single cells and Mean). By contrast, in cells in which Arp2/3 was inhibited by CK-666, the movement was slower and linear (Fig. 5.8B, CK-666 single cells and Mean). Thus, although the treatment does not block apical expansion, it changes its dynamics at anaphase onset.

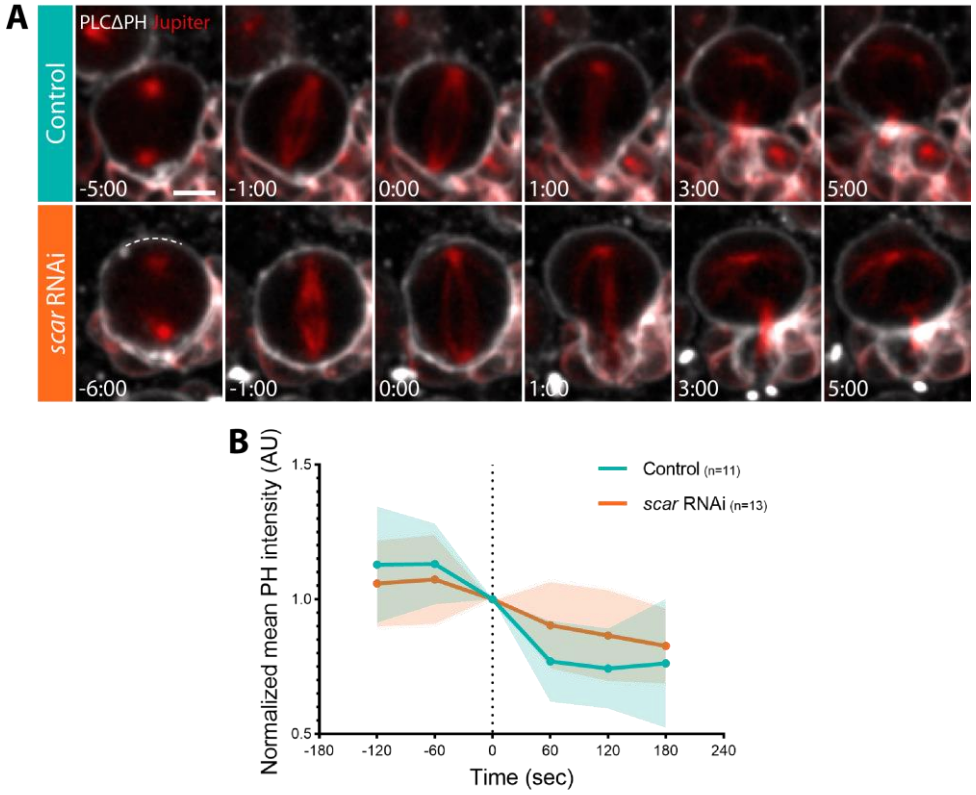

Figure 5.7. SCAR helps organise the apical membrane in NBs progressing through mitosis. A. Genotype: Wor-Gal4/Cyo::ActGFP; Jupiter::GFP, neur-PLCΔPH::RFP/TM6B x UAS-SCAR-RNAi. Live imaging of cells expressing UAS-scar-dsRNA/Cyo::GFP (control) or UAS-scar-dsRNA/WorGal4 (scar RNAi) and fluorescent markers Jupiter::GFP and neur-PH::RFP. Dotted line represents line traced for analysis of PH signal intensity. **B.** Plot showing changes in PH intensity during time in control and scar-dsRNA cells. $N_{replicates}$ = 2.
Scale bar: 5 µm. Central and error bars: mean and SD.

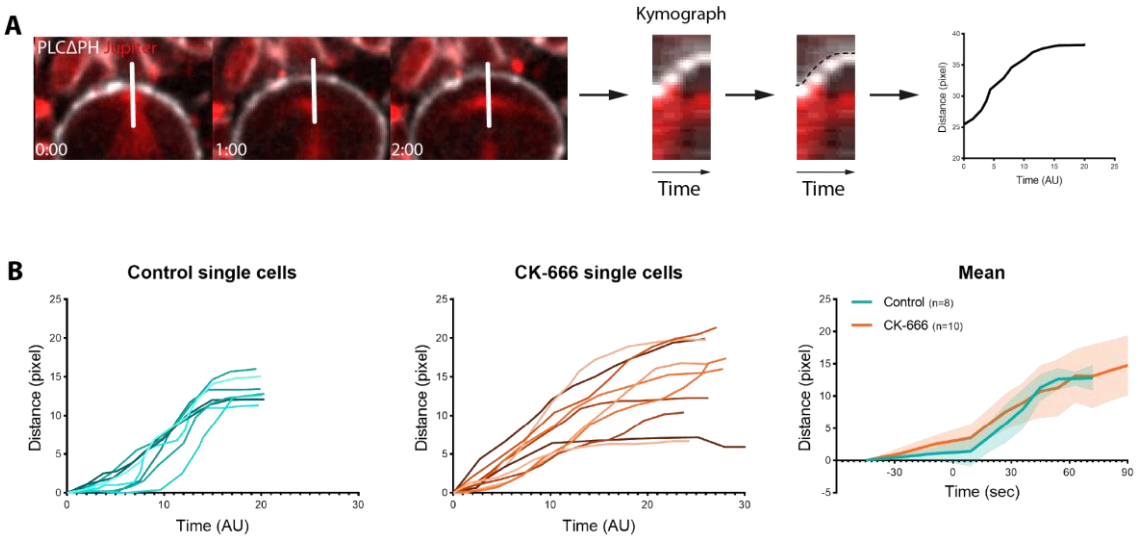

Figure 5.8. Arp2/3 inhibition alters the dynamics of cortical expansion. A. Genotype: Wor-Gal4, UAS-cherry::Jupiter/Cyo x L/Cyo ; UAS-PLCΔPH::GFP/TM6B. Kymographs were generated drawing a line like shown in figure, the movement of the membrane was manually traced and coordinates were exported and plotted. The final result is represented by the graph on the right. **B.** Graphs showing single cell tracks and mean of membrane movement during anaphase, for control (CK-689, 400 µM) and CK-666 treated cells (400 µM). Single cells graphs show coordinates from kymographs. Coordinates were centred to start at (x=0, y=0). To plot the mean, a linear interpolation of coordinates was performed.
$N_{replicates}$ = 2. Central and error bars: mean and SD.

Next, to understand how inhibition of the Arp2/3 complex alters membrane flow and movement of membrane domains at the metaphase-anaphase transition (as seen in Fig. 5.1), I generated kymographs for both control cells (treated with CK-689) and CK-666 treated cells. In both cases, a line was drawn from the apical plasma membrane and across one of the discrete membrane domains to track its movement during passage through mitosis. As shown in Fig. 5.1, in control cells membrane domains (orange lines) were seen moving at a relatively fixed speed towards the apical side of the cell in prophase, before suddenly reversing their direction to move downward at the onset of anaphase. In parallel, the previously stable plasma membrane (blue lines) moved rapidly upward and away from the apical centrosome as the apical domain expanded at the metaphase-anaphase transition (Fig. 5.9 Control), before quickly stabilizing its position. The dynamics of these movements were altered in CK-666 treated cells. Indeed, the majority of PH::GFP bright membrane domains appeared relatively static during progression from prophase into metaphase (Fig. 5.9 CK-666). In addition, at the onset of anaphase, the inhibition of the Arp2/3 complex suppressed apical expansion and the basal flow of membrane, which was ~50% slower in CK-666 treated cells relative to the control, in line with what observed previously for the other processes analysed related to the membrane and PH intensity.

Earlier in this chapter, I showed that metaphase NBs possess finger-like membrane protrusions that appear positive for SCAR and actin filaments. These data suggested a role for the SCAR and Arp2/3 complexes in protrusion formation likely through the nucleation of branched actin filaments. To test this hypothesis, I treated NBs expressing the PH membrane marker with CK-666 and then imaged the treated cells at high resolution. While CK-666 treated cells possessed patches of PH::GFP in metaphase, which I interpreted as local accumulations of membrane, like those seen in the control, this membrane domain was not as organized as it was in control cells (Fig. 5.10A, B, D, E). Furthermore, when the Arp2/3 complex was inhibited, the excess membrane was observed forming small rounded structures, some of which resembled budding vesicles (Fig. 5.10E), rather than finger-like protrusions. Thus, the Arp2/3 complex is not required for the accumulation of an apical membrane reservoir, but is required for the proper organisation of the plasma membrane. During the metaphase-anaphase

transition, these membrane domains then became smoothed out so that they were no longer visible by cytokinesis (Fig. 5.10G, H), with similar kinetics to the loss of membrane protrusions in the control. This is in line with the observation made in Fig. 5.9, showing that the membrane still flows downward during anaphase following treatment with CK-666, suggesting that the Arp2/3 complex is required for organisation of the apical membrane, but not for the changes in movement and organisation that occur at anaphase.

Taking this further, to determine the role played by all types of actin filaments in the formation of the polarized membrane protrusions, I treated cells with Latrunculin B (LatB). LatB sequesters actin monomers to inhibit actin nucleation and polymerisation (Morton, Ayscough, and Mclaughlin 2000). As a result, cells treated with LatB cannot assemble Formin- or Arp2/3-nucleated actin filaments, or the acto-myosin ring necessary for division (Wakatsuki et al. 2001). Nevertheless, as expected, the mitotic spindle was formed and underwent its normal anaphase movements in LatB treated NBs, since mitosis is not dependent on the actin cytoskeleton (Ramkumar and Baum 2016) (Fig. 5.10C). This enabled me to look for changes in the membrane organisation in mitotic LatB-treated neuroblasts. These cells developed local patches of apical membrane enrichment in metaphase. However, these seemed disorganised and appeared to protrude into the cell (Fig. 5.10F), which appeared very different from the spike-like outward-facing protrusions seen in control cells (Fig. 5.10D-E). LatB also blocked all membrane flow (Fig. 5.10I). Taken together, these results suggest that the actin cortex is likely required for membrane organisation and directional membrane flows during mitosis in NBs.

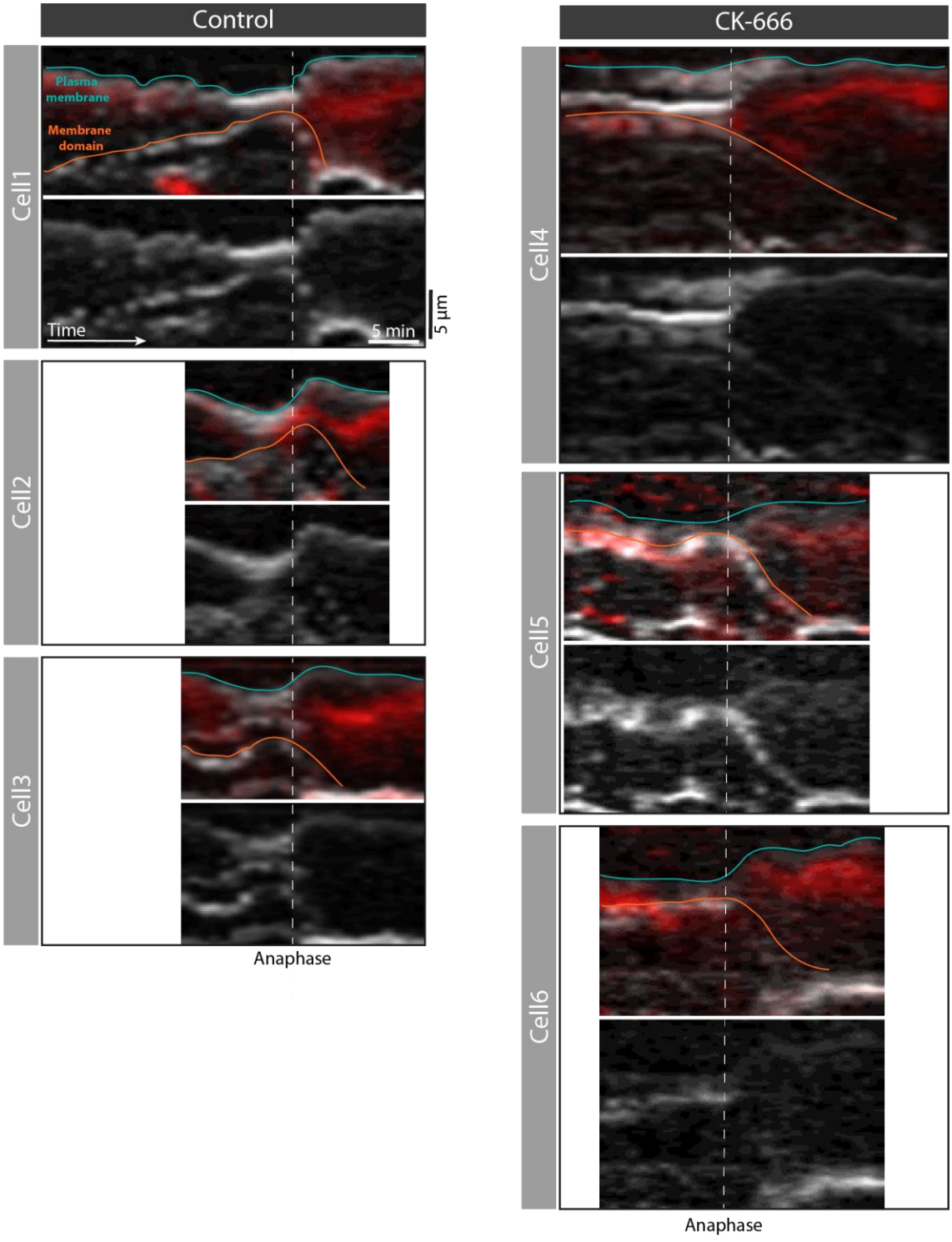

Figure 5.9. Arp2/3 inhibition affects the movement of membrane domains during cell division in NBs. Genotype: Wor-Gal4, UAS-cherry::Jupiter/Cyo x L/Cyo ; UAS-PLCΔPH::GFP/TM6B. Kymographs of control (CK-689 treatment, 400 µM) and CK-666 treated cells (400 µM), expressing PH::GFP and cherry::Jupiter, and showing movement of plasma membrane (blue lines) and membrane domain (orange lines) starting from prophase to cytokinesis.

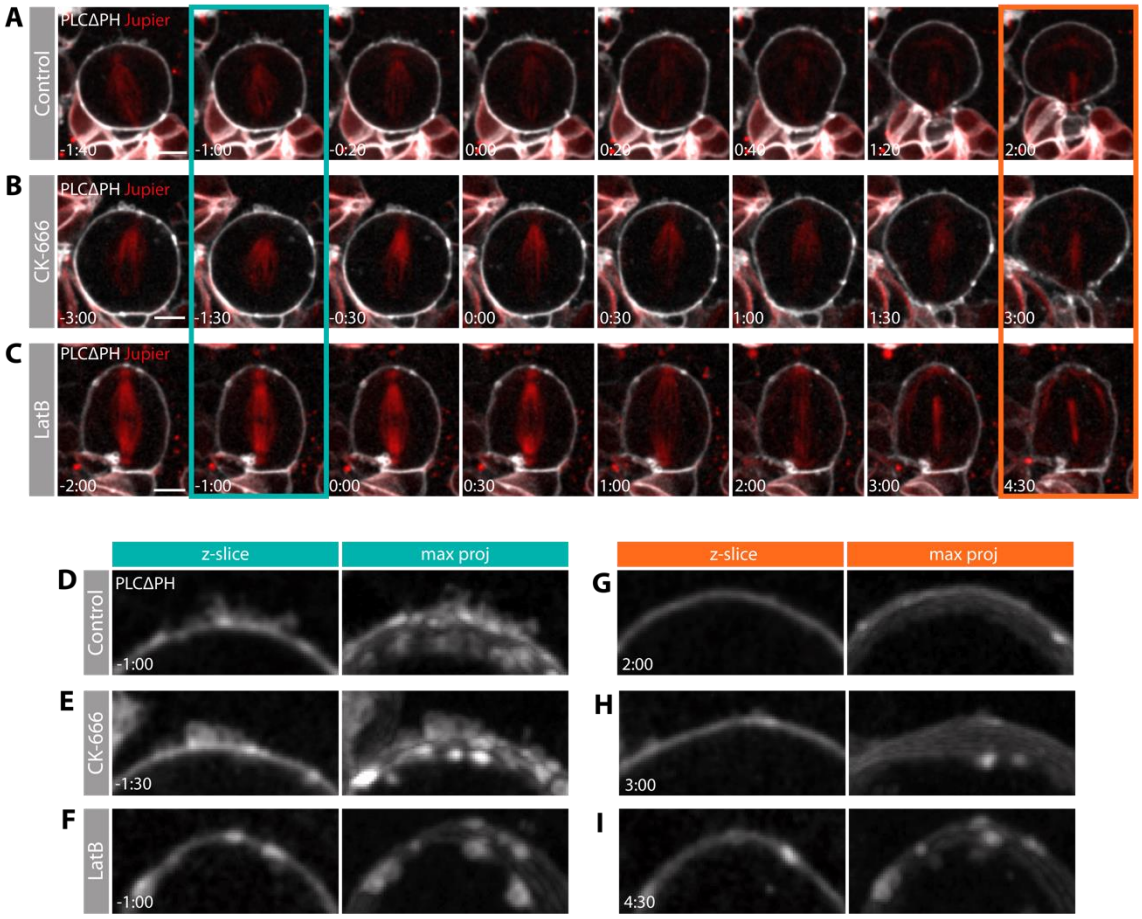

Figure 5.10. Inhibition of actin nucleation affects the apical membrane organization of mitotic NBs. A-C. Genotype: Wor-Gal4, UAS-cherry::Jupiter/Cyo x L/Cyo ; UAS-PLCΔPH::GFP/TM6B. High resolution imaging of dividing NBs treated with CK-689 (400 µM) (**A**), CK-666 (400 µM) (**B**) and Latrunculin B (10 µM) (**C**). **D-F.** Inserts depicting z-slice and maximum intensity projection of apical side of metaphase NBs highlighted by blue frame, showing polarized membrane protrusions in control (**D**) and the effect of CK-666 (**E**) and Latrunculin B (**F**). **G-I.** Inserts depicting z-slice and maximum intensity projection of apical side of cytokinetic NBs highlighted by orange frame, showing the absence of apical protrusions in control (**G**) and CK-666 treated cells (**H**), and the presence of the same ones in cells treated with Latrunculin B (**I**).
Scale bar: 5 µm.

5.4 Arp2/3 helps regulate apical Myosin clearance.

To determine how membrane remodelling events at the metaphase-anaphase transition are coordinated with changes in the actomyosin cortex, I imaged non-muscle Myosin II, using the Sqh::GFP reporter, together with cherry::Jupiter as a microtubule marker, at higher temporal (15 sec/frame) and spatial resolution (Fig. 5.11A). I then quantified Myosin levels at both the apical and basal side of the NB. The result of the analysis shows that Myosin is first cleared from the apical cortex around 15 seconds after anaphase onset. This is followed by basal Myosin clearance 45 seconds later (Fig. 5.11B, black arrows), in line with previously reported data (Roubinet et al. 2017). The comparison of this timing with that measured in Figure 5.2 shows that membrane dynamics and Myosin dynamics follow the same temporal pattern, suggesting a possible correlation between the two events.

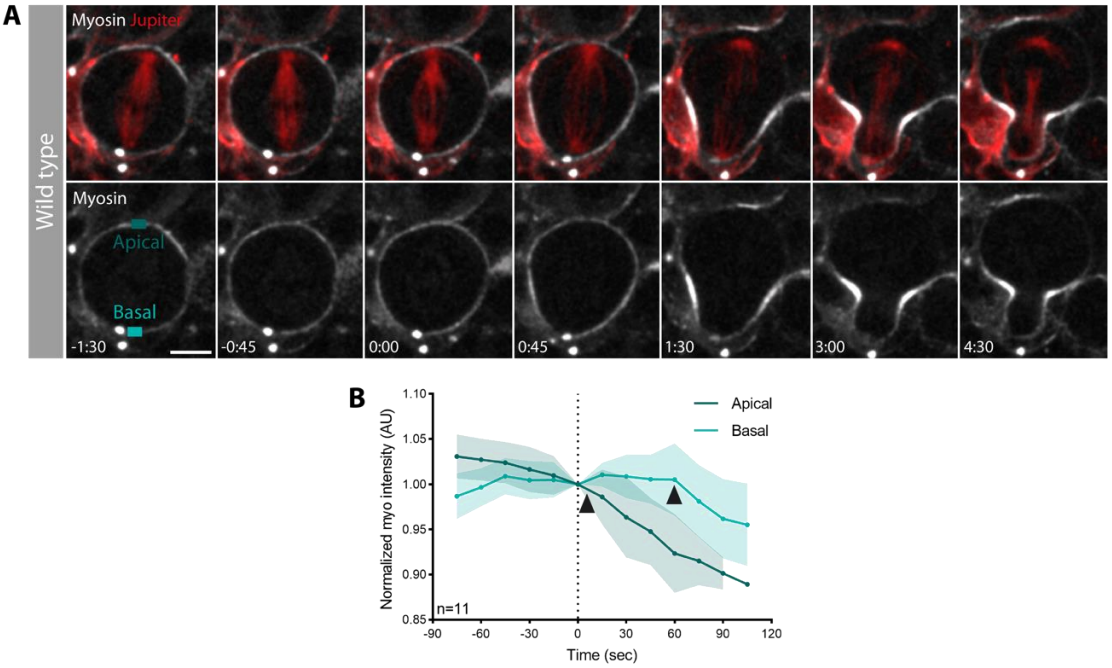

Figure 5.11. Myosin starts to be cleared apically around the time of anaphase onset. A. Genotype: Wor-Gal4, UAS-cherry::Jupiter, Sqh::GFP / Cyo. High resolution time-lapse image of dividing NB expressing Myosin marker (Sqh::GFP) and microtubule marker (cherry::Jupiter). Apical and basal rectangles indicate the areas measured for the graph in B. **B.** Graph shows apical and basal Myosin intensity changes with time. Arrowheads mark time points at which Myosin starts to be cleared. $N_{replicates}$ = 2.
Scale bar: 5 µm. Central and error bars: mean and SD.

Next, I wanted to correlate changes in the pattern of apical Myosin with changes in apical SCAR localisation. To help remove the background signal coming from surrounding tissue, for this experiment I dissociated brains and imaged single NBs expressing SCAR::GFP and Sqh::cherry via the UAS/wor-GAL4 system. Time-lapse montages of NBs revealed that levels of apical SCAR and Myosin starts to decrease just before the onset of anaphase cell elongation (Fig. 5.12A). The SCAR::GFP signal then increases at the furrow, beginning in late anaphase and peaking just before cytokinesis completion (Fig. 5.12B). By comparing the timing of NB division in this experiment to that seen in previous experiments, we can see that there is a delay in mitotic progression. This may be due to the stress induced by brain dissociation. It should also be noted that the time of anaphase onset in this experiment could not be precisely defined, due to the lack of a microtubule marker. However, when the dynamics of SCAR and Myosin are compared in these movies, it is clear that the two reporters follow the same temporal dynamics.

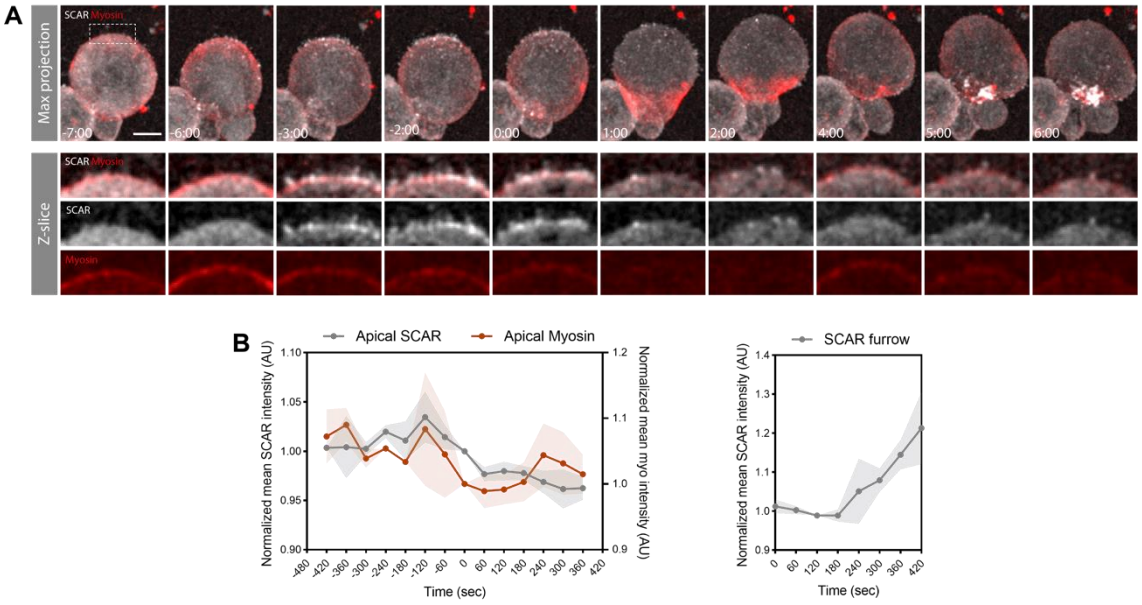

Figure 5.12. Apical Myosin and SCAR undergo parallel changes in their localisation at the metaphase-anaphase transition. A. Genotype: Wor-Gal4/Cyo ; UAS-Sqh::mCherry/TM6B x UAS-SCAR::GFP. High resolution imaging of dissociated NB expressing a SCAR reporter, UAS-SCAR::GFP and a non-muscle Myosin II marker, UAS-Sqh::cherry, which expressions is driven by wor-GAL4. Inserts show apical SCAR and Myosin signals. **B.** Graph showing SCAR and Myosin intensity during NB division. SCAR::GFP accumulating at the furrow starts at around anaphase onset and peaks at cytokinesis.
$N_{replicates}$ = 2, n = 3. Scale bar: 5 µm. Central and error bars: mean and SD.

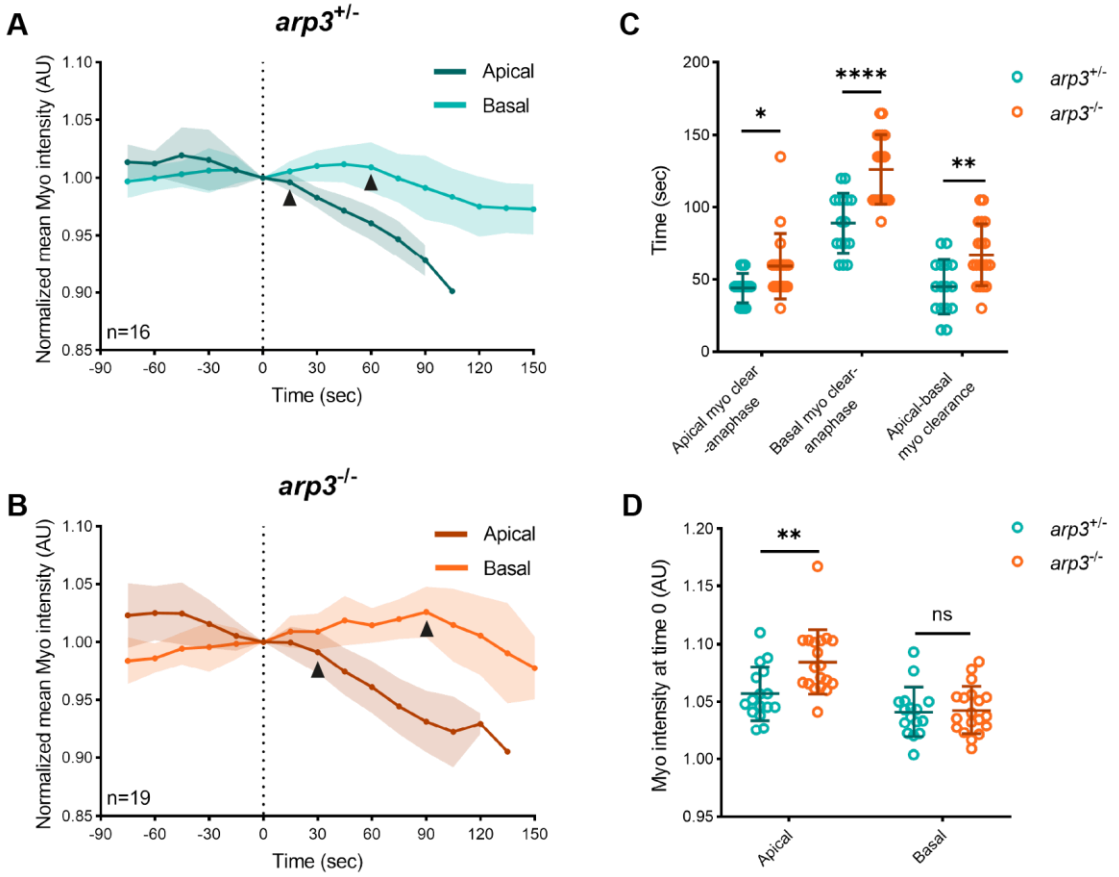

Figure 5.13. Arp2/3 controls apical Myosin dynamics in mitotic NBs. A-B. Graphs showing Myosin intensity changes during metaphase-anaphase transition in heterozygous *arp3*$^{+/-}$ (**A**) and mutant *arp3*$^{-/-}$ (**B**) expressing Sqh::GFP and cherry::Jupiter. Arrowheads mark the start of Myosin clearance. **C.** Plot showing time of Myosin clearance at the apical side, basal side and difference between the two sides, in heterozygous *arp3*$^{+/-}$ and mutant *arp3*$^{-/-}$. **D.** Myosin intensity at time 0 at the apical and basal sides, compared between the two conditions. $N_{replicates}$ = 3. Asterisks denote statistical significance. ns, not significant P > 0.05, *P ≤ 0.05, **P ≤ 0.01, ***P ≤ 0.001 and ****P ≤ 0.0001 (Tukey's multiple comparison test).
Central and error bars: mean and SD.

Previously I showed that Myosin, PH and SCAR follow the same temporal and spatial dynamics at the apical side of the NB, indicating a possible relationship between these proteins. To understand if Arp2/3 helps regulate Myosin clearance, I measured Myosin intensity at the apical and basal sides of the NB in Arp3 mutant and heterozygous control. The heterozygous behaves like the wild type (Fig. 5.11), with apical Myosin being cleared around 15 seconds after anaphase onset and basal around 60 seconds (Fig. 5.13A). On the other hand, in the mutant we can observe a delay in Myosin clearance on both sides: 15 seconds for the apical, and 30 seconds for the basal side (Fig. 5.13B, C). The extra 15 seconds of delay of the basal side are possibly due to cumulative effects of the delay in apical Myosin clearance.

I also compared Myosin intensity at time 0 in mutant and heterozygous animals. Interestingly, there is significantly more Myosin in mutant compared to the control, but only at the apical side (Fig. 5.13D). This strongly suggests that SCAR and the Arp2/3 complex regulate the amount of apical Myosin in cells entering mitosis through nucleation of branched actin. As a result, removing one element of this pathway leads to an excess of cortical Myosin and to a delay in apical Myosin clearance, with consequences for later stages of cell division.

5.5 Conclusion

In this chapter, I have characterized membrane movement and organization, and Myosin and SCAR temporal dynamics in the wild type NB, during metaphase-anaphase transition. I have shown that all of these processes happen with the same dynamics and are possibly connected together.

I have also shown that inhibiting SCAR or the Arp2/3 complex slows down membrane flow and leads to defects of the apical membrane organization at metaphase. Furthermore, in the *arp3* mutant, more Myosin accumulates at the apical side of the metaphase NB and its clearance is delayed. These effects on the membrane and Myosin are likely to be the cause of the cytokinetic phenotype described in the previous chapters.

Chapter 6.

Discussion.

6.1 Introduction

Cells undergo major shape changes through the different stages of cell division. These changes include rounding up at mitotic entry and forming the cleavage furrow at cytokinesis. Remodeling of the cortex is carried out by rearrangements of the actin cytoskeleton, which in turn is mainly nucleated by Diaphanous-family Formins in mitosis (Ramkumar and Baum 2016). Cells that undergo asymmetric divisions face additional challenges as they divide, since they have to coordinate shape changes with polarity establishment and fate determinant segregation. With the work in this thesis, I have shown that another actin nucleator, the Arp2/3 complex, is involved in the precise regulation of cortical dynamics. I have used the *Drosophila* neuroblasts to explore the role of branched actin network in asymmetric cell division, and I have shown that it is required at metaphase to pattern membrane domains at the cortex and to help break the symmetry of the actomyosin cortex.

I have analyzed Arp2/3 nucleation promoting factors, and have identified SCAR as the main activator in the dividing neuroblast. I have explored SCAR polarized localization and its relationship with the plasma membrane. Finally, I have observed the effects of SCAR and Arp2/3 inhibition on the neuroblast.

In this chapter, I discuss the details of these findings and place them in the wider context of the known literature. I also present a model that collates the results of this work and discuss further experiments to test the model.

6.2 Phenotypic discrepancies between different inhibition strategies.

While most of my data were consistent, I observed significant differences between drug, RNAi and mutants and, in the case of WASp and WASH, phenotypes observed using RNAi could not be replicated by other means. Cells where *wasp* was inhibited by RNAi showed a myosin ring moving from the basal side of newly formed NB to the apical side after cytokinesis, but this phenotype was not observed in the mutant (Fig. 4.3). This mutant has been used previously to show that myoblasts do not fuse in the embryo, indicating that the mutation

might be more reliable than the dsRNA, which might have off-target effects (Berger et al. 2008b). Furthermore, when WASp localization was observed, I could not see it enriched in any particular subcellular structure (Fig. 4.6).

By contrast, the cortical defects I observed in dividing cells in which either *scar* or *wash* was knocked-down by RNAi at first glance appeared similar to those seen in *arp3* RNAi flies. This indicates that one or both of these NPFs could be involved in Arp2/3 activation in these cells (Fig. 4.1, 4.2, 3.5). However, *wash* mutant NBs did not exhibit any evident phenotypes. This implies that the dsRNA I used had some off-target effect. Furthermore, WASH::GFP seemed to mark cytoplasmic spots in interphase, likely endosomes (Derivery et al. 2009; Gomez and Billadeau 2009), but did not have any specific localization during mitosis or division (Fig. 4.6) (Derivery et al., 2009; Gomez & Billadeau, 2009). For these reasons my data cannot be used to conclude that WASH plays an important role in the control of the mitotic NB cortex.

SCAR was the only NPF that when inhibited by RNAi or in loss of function clones led to phenotypes comparable to those observed in flies expressing dsRNAs targeting *arp3* and in the *arp3* mutant. Indeed, *scar* mutant clones also exhibited cortical defects at cytokinesis (Fig. 4.4). This is in line with the previously suggestion that SCAR is the NPF whose loss of function phenotype most closely resembles that of the Arp2/3 complex (Zallen et al. 2002). Furthermore, in this system I found that SCAR has a similar pattern of localization to tagged components of the Arp2/3 complex. Thus, confocal microscopy of entire brain lobes revealed that SCAR::GFP and two GFP-tagged components of the Arp2/3 complex, ArpC1 and Arp3, all localize at the furrow at cytokinesis (Fig. 4.5, 4.6). Two caveats of this experiment are that proteins may not behave normally when tagged nor when overexpressed using the UAS/GAL4 system. Moreover, I was not able to confirm whether the endogenous proteins had a similar localization using antibodies. Nevertheless, the localisation of these proteins to the contact site of the two new daughter cells is in line with previously published observations (Herszterg et al. 2013). Moreover, I was able to confirm the localization of the Arp2/3 complex using two distinct tagged components of the complex. Similarly,

SCAR localization was confirmed by looking at the localisation of Abi, a binding SCAR partner (Fig. 4.5, 4.9).

More strikingly, when observed at higher spatial resolution, both Arp3 and SCAR exhibited an asymmetric cortical localization at metaphase that to my knowledge has not been described previously. The apical cortical localization for SCAR was clearest when SCAR::GFP was imaged in dissociated NBs. While the cortical Arp3::GFP signal was less bright, it was still clearly concentrated at the apical pole of metaphase cells (Fig. 4.5, 4.7, 4.8). Thus, in neuroblasts it is clear that Arp2/3 and SCAR complexes co-localise both at metaphase and at cytokinesis.

In my study I also observed differences in the phenotypic consequences of perturbations of Arp2/3 activity which depended on the method used. Thus, the cortical defects that resulted from dsRNA mediated interference of *arp3* or from null mutants in the same gene led to milder phenotypes than those observed after chemical inhibition of the complex using CK-666 (Fig. 3.2, 3.5, 3.6). This could be due to secondary effects of the drug. It should also be noted that the treatment of brains with a control inactive version of the CK-666, CK-689, also led to the accumulation of ectopic Myosin in around 22% of cells (Fig. 3.1). Thus, there are likely to be non-specific effects that result from the high concentrations of small molecules and/or the solvent (DMSO). Note that it was necessary to add this volume of inhibitor solution because of the limited solubility of these small molecules and because of the need to penetrate the brain in a timely manner for use in these experiments.

Taken together, however, the similar cortical localization patterns of the tagged proteins and the similar cortical phenotypes observed using different tools to perturb the function of the Arp2/3 and SCAR complexes confirm a likely common role for these two complexes acting in tandem to control actin polymerization in the dividing neuroblast.

6.2.1 Discussion on cell size

There were also some perplexing differences in cell size following the chemical or genetic inhibition of Arp2/3 complex activity. In the first case, both the daughter NB and GMC were bigger than control; indicating a change in cell growth or a delay in division. By contrast, in the *arp3* mutant, the NB was smaller while the GMC was not affected. It is possible that differences in the nature of the phenotype affect cell growth or the size at division in complex ways, for example by affecting other proteins involved in defining the position of the furrow (e.g. Ect2/Pebble) (Montembault et al. 2022).

The difference may also be due to the impact of perturbations on different populations of cells. Thus, chemical inhibition is likely to affect all the cells in the tissue surrounding the dividing NB. This will include glia, which in the developing *Drosophila* brain play essential roles in regulating the proliferation of NBs, and could influence NB size too (Kanai et al. 2018). Conversely, the loss of function mutant may differentially affect cells depending on the time at which endogenous Arp2/3 complex runs out, and the use of a driver to drive RNAi will only affect cells in the NB lineage.

6.3 The role of the microtubules in the Arp2/3-dependent phenotype.

The delay in early mitotic stages observed in the perturbations used in this study could derive from a delay in the satisfaction of the spindle assembly checkpoint, due to microtubule defects (Musacchio and Salmon 2007). This led me to explore the role of microtubules in cells in which Arp2/3 was inhibited. This analysis revealed microtubules mis-localizing to the cortex at telophase-cytokinesis in 70% of CK-666 treated cells. Within this group, 64% also show spindle defects at metaphase, indicating that the membrane defects observed later are caused by defects at the spindle and possibly by microtubules nucleating in the wrong subcellular localization (Fig. 3.7). However, removing either the centrosome microtubules or all microtubules did not rescue the phenotype at cytokinesis, indicating that these misplaced microtubules themselves are unlikely to be

responsible for ectopic cleavage furrow formation. Instead, the microtubule phenotype is likely to be a separate consequence of Arp2/3 inhibition (Fig. 3.8, 3.9). In fact, removing centrosomes led to an increase of the penetrance of the cortical phenotype in cells in which Arp2/3 was inhibited, when compared with cells with centrosomes. Thus, the impact of defects in cortical actin are even more extreme when combined with defects in the microtubule cytoskeleton.

6.4 Role of Arp2/3 on apical cortical remodeling.

Using the reporter PLCΔ1PH::GFP, which has been proved effective in marking membrane domains in both *Drosophila* and *C. elegans* (LaFoya and Prehoda 2021; Scholze et al. 2018), I found that PH-rich membrane domains move towards the apical side of the NB during prophase, and then reverse their direction of motion in anaphase. These data indicate that the direction of membrane flow is coordinated with mitosis phases, as previously reported (Fig. 5.1) (LaFoya and Prehoda 2021; Oon and Prehoda 2021). However, although Latrunculin treatment completely abolishes membrane flows, as these studies and my own data show, I found that Arp2/3 inhibition by CK-666 did not eliminate these membrane movements, but only delayed their dynamics (Fig. 5.9). Similarly, in cells in which *scar* was knocked-down via RNAi, I observed changes in apical PH intensity rather than changes in membrane flow, suggesting a role for SCAR in the organisation of protrusions (Fig. 5.5-5.7). Similarly, when the Arp2/3 complex was inhibited, protrusions were lost, while excess membrane was still observed in patches on the apical cortex (Fig. 5.10). These data suggest that SCAR and the Arp2/3 complex nucleate a branched-actin network which creates the scaffold for the membrane protrusions, as previously suggested (Biyasheva et al. 2004; Georgiou and Baum 2010), but is not responsible for the local accumulation of excess membrane, which is more likely carried out by cortical flow driven by Myosin acting on a Formin-nucleated cortical mesh (Chugh and Paluch 2018; LaFoya and Prehoda 2021; Scholze et al. 2018).

The SCAR and Arp2/3-dependent membrane protrusions were absorbed when the cell entered anaphase and underwent cortical expansion (Fig. 5.3, 6.1). While this might lead to the suggestion that these protrusions provide excess

membrane that is released for use during cortical expansion, inhibiting the Arp2/3 complex did not block membrane flows during mitosis and did not prevent the cell from completing division. Thus, my data suggest that these protrusions do not act as a membrane reservoir, as has been suggested by a paper on bioRxiv (LaFoya and Prehoda 2022). Interestingly, excess membrane was still visible after Latrunculin B treatment, which abolishes completely actin nucleation (Fig. 5.10). In this case, excess membrane formed structures under the plasma membrane, rather than protrusions. While these types of experiment using Latrunculin are crude, this suggests the possibility that a Formin-dependent actin cortex constitutes a scaffold that prevents the membrane from collapsing inwards.

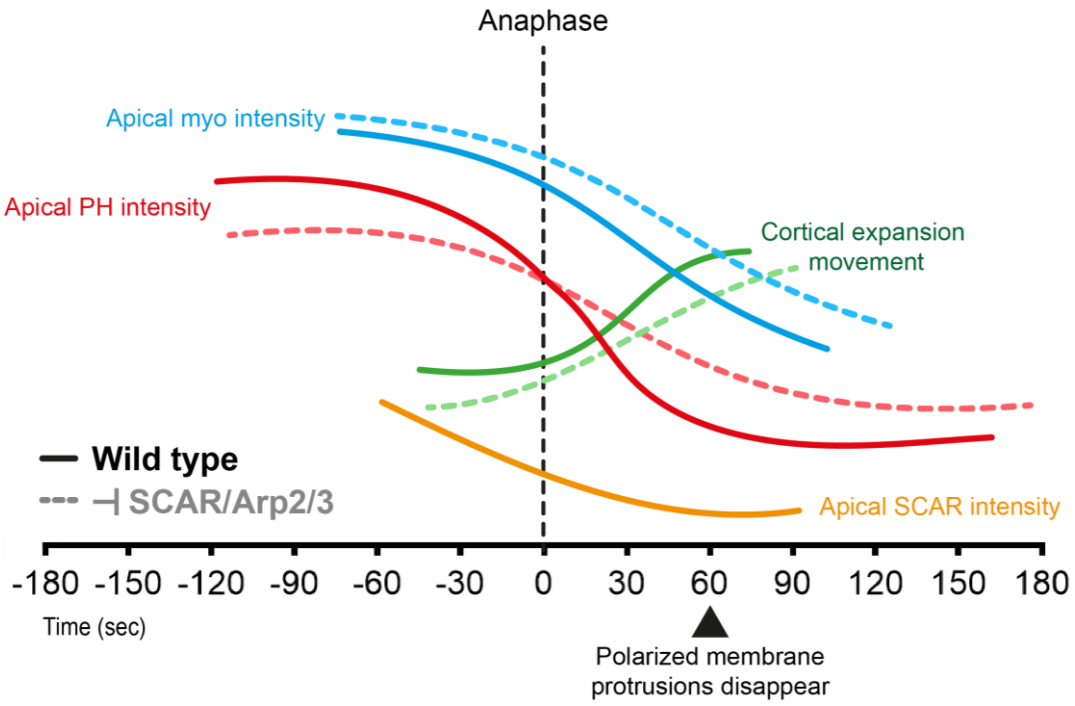

Figure 6.1. Summary of the cortical processes at metaphase-anaphase transition. Representation of processes happening at anaphase onset in wild-type and cells where Arp2/3 or SCAR have been inhibited .

6.4.1 Role of Arp2/3 in regulating cortical Myosin.

Arp2/3 inhibition also affected Myosin dynamics. Both apical and basal Myosin clearance were delayed in *arp3* mutant (Fig. 5.13). Even though the basal clearance of Myosin is delayed more compared to the apical clearance, this could possibly reflect the general delay of mitotic phases observed in the *arp3* mutant and other conditions where Arp2/3 is inhibited (Fig. 3.4, 3.5, 3.6, 4.2). More interestingly, absolute Myosin signal intensity was also increased at the apical, but not basal, cortex. As a result, wildtype cells enter anaphase with lower levels of apical Myosin, something that might serve to help break the symmetry in the system (Fig. 5.13, 6.1). In *Drosophila* salivary glands, where the actomyosin cortex generates the force required to collapse large spherical secretory vesicles, the Arp2/3 complex has been proposed to form stripes of branched actin that break the symmetry of the Formin-nucleated actomyosin cortex around the vesicle (Rousso, Schejter, and Shilo 2016). Recently in vitro work has also been published that shows how a branched actin network can prevent the accumulation of stress in an actomyosin network, by inhibiting the processivity of Myosin motors (Muresan et al. 2022). Here I propose that the SCAR and the Arp2/3 complex act in a similar way in the cortex of mitotic neuroblasts to construct a branched actin network that reduces the ability of Myosin to be recruited to and act on the apical cortex - aiding asymmetrical cortical expansion and asymmetric cell division.

Another effect of Arp2/3 inhibition is the delay in cortical expansion in cells treated with CK-666 (Fig. 5.8). While in control cells the apical membrane exhibits a fast and sharp movement, treated cells show a slow and gradual expansion (Fig. 5.8, 5.9). While it is not clear precisely how these changes in cortical remodelling dynamics are linked together, one possibility is that the apical accumulation of Myosin in Arp2/3 loss of function cells delays cortical expansion. An alternative hypothesis is that this delay is instead caused by the disorganized membrane protrusions. It is also unclear which of these processes are responsible for the phenotypes observed at cytokinesis when either Arp2/3 or SCAR are inhibited. These could even result from the effects of perturbations on other structures, e.g. microtubules or the actin forming at the new interface between daughter cells.

Nevertheless, it remains possible that the loss of branched actin from the apical cortex has effects on the system that alter cortical instability in more indirect ways.

6.4.2 Relationship between membrane dynamics and WASp family proteins and Arp2/3.

In the model proposed by this work, filopodia-like protrusions would be generated by SCAR and the Arp2/3 complex. While many studies have assumed a clear separation of function between the different Arp2/3 nucleation promoting factors, with SCAR being responsible for lamellipodia formation, and WASp being involved in filopodia, this is not always the case (Campellone and Welch 2010; Chesarone and Goode 2009). In fact, previous work suggests that in *Drosophila*, while SCAR-depleted cells lose both lamellipodia and filopodia, WASp removal does not lead to a significant cortical phenotype, arguing that both cortical actin structures are largely regulated by SCAR (Biyasheva et al. 2004; Georgiou and Baum 2010).

The filopodia-like membrane protrusions seem enriched in phospholipid PIP_2, which is a Cdc42-WASp activator. By contrast, SCAR is usually activated by Rac and PIP_3 (Campellone and Welch 2010). However, a more detailed analysis of the lipid composition of these protrusions is required to determine if they are also rich in PIP_3. A study in the *C. elegans* zygote shows a link between PIP_2 membrane domains, Cdc42 and polarity proteins Par-3/Par-6, and proposes that the lipid membrane component modulates actin organization and cell polarity (Scholze et al. 2018). However, in several of *Drosophila* cell types, including NBs, it has been shown that Baz preferentially binds PIP_3 (Krahn et al. 2010), indicating that the relationship between polarity and actin nucleators might be different in different systems. Therefore, it would be interesting in the future to explore the distribution of specific phospholipids in the NB membrane during division. In conclusion, SCAR depletion appears clear and fits that described by previous studies that implicated SCAR in the formation of thin actin-based protrusions, making this factor the best candidate nucleator for the actin network at the membrane protrusions (Georgiou and Baum 2010; Trylinski and Schweisguth 2019; Zallen et al. 2002).

6.5 The case for a role of Arp2/3 in mitosis.

Having observed a role for the Arp2/3 complex in cortical dynamics upon mitotic exit (Fig. 3.1, 3.2, 3.5, 3.6) my initial hypothesis was that Arp2/3 was inactive in metaphase but then reactivated at cytokinesis in the NB, as has been shown in other systems. For example, the Arp2/3 complex is activated at mitotic exit in human cells (Farina et al. 2019), and has a role in regulation of the cortex in the *C. elegans* zygote and in *Drosophila* SOPs during cytokinesis (Chan et al. 2019; Trylinski and Schweisguth 2019). However, upon further examination my data suggest that the Arp2/3 complex has a role within mitosis. This is much more surprising, since it is believed a general switch from Arp2/3 to Formin nucleated actin filament formation exists upon entry into mitosis, and that it is reversed at mitotic exit (Ramkumar and Baum 2016).

My data include the observation that Arp2/3 inhibition leads to a delay of one or more mitotic phases (Fig. 3.4, 3.5, 3.6). In particular, the time from NEB and anaphase onset was longer in all conditions, while the time from anaphase to cytokinesis was longer in CK-666 treated cells and *arp3* RNAi experiment but not in arp3 mutant cells. By contrast, the third phase, from cytokinesis to NER was the same as control in all cases. This suggests that even though the most evident phenotypes like cortical instability and the ectopic cleavage furrow are seen at the end of division, Arp2/3 inhibition might exert its function in mitosis. In addition, the Arp2/3 membrane protrusions I observe on the apical cortex are assembled in prophase or early metaphase. While this is the case, I was not able to observe any strong gross cellular defects in Arp2/3 loss of function NBs during metaphase. This changes when cells enter anaphase (Fig. 6.1). As soon as this occurs, Arp2/3 inhibition leads to cortical instabilities, like those seen by Rousso et al. in *Drosophila* salivary glands. In vesicles in the salivary gland, Arp2/3 and Formin pattern the cortex to enable smooth changes in shape. The same mechanism may be in place in the NB cortex. Both types of actomyosin-mediated changes in membrane organisation require precision. Thus, even though the Arp2/3 complex does not contribute to the forces that drive cell rounding or to cytokinesis, the results observed in this work suggest that it might be needed to fine tune the mechanics to add precision and robustness to the system. This is

shown by the fact that while cells without Arp2/3 still divide, further perturbations of the system, for example the loss of Sas4, lead to a profound increase in the prevalence of defects.

Based on my observations, I will now present a working model for the function of branched actin in asymmetric NB division. First, SCAR and Arp2/3 are recruited to the apical side of the NB in prophase-metaphase, perhaps by the polarity machinery, where they nucleate branched actin network that supports the formation of filopodia-like membrane protrusions (Fig. 6.1). I anticipate that Formin-dependent actin filament formation will also be required for the formation for these protrusions. At the same time, this network of branched actin limits the accumulation of Myosin at apical pole of the cell, as has been shown to occur in vitro (Muresan et al. 2022). Arp2/3 activity would therefore aid the polarity machinery in breaking the symmetry of the actomyosin cortex that leads to Myosin flow. Arp2/3 activity alone can not substitute the activity of the polarity complex in affecting Myosin localization, as demonstrated by the drastic effect of polarity inhibition compared to the mild effect of Arp2/3 inhibition. However, I believe this mechanism to be necessary to fine tune the complex rearrangements of the cortex happening at metaphase-anaphase transition, which is in turn required for proper asymmetry establishment in the NB. Indeed, the loss of Arp2/3 function leads to a disorganized apical membrane at anaphase onset. This in turn leads to affected dynamics of cortical expansion, and possibly to cortical instabilities and defects at cytokinesis (Fig. 6.2). Further work will be required to fully test this model. For example, in the long term future it would be great to know if the cortex has an asymmetric distribution of branched and unbranched actin as predicted by this model, e.g. using electron microscopy.

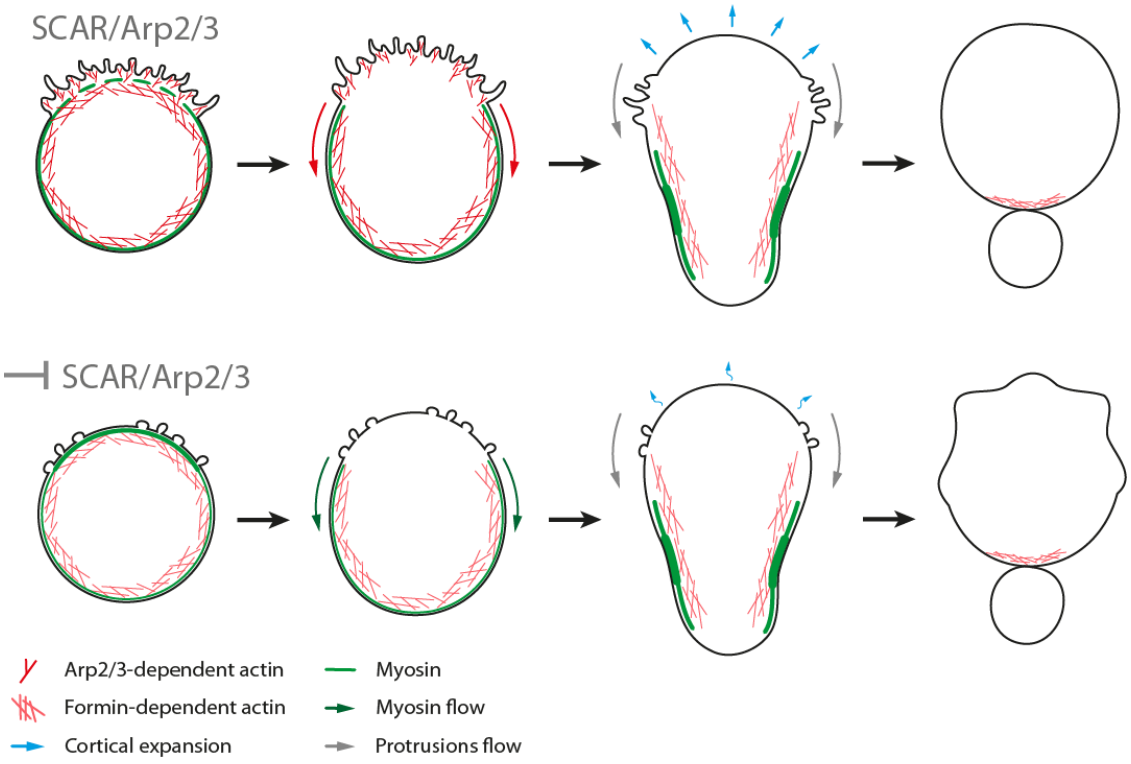

Figure 6.2. Model for the role of SCAR/Arp2/3 during metaphase-anaphase transition in the NB. Schematics representing how SCAR and Arp2/3 regulate cortical remodelling at anaphase onset in the NB.

6.6 Conclusions and future perspective.

With this work, I present a new model for the role of SCAR and Arp2/3 complex in shaping the cortex at metaphase-anaphase transition in dividing NBs. In this system perturbations to SCAR or the Arp2/3 complex delay cortical expansion, and lead to cortical instability and to defects in the precisely choreographed changes in shape cells undergo to achieve an asymmetric division (Fig. 6.1A). In this process, we propose that the SCAR complex provides a polarised cue to bias the accumulation of Arp2/3 leading to the formation of a branched apical actin network.

To better understand if the delayed cortical expansion and phenotypes at cytokinesis in Arp2/3 loss of function cells are driven by excess Myosin or by the disorganized membrane protrusions, these two processes should be inhibited one at a time and in a specific way. It is challenging to selectively inhibit PIP_2 and PIP_3 rich membrane domains, without affecting the overall organization of the membrane. An approach to directly test whether the Arp2/3 loss of function phenotypes arise from overactive Myosin would be to use nanobodies to over-activate Myosin to the apical side of the NB to reproduce the effect of Arp2/3 inhibition.

I also showed that SCAR localizes asymmetrically in metaphase, in a manner that resembles that of aPKC and Par3 (Loyer and Januschke 2020; Petronczki and Knoblich 2000; Wodarz et al. 2000). In both *Drosophila* neuroblasts and *C. elegans* a link between these proteins and F-actin, Myosin and membrane domains has been clearly established (LaFoya and Prehoda 2021; Oon and Prehoda 2021; Scholze et al. 2018). Future work will be necessary to elucidate how SCAR is recruited apically and the mechanisms involved. This could be explored by studying the role of PIP_3, PIP_2, Rac and Cdc42 in activating SCAR, and how each in turn is recruited to the apical cortex.

The apical localization of SCAR and of the membrane protrusions suggest that this mechanism might be recruited through polarity and the Par complex. Indeed, epithelial cells often present membrane protrusions like filopodia or microvilli at their apical side, and these are regulated by the Par complex via Cdc42 and Rac,

that in turn induce activation of WASp and SCAR/WAVE, respectively, to form branched actin networks. Therefore, even though I have not explored the role of polarity in formation of protrusions in the NB, my work fit with what is known about polarized membrane protrusions. Usually protrusions in epithelial cells are either driving cell migration, necessary to contact neighbouring cells, or used to increase cell surface. In this thesis I was not able to show what is the exact function of the membrane protrusions, but they could be either similar to microvilli as in they are used by the cell to store excess membrane necessary for cortical expansion, or they could have a similar function to blebs and be used to stabilize the cortex and maintain/release membrane tension. Several cell types, like HeLa and *Drosophila* SOPs undergo blebbing at the poles during anaphase to release tension. Therefore, the observations in the NB in this thesis could show how a mechanism that is well understood in a specific biological context can be adapted for specific use in a different situation, specifically in this case, in asymmetric cell division in non-epithelial cells.

Bibliography

Abeysundara, Namal, Andrew J. Simmonds, and Sarah C. Hughes. 2018. “Moesin Is Involved in Polarity Maintenance and Cortical Remodeling during Asymmetric Cell Division.” *Molecular Biology of the Cell* 29(4):419–34. doi: 10.1091/MBC.E17-05-0294/ASSET/IMAGES/LARGE/MBC-29-419-G009.JPEG.

Albertson, Roger, and Chris Q. Doe. 2003. “Dlg, Scrib and Lgl Regulate Neuroblast Cell Size and Mitotic Spindle Asymmetry.” *Nature Cell Biology* 5(2):166–70. doi: 10.1038/ncb922.

Amann, K. J., and T. D. Pollard. 2001. “The Arp2/3 Complex Nucleates Actin Filament Branches from the Sides of Pre-Existing Filaments.” *Nature Cell Biology 2001 3:3* 3(3):306–10. doi: 10.1038/35060104.

Artavanis-Tsakonas, Spyros, Matthew D. Rand, and Robert J. Lake. 1999. “Notch Signaling: Cell Fate Control and Signal Integration in Development.” *Science (New York, N.Y.)* 284(5415):770–76. doi: 10.1126/SCIENCE.284.5415.770.

Ashraf, Shovon I., Xiaodi Hu, John Roote, and Y. Tony Ip. 1999. “The Mesoderm Determinant Snail Collaborates with Related Zinc-Finger Proteins to Control Drosophila Neurogenesis.” *EMBO Journal* 18(22):6426–38. doi: 10.1093/EMBOJ/18.22.6426.

Atwood, Scott X., Chiswili Chabu, Rhiannon R. Penkert, Chris Q. Doe, and Kenneth E. Prehoda. 2007. “Cdc42 Acts Downstream of Bazooka to Regulate Neuroblast Polarity through Par-6/APKC.” *Journal of Cell Science* 120(Pt 18):3200. doi: 10.1242/JCS.014902.

Atwood, Scott X., and Kenneth E. Prehoda. 2009. “APKC Phosphorylates Miranda to Polarize Fate Determinants during Neuroblast Asymmetric Cell Division.” *Current Biology : CB* 19(9):723–29. doi: 10.1016/J.CUB.2009.03.056.

Barros, Claudia S., Chris B. Phelps, and Andrea H. Brand. 2003. “Drosophila Nonmuscle Myosin II Promotes the Asymmetric Segregation of Cell Fate

Determinants by Cortical Exclusion Rather Than Active Transport." *Developmental Cell* 5(6):829–40. doi: 10.1016/S1534-5807(03)00359-9.

Basant, Angika, and Michael Glotzer. 2018. "Spatiotemporal Regulation of RhoA during Cytokinesis." *Current Biology* 28(9):R570–80. doi: 10.1016/j.cub.2018.03.045.

Bassi, Zuni I., Koen J. Verbrugghe, Luisa Capalbo, Stephen Gregory, Emilie Montembault, David M. Glover, and Pier Paolo D'Avino. 2011. "Sticky/Citron Kinase Maintains Proper RhoA Localization at the Cleavage Site during Cytokinesis." *The Journal of Cell Biology* 195(4):595–603. doi: 10.1083/JCB.201105136.

Basto, Renata, Rui Gomes, and Roger E. Karess. 2000. *Rough Deal and Zw10 Are Required for the Metaphase Checkpoint in Drosophila*. Vol. 2. Nature Publishing Group.

Basto, Renata, Joyce Lau, Tatiana Vinogradova, Alejandra Gardiol, C. Geoffrey Woods, Alexey Khodjakov, and Jordan W. Raff. 2006. "Flies without Centrioles." *Cell* 125(7):1375–86. doi: 10.1016/j.cell.2006.05.025.

Bello, Bruno C., Natalya Izergina, Emmanuel Caussinus, and Heinrich Reichert. 2008. "Amplification of Neural Stem Cell Proliferation by Intermediate Progenitor Cells in Drosophila Brain Development." *Neural Development* 3(1):1–18. doi: 10.1186/1749-8104-3-5/FIGURES/8.

Bello, Bruno, Heinrich Reichert, and Frank Hirth. 2006. "The Brain Tumor Gene Negatively Regulates Neural Progenitor Cell Proliferation in the Larval Central Brain of Drosophila." *Development (Cambridge, England)* 133(14):2639–48. doi: 10.1242/DEV.02429.

Ben-Yaacov, Sari, Roland le Borgne, Irit Abramson, Francois Schweisguth, and Eyal D. Schejter. 2001a. "Wasp, the Drosophila Wiskott-Aldrich Syndrome Gene Homologue, Is Required for Cell Fate Decisions Mediated by Notch Signaling." *Journal of Cell Biology* 152(1):1–13. doi: 10.1083/JCB.152.1.1.

Ben-Yaacov, Sari, Roland le Borgne, Irit Abramson, Francois Schweisguth, and Eyal D. Schejter. 2001b. “Wasp, the Drosophila Wiskott-Aldrich Syndrome Gene Homologue, Is Required for Cell Fate Decisions Mediated by Notch Signaling.” *The Journal of Cell Biology* 152(1):1–14. doi: 10.1083/jcb.152.1.1-b.

Berger, Susanne, Gritt Schäfer, Dörthe A. Kesper, Anne Holz, Therese Eriksson, Ruth H. Palmer, Lothar Beck, Christian Klämbt, Renate Renkawitz-Pohl, and Susanne Filiz Önel. 2008a. “WASP and SCAR Have Distinct Roles in Activating the Arp2/3 Complex during Myoblast Fusion.” *Journal of Cell Science* 121(8):1303–13. doi: 10.1242/JCS.022269.

Berger, Susanne, Gritt Schäfer, Dörthe A. Kesper, Anne Holz, Therese Eriksson, Ruth H. Palmer, Lothar Beck, Christian Klämbt, Renate Renkawitz-Pohl, and Susanne Filiz Önel. 2008b. “WASP and SCAR Have Distinct Roles in Activating the Arp2/3 Complex during Myoblast Fusion.” *Journal of Cell Science* 121(8):1303–13. doi: 10.1242/JCS.022269.

Biyasheva, Assel, Tatyana Svitkina, Patricia Kunda, Buzz Baum, and Gary Borisy. 2004. “Cascade Pathway of Filopodia Formation Downstream of SCAR.” *Journal of Cell Science* 117(6):837–48. doi: 10.1242/JCS.00921.

Bogdan, Sven, Oliver Grewe, Mareike Strunk, Alexandra Mertens, and Christian Klämbt. 2004. “Sra-1 Interacts with Kette and Wasp and Is Required for Neuronal and Bristle Development in Drosophila.” *Development (Cambridge, England)* 131(16):3981–89. doi: 10.1242/DEV.01274.

Boone, Jason Q., and Chris Q. Doe. 2008. “Identification of Drosophila Type II Neuroblast Lineages Containing Transit Amplifying Ganglion Mother Cells.” *Developmental Neurobiology* 68(9):1185–95. doi: 10.1002/DNEU.20648.

Bosticardo, Marita, Francesco Marangoni, Alessandro Aiuti, Anna Villa, and Maria Grazia Roncarolo. 2009. “Recent Advances in Understanding the Pathophysiology of Wiskott-Aldrich Syndrome.” *Blood* 113(25):6288–95. doi: 10.1182/BLOOD-2008-12-115253.

Boulianne, G. L., A. De La Concha, J. A. Campos-Ortega, L. Y. Jan, and Y. N. Jan. 1991. “The Drosophila Neurogenic Gene Neuralized Encodes a Novel Protein and Is Expressed in Precursors of Larval and Adult Neurons.” *EMBO Journal* 10(10):2975–84. doi: 10.1002/J.1460-2075.1991.TB07848.X.

Bovellan, Miia, Yves Romeo, Maté Biro, Annett Boden, Priyamvada Chugh, Amina Yonis, Malti Vaghela, Marco Fritzsche, Dale Moulding, Richard Thorogate, Antoine Jégou, Adrian J. Thrasher, Guillaume Romet-Lemonne, Philippe P. Roux, Ewa K. Paluch, and Guillaume Charras. 2014. “Cellular Control of Cortical Actin Nucleation.” *Current Biology* 24(14):1628–35. doi: 10.1016/j.cub.2014.05.069.

Bowman, Sarah K., Ralph A. Neumüller, Maria Novatchkova, Quansheng Du, and Juergen A. Knoblich. 2006a. “The Drosophila NuMA Homolog Mud Regulates Spindle Orientation in Asymmetric Cell Division.” 10(6):731–42. doi: 10.1016/J.DEVCEL.2006.05.005.

Bowman, Sarah K., Ralph A. Neumüller, Maria Novatchkova, Quansheng Du, and Juergen A. Knoblich. 2006b. “The Drosophila NuMA Homolog Mud Regulates Spindle Orientation in Asymmetric Cell Division.” *Developmental Cell* 10(6):731–42. doi: 10.1016/J.DEVCEL.2006.05.005.

Brand, Andrea H., Armen S. Manoukian, and Norbert Perrimon. 1994. “Ectopic Expression in Drosophila.” *Methods in Cell Biology* 44(C):635–54. doi: 10.1016/S0091-679X(08)60936-X.

Brinkley, B. R., Elton Stubblefield, and T. C. Hsu. 1967. “The Effects of Colcemid Inhibition and Reversal on the Fine Structure of the Mitotic Apparatus of Chinese Hamster Cells in Vitro.” *Journal of Ultrastructure Research* 19(1):1–18. doi: 10.1016/S0022-5320(67)80057-1.

Burkel, Brian M., George Von Dassow, and William M. Bement. 2007. “Versatile Fluorescent Probes for Actin Filaments Based on the Actin-Binding Domain of Utrophin.” doi: 10.1002/cm.20226.

Cabernard, Clemens, and Chris Q. Doe. 2009. “Apical/Basal Spindle Orientation Is Required for Neuroblast Homeostasis and Neuronal Differentiation in Drosophila.” *Developmental Cell* 17(1):134–41. doi: 10.1016/j.devcel.2009.06.009.

Cabernard, Clemens, Kenneth E. Prehoda, and Chris Q. Doe. 2010. “A Spindle-Independent Cleavage Furrow Positioning Pathway.” *Nature* 467(7311):91–94. doi: 10.1038/nature09334.

Campellone, Kenneth G., and Matthew D. Welch. 2010. “A Nucleator Arms Race: Cellular Control of Actin Assembly.” *Nature Reviews Molecular Cell Biology* 11(4):237–51. doi: 10.1038/nrm2867.

Carlier, Marie France, Dominique Pantaloni, John A. Evans, Peter K. Lambooy, Edward D. Korn, and Martin R. Webb. 1988. “The Hydrolysis of ATP That Accompanies Actin Polymerization Is Essentially Irreversible.” *FEBS Letters* 235(1–2):211–14. doi: 10.1016/0014-5793(88)81264-X.

Caygill, Elizabeth E., and Andrea H. Brand. 2016. “The GAL4 System: A Versatile System for the Manipulation and Analysis of Gene Expression.” Pp. 33–52 in *Methods in Molecular Biology*. Vol. 1478.

Chan, Fung Yi, Ana M. Silva, Joana Saramago, Joana Pereira-Sousa, Hailey E. Brighton, Marisa Pereira, Karen Oegema, Reto Gassmann, and Ana Xavier Carvalho. 2019. “The ARP2/3 Complex Prevents Excessive Formin Activity during Cytokinesis.” *Molecular Biology of the Cell* 30(1):96–107. doi: 10.1091/mbc.E18-07-0471.

Chan, L. N., and W. Gehring. 1971. “Determination of Blastoderm Cells in Drosophila Melanogaster.” *Proceedings of the National Academy of Sciences* 68(9):2217–21. doi: 10.1073/PNAS.68.9.2217.

Chereau, David, Frederic Kerff, Philip Graceffa, Zenon Grabarek, Knut Langsetmo, and Roberto Dominguez. 2005. “Actin-Bound Structures of Wiskott-Aldrich Syndrome Protein (WASP)-Homology Domain 2 and the Implications for Filament Assembly.” *Proceedings of the National Academy*

of Sciences of the United States of America 102(46):16644–49. doi: 10.1073/PNAS.0507021102.

Chesarone, Melissa A., and Bruce L. Goode. 2009. “Actin Nucleation and Elongation Factors: Mechanisms and Interplay.” *Current Opinion in Cell Biology* 21(1):28–37. doi: 10.1016/j.ceb.2008.12.001.

Choksi, Semil P., Tony D. Southall, Torsten Bossing, Karin Edoff, Elzo de Wit, Bettina E. E. Fischer, Bas van Steensel, Gos Micklem, and Andrea H. Brand. 2006. “Prospero Acts as a Binary Switch between Self-Renewal and Differentiation in Drosophila Neural Stem Cells.” *Developmental Cell* 11(6):775–89. doi: 10.1016/J.DEVCEL.2006.09.015.

Chugh, Priyamvada, and Ewa K. Paluch. 2018. “The Actin Cortex at a Glance.” *Journal of Cell Science* 131(14). doi: 10.1242/JCS.186254/56817.

Connell, Marisa, Clemens Cabernard, Derek Ricketson, Chris Q. Doe, and Kenneth E. Prehoda. 2011. “Asymmetric Cortical Extension Shifts Cleavage Furrow Position in Drosophila Neuroblasts.” *Molecular Biology of the Cell* 22(22):4220–26. doi: 10.1091/mbc.E11-02-0173.

Davidson, Andrew J., Seiji Ura, Peter A. Thomason, Gabriela Kalna, and Robert H. Insall. 2013. “Abi Is Required for Modulation and Stability but Not Localization or Activation of the SCAR/WAVE Complex.” *Eukaryotic Cell* 12(11):1509–16. doi: 10.1128/EC.00116-13.

D’Avino, Pier Paolo, Maria Grazia Giansanti, and Mark Petronczki. 2015. “Cytokinesis in Animal Cells.” *Cold Spring Harbor Perspectives in Biology* 7(4):1–17. doi: 10.1101/cshperspect.a015834.

Derivery, Emmanuel, Carla Sousa, Jérémie J. Gautier, Bérangère Lombard, Damarys Loew, and Alexis Gautreau. 2009. “The Arp2/3 Activator WASH Controls the Fission of Endosomes through a Large Multiprotein Complex.” *Developmental Cell* 17(5):712–23. doi: 10.1016/j.devcel.2009.09.010.

Doe, Chris Q., Quynh Chu-LaGraff, Dorothy M. Wright, and Matthew P. Scott. 1991. “The Prospero Gene Specifies Cell Fates in the Drosophila Central Nervous System.” *Cell* 65(3):451–64. doi: 10.1016/0092-8674(91)90463-9.

Dominguez, Roberto, and Kenneth C. Holmes. 2011. “Actin Structure and Function.” *Annual Review of Biophysics* 40(1):169–86. doi: 10.1146/annurev-biophys-042910-155359.

Eden, Sharon, Rajat Rohatgi, Alexandre V. Podtelejnikov, Matthias Mann, and Marc W. Kirschner. 2002. “Mechanism of Regulation of WAVE1-Induced Actin Nucleation by Rac1 and Nck.” *Nature 2002 418:6899* 418(6899):790–93. doi: 10.1038/nature00859.

Egile, Coumaran, Isabelle Rouiller, Xiao Ping Xu, Niels Volkmann, Rong Li, and Dorit Hanein. 2005. “Mechanism of Filament Nucleation and Branch Stability Revealed by the Structure of the Arp2/3 Complex at Actin Branch Junctions.” *PLOS Biology* 3(11):e383. doi: 10.1371/JOURNAL.PBIO.0030383.

Farina, Francesca, Nitya Ramkumar, Louise Brown, Dureen Samandar Eweis, Jannis Anstatt, Thomas Waring, Jessica Bithell, Giorgio Giogio Scita, Manuel Thery, Laurent Blanchoin, Tobias Zech, Buzz Baum, Durren Samander-, Jannis Anstatt, Thomas Waring, Jessica Bithell, Giorgio Giogio Scita, Laurent Blanchoin, Tobias Zech, Buzz Baum, Dureen Samandar Eweis, Jannis Anstatt, Thomas Waring, Jessica Bithell, Giorgio Giogio Scita, Manuel Thery, Laurent Blanchoin, Tobias Zech, and Buzz Baum. 2019. “Local Actin Nucleation Tunes Centrosomal Microtubule Nucleation during Passage through Mitosis.” *The EMBO Journal* 38(11):1–16. doi: 10.15252/embj.201899843.

Field, Christine M. 2011. “Bulk Cytoplasmic Actin and Its Functions in Meiosis and Mitosis Minireview.” 825–30. doi: 10.1016/j.cub.2011.07.043.

Field, Christine M., Margaret Coughlin, Steve Doberstein, Thomas Marty, and William Sullivan. 2005. “Characterization of Anillin Mutants Reveals Essential Roles in Septin Localization and Plasma Membrane Integrity.” *Development* 132(12):2849–60. doi: 10.1242/DEV.01843.

Field, Christine M., Martin Wühr, Graham A. Anderson, Hao Yuan Kueh, Devin Strickland, and Timothy J. Mitchison. 2011. “Actin Behavior in Bulk Cytoplasm Is Cell Cycle Regulated in Early Vertebrate Embryos.” *Journal of Cell Science* 124(12):2086–95. doi: 10.1242/JCS.082263.

Fink, Jenny, Nicolas Carpi, Timo Betz, Angelique Bétard, Meriem Chebah, Ammar Azioune, Michel Bornens, Cecile Sykes, Luc Fetler, Damien Cuvelier, and Matthieu Piel. 2011. “External Forces Control Mitotic Spindle Positioning.” *Nature Cell Biology* 13(7):771–78. doi: 10.1038/NCB2269.

Gallaud, Emmanuel, Tri Pham, and Clemens Cabernard. 2017. “Drosophila Melanogaster Neuroblasts: A Model for Asymmetric Stem Cell Divisions.” Pp. 351–73 in Vol. 61.

Gautreau, Alexis, Hsin Yi H. Ho, Jiaxu Li, Hanno Steen, Steven P. Gygi, and Marc W. Kirschner. 2004. “Purification and Architecture of the Ubiquitous Wave Complex.” *Proceedings of the National Academy of Sciences of the United States of America* 101(13):4379–83. doi: 10.1073/PNAS.0400628101.

Georgiou, Marios, and Buzz Baum. 2010. “Polarity Proteins and Rho GTPases Cooperate to Spatially Organise Epithelial Actin-Based Protrusions.” *Journal of Cell Science* 123(7):1089–98. doi: 10.1242/jcs.060772.

Goley, Erin D., and Matthew D. Welch. 2006. “The ARP2/3 Complex: An Actin Nucleator Comes of Age.” *Nature Reviews Molecular Cell Biology* 7(10):713–26. doi: 10.1038/nrm2026.

Gomez, Timothy S., and Daniel D. Billadeau. 2009. “A FAM21-Containing WASH Complex Regulates Retromer-Dependent Sorting.” *Dev. Cell* 17(5):699–711. doi: 10.1016/j.devcel.2009.09.009.

Gönczy, Pierje, Silke Pichler, Matthew Kirkham, and Anthony A. Hyman. 1999. “Cytoplasmic Dynein Is Required for Distinct Aspects of Mtoc Positioning, Including Centrosome Separation, in the One Cell Stage Caenorhabditis Elegans Embryo.” *Journal of Cell Biology* 147(1):135–50. doi: 10.1083/JCB.147.1.135.

Gönczy, Pierre. 2008. “Mechanisms of Asymmetric Cell Division: Flies and Worms Pave the Way.” *Nature Reviews Molecular Cell Biology 2008 9:5* 9(5):355–66. doi: 10.1038/nrm2388.

Goode, Bruce L., Avital A. Rodal, Georjana Barnes, and David G. Drubin. 2001. “Activation of the Arp2/3 Complex by the Actin Filament Binding Protein Abp1p.” *The Journal of Cell Biology* 153(3):627. doi: 10.1083/JCB.153.3.627.

Gournier, Helene, Erin D. Goley, Hanspeter Niederstrasser, Thong Trinh, and Matthew D. Welch. 2001. “Reconstitution of Human Arp2/3 Complex Reveals Critical Roles of Individual Subunits in Complex Structure and Activity.” *Molecular Cell* 8(5):1041–52. doi: 10.1016/S1097-2765(01)00393-8.

Hannaford, Matthew, Nicolas Loyer, Francesca Tonelli, Martin Zoltner, and Jens Januschke. 2019. “A Chemical-Genetics Approach to Study the Role of Atypical Protein Kinase C in Drosophila.” *Development (Cambridge)* 146(2). doi: 10.1242/dev.170589.

Hannaford, Matthew Robert, Anne Ramat, Nicolas Loyer, and Jens Januschke. 2018. “APKC-Mediated Displacement and Actomyosin-Mediated Retention Polarize Miranda in Drosophila Neuroblasts.” *ELife* 7. doi: 10.7554/eLife.29939.

Hanson, Jean, and J. Lowy. 1963. “The Structure of F-Actin and of Actin Filaments Isolated from Muscle.” *Journal of Molecular Biology* 6(1):46-IN5. doi: 10.1016/S0022-2836(63)80081-9.

Harding, Katherine, and Kristin White. 2018. “Drosophila as a Model for Developmental Biology: Stem Cell-Fate Decisions in the Developing Nervous System.” *Journal of Developmental Biology* 6(4). doi: 10.3390/JDB6040025.

Heimsath, Ernest G., and Henry N. Higgs. 2012. “The C Terminus of Formin FMNL3 Accelerates Actin Polymerization and Contains a WH2 Domain-like

Sequence That Binds Both Monomers and Filament Barbed Ends." *Journal of Biological Chemistry* 287(5):3087–98. doi: 10.1074/jbc.M111.312207.

Herszterg, Sophie, Andrea Leibfried, Floris Bosveld, Charlotte Martin, and Yohanns Bellaiche. 2013. "Interplay between the Dividing Cell and Its Neighbors Regulates Adherens Junction Formation during Cytokinesis in Epithelial Tissue." *DEVCEL* 24(3):256–70. doi: 10.1016/j.devcel.2012.11.019.

Hetrick, Byron, Min Suk Han, Luke A. Helgeson, and Brad J. Nolen. 2013. "Small Molecules CK-666 and CK-869 Inhibit Actin-Related Protein 2/3 Complex by Blocking an Activating Conformational Change." *Chemistry and Biology* 20(5):701–12. doi: 10.1016/j.chembiol.2013.03.019.

Homem, Catarina C. F., and Juergen A. Knoblich. 2012. "Drosophila Neuroblasts: A Model for Stem Cell Biology." *Development (Cambridge)* 139(23):4297–4310. doi: 10.1242/dev.080515.

Hudson, Andrew M., and Lynn Cooley. 2002a. "A Subset of Dynamic Actin Rearrangements in Drosophila Requires the Arp2/3 Complex." *The Journal of Cell Biology* 156(4):677. doi: 10.1083/JCB.200109065.

Hudson, Andrew M., and Lynn Cooley. 2002b. "A Subset of Dynamic Actin Rearrangements in Drosophila Requires the Arp2/3 Complex." *The Journal of Cell Biology* 156(4):677–87. doi: 10.1083/JCB.200109065.

Hudson, Andrew M., and Lynn Cooley. 2002c. "A Subset of Dynamic Actin Rearrangements in Drosophila Requires the Arp2/3 Complex." *The Journal of Cell Biology* 156(4):677. doi: 10.1083/JCB.200109065.

Hudson, Andrew M., and Lynn Cooley. 2002d. "A Subset of Dynamic Actin Rearrangements in Drosophila Requires the Arp2/3 Complex." *The Journal of Cell Biology* 156(4):677–87. doi: 10.1083/JCB.200109065.

Ibarra, N., A. Pollitt, and R. H. Insall. 2005. "Regulation of Actin Assembly by SCAR/WAVE Proteins." *Biochemical Society Transactions* 33(Pt 6):1243–46. doi: 10.1042/BST20051243.

Ideses, Yaron, Yifat Brill-Karniely, Lior Haviv, Avinoam Ben-Shaul, and Anne Bernheim-Groswasser. 2008. “Arp2/3 Branched Actin Network Mediates Filopodia-like Bundles Formation in Vitro.” *PLoS ONE* 3(9). doi: 10.1371/JOURNAL.PONE.0003297.

Ikeshima-Kataoka, H., J. B. Skeath, Y. I. Nabeshima, C. Q. Doe, and F. Matsuzaki. 1997. “Miranda Directs Prospero to a Daughter Cell during Drosophila Asymmetric Divisions.” *Nature* 390(6660):625–29. doi: 10.1038/37641.

Illukkumbura, Rukshala, Tom Bland, and Nathan W. Goehring. 2020. “Patterning and Polarization of Cells by Intracellular Flows.” *Current Opinion in Cell Biology* 62:123–34. doi: 10.1016/J.CEB.2019.10.005.

Izumi, Yasushi, Nao Ohta, Kanako Hisata, Thomas Raabe, and Fumio Matsuzaki. 2006. “Drosophila Pins-Binding Protein Mud Regulates Spindle-Polarity Coupling and Centrosome Organization.” *Nature Cell Biology* 8(6):586–93. doi: 10.1038/NCB1409.

Januschke, Jens, and Cayetano Gonzalez. 2010. “The Interphase Microtubule Aster Is a Determinant of Asymmetric Division Orientation in Drosophila Neuroblasts.” *Journal of Cell Biology* 188(5):693–706. doi: 10.1083/JCB.200905024.

Jia, Da, Timothy S. Gomez, Zoltan Metlagel, Junko Umetani, Zbyszek Otwinowski, Michael K. Rosen, and Daniel D. Billadeau. 2010. “WASH and WAVE Actin Regulators of the Wiskott-Aldrich Syndrome Protein (WASP) Family Are Controlled by Analogous Structurally Related Complexes.” *Proceedings of the National Academy of Sciences of the United States of America* 107(23):10442–47. doi: 10.1073/pnas.0913293107.

Jin, Meiyan, Cyna Shirazinejad, Bowen Wang, Amy Yan, Johannes Schöneberg, Srigokul Upadhyayula, Ke Xu, and David G. Drubin. 2022. “Branched Actin Networks Are Organized for Asymmetric Force Production during Clathrin-Mediated Endocytosis in Mammalian Cells.” *Nature Communications 2022 13:1* 13(1):1–12. doi: 10.1038/s41467-022-31207-5.

Johnston, Christopher A., Keiko Hirono, Kenneth E. Prehoda, and Chris Q. Doe. 2009. “Identification of an Aurora-A/PinsLINKER/Dlg Spindle Orientation Pathway Using Induced Cell Polarity in S2 Cells.” *Cell* 138(6):1150–63. doi: 10.1016/J.CELL.2009.07.041.

Joseph, Jayabalan M., Petra Fey, Nagendran Ramalingam, Xiao I. Liu, Meino Rohlfs, Angelika A. Noegel, Annette Müller-Taubenberger, Gernot Glöckner, and Michael Schleicher. 2008. “The Actinome of Dictyostelium Discoideum in Comparison to Actins and Actin-Related Proteins from Other Organisms.” *PLOS ONE* 3(7):e2654. doi: 10.1371/JOURNAL.PONE.0002654.

Kanai, Makoto I., Myung Jun Kim, Takuya Akiyama, Masahiko Takemura, Kristi Wharton, Michael B. O’Connor, and Hiroshi Nakato. 2018. “Regulation of Neuroblast Proliferation by Surface Glia in the Drosophila Larval Brain.” *Scientific Reports 2018 8:1* 8(1):1–15. doi: 10.1038/s41598-018-22028-y.

Karpova, Nina, Yves Bobinnec, Sylvaine Fouix, Philippe Huitorel, and Alain Debec. 2006. “Jupiter, a New Drosophila Protein Associated with Microtubules.” *Cell Motility and the Cytoskeleton* 63(5):301–12. doi: 10.1002/CM.20124.

Kim, Annette S., Lazaros T. Kakalis, Norzehan Abdul-Manan, Grace A. Liu, and Michael K. Rosen. 2000. “Autoinhibition and Activation Mechanisms of the Wiskott–Aldrich Syndrome Protein.” *Nature 2000 404:6774* 404(6774):151–58. doi: 10.1038/35004513.

Kobayashi, K., S. Kuroda, M. Fukata, T. Nakamura, T. Nagase, N. Nomura, Y. Matsuura, N. Yoshida-Kubomura, A. Iwamatsu, and K. Kaibuchi. 1998. “P140Sra-1 (Specifically Rac1-Associated Protein) Is a Novel Specific Target for Rac1 Small GTPase.” *J. Biol. Chem.* 273:291–95.

Krahn, Michael P., Dieter R. Klopfenstein, Nannette Fischer, and Andreas Wodarz. 2010. “Membrane Targeting of Bazooka/PAR-3 Is Mediated by Direct Binding to Phosphoinositide Lipids.” *Current Biology* 20(7):636–42. doi: 10.1016/J.CUB.2010.01.065.

Kraut, Rachel, William Chia, Lily Yeh Jan, Yuh Nung Jan, and Jürgen A. Knoblich. 1996. “Role of Inscuteable in Orienting Asymmetric Cell Divisions in Drosophila.” *Nature 1996 383:6595* 383(6595):50–55. doi: 10.1038/383050a0.

Kunda, Patricia, Gavin Craig, Veronica Dominguez, and Buzz Baum. 2003. “Abi, Sra1, and Kette Control the Stability and Localization of SCAR/WAVE to Regulate the Formation of Actin-Based Protrusions.” *Current Biology* 13(21):1867–75. doi: 10.1016/j.cub.2003.10.005.

LaFoya, Bryce, and Kenneth E. Prehoda. 2021. “Actin-Dependent Membrane Polarization Reveals the Mechanical Nature of the Neuroblast Polarity Cycle.” *Cell Reports* 35(7):109146. doi: 10.1016/j.celrep.2021.109146.

LaFoya, Bryce, and Kenneth E. Prehoda. 2022. “An Actomyosin-Polarized Membrane Reservoir Mediates the Unequal Divisions of Drosophila Neural Stem Cells.” *BioRxiv* 2022.05.03.490551. doi: 10.1101/2022.05.03.490551.

Lang, Charles F., and Edwin Munro. 2017. “The PAR Proteins: From Molecular Circuits to Dynamic Self-Stabilizing Cell Polarity.” *Development* 144(19):3405–16. doi: 10.1242/DEV.139063.

Lara-Gonzalez, Pablo, Frederick G. Westhorpe, and Stephen S. Taylor. 2012. “The Spindle Assembly Checkpoint.” *Current Biology : CB* 22(22):R966-80. doi: 10.1016/j.cub.2012.10.006.

Lebensohn, Andres M., and Marc W. Kirschner. 2009. “Activation of the WAVE Complex by Coincident Signals Controls Actin Assembly.” *Molecular Cell* 36(3):512–24. doi: 10.1016/j.molcel.2009.10.024.

Lee, Cheng Yu, Brian D. Wilkinson, Sarah E. Siegrist, Robin P. Wharton, and Chris Q. Doe. 2006. “Brat Is a Miranda Cargo Protein That Promotes Neuronal Differentiation and Inhibits Neuroblast Self-Renewal.” *Developmental Cell* 10(4):441–49. doi: 10.1016/J.DEVCEL.2006.01.017.

Linardopoulou, Elena v., Sean S. Parghi, Cynthia Friedman, Gregory E. Osborn, Susan M. Parkhurst, and Barbara J. Trask. 2007. “Human Subtelomeric

WASH Genes Encode a New Subclass of the WASP Family." *PLOS Genetics* 3(12):e237. doi: 10.1371/JOURNAL.PGEN.0030237.

Liu, Jinghe, Gregory D. Fairn, Derek F. Ceccarelli, Frank Sicheri, and Andrew Wilde. 2012. "Cleavage Furrow Organization Requires PIP(2)-Mediated Recruitment of Anillin." *Current Biology : CB* 22(1):64–69. doi: 10.1016/J.CUB.2011.11.040.

Liu, Raymond, Maria Teresa Abreu-Blanco, Kevin C. Barry, Elena v. Linardopoulou, Gregory E. Osborn, and Susan M. Parkhurst. 2009. "Wash Functions Downstream of Rho and Links Linear and Branched Actin Nucleation Factors." *Development* 136(16):2849–60. doi: 10.1242/dev.035246.

Liu, Yuechueng, Daniel A. Fisher, and Daniel R. Storm. 1994. "Intracellular Sorting of Neuromodulin (GAP-43) Mutants Modified in the Membrane Targeting Domain." *The Journal of Neuroscience : The Official Journal of the Society for Neuroscience* 14(10):5807–17. doi: 10.1523/JNEUROSCI.14-10-05807.1994.

Loyer, Nicolas, and Jens Januschke. 2018. "The Last-Born Daughter Cell Contributes to Division Orientation of Drosophila Larval Neuroblasts." *Nature Communications* 9(1):1–12. doi: 10.1038/s41467-018-06276-0.

Loyer, Nicolas, and Jens Januschke. 2020. "Where Does Asymmetry Come from? Illustrating Principles of Polarity and Asymmetry Establishment in Drosophila Neuroblasts." *Current Opinion in Cell Biology* 62:70–77.

Lu, Bingwei, Michael Rothenberg, Lily Y. Jan, and Yuh Nung Jan. 1998. "Partner of Numb Colocalizes with Numb during Mitosis and Directs Numb Asymmetric Localization in Drosophila Neural and Muscle Progenitors." *Cell* 95(2):225–35. doi: 10.1016/S0092-8674(00)81753-5.

Machesky, Laura M., Simon J. Atkinson, Christophe Ampe, Joel Vandekerckhove, and Thomas D. Pollard. 1994. "Purification of a Cortical Complex Containing Two Unconventional Actins from Acanthamoeba by

Affinity Chromatography on Profilin-Agarose." *The Journal of Cell Biology* 127(1):107. doi: 10.1083/JCB.127.1.107.

Marchand, Jean Baptiste, Donald A. Kaiser, Thomas D. Pollard, and Henry N. Higgs. 2001. "Interaction of WASP/Scar Proteins with Actin and Vertebrate Arp2/3 Complex." *Nature Cell Biology* 3(1):76–82. doi: 10.1038/35050590.

Martin, Adam C., Michael Gelbart, Rodrigo Fernandez-Gonzalez, Matthias Kaschube, and Eric F. Wieschaus. 2010. "Integration of Contractile Forces during Tissue Invagination." *Journal of Cell Biology* 188(5):735–49. doi: 10.1083/JCB.200910099/VIDEO-10.

Merdes, Andreas, Kasra Ramyar, Janet D. Vechio, and Don W. Cleveland. 1996. "A Complex of NuMA and Cytoplasmic Dynein Is Essential for Mitotic Spindle Assembly." *Cell* 87(3):447–58. doi: 10.1016/S0092-8674(00)81365-3.

Mitsushima, Masaru, Kazuhiro Aoki, Miki Ebisuya, Shigeru Matsumura, Takuya Yamamoto, Michiyuki Matsuda, Fumiko Toyoshima, and Eisuke Nishida. 2010. "Revolving Movement of a Dynamic Cluster of Actin Filaments during Mitosis." *Journal of Cell Biology* 191(3):453–62. doi: 10.1083/jcb.201007136.

Montembault, Emilie, Irène Deduyer, Marie-Charlotte Claverie, Lou Bouit, Nicolas Tourasse, Denis Dupuy, Derek McCusker, and Anne Royou. 2022. "Two RhoGEF Isoforms with Distinct Localisation Act in Concert to Control Asymmetric Cell Division." *BioRxiv* 33(8.5.2017):2003–5.

Morton, Walter M., Kathryn R. Ayscough, and Paul J. Mclaughlin. 2000. "Latrunculin Alters the Actin-Monomer Subunit Interface to Prevent Polymerization." *Nature Cell Biology 2000 2:6* 2(6):376–78. doi: 10.1038/35014075.

Moulding, Dale A., Michael P. Blundell, David G. Spiller, Michael R. H. White, Giles O. Cory, Yolanda Calle, Helena Kempski, Jo Sinclair, Phil J. Ancliff, Christine Kinnon, Gareth E. Jones, and Adrian J. Thrasher. 2007. "Unregulated Actin Polymerization by WASp Causes Defects of Mitosis and

Cytokinesis in X-Linked Neutropenia." *Journal of Experimental Medicine* 204(9):2213–24. doi: 10.1084/jem.20062324.

Moulding, Dale A., Emad Moeendarbary, Leo Valon, Julien Record, Guillaume T. Charras, and Adrian J. Thrasher. 2012. "Excess F-Actin Mechanically Impedes Mitosis Leading to Cytokinesis Failure in X-Linked Neutropenia by Exceeding Aurora B Kinase Error Correction Capacity." *Blood* 120(18):3803–11. doi: 10.1182/blood-2012-03-419663.

Muller, Jean, Yukako Oma, Laurent Vallar, Evelyne Friederich, Olivier Poch, and Barbara Winsor. 2005. "Sequence and Comparative Genomic Analysis of Actin-Related Proteins." *Molecular Biology of the Cell* 16(12):5736–48. doi: 10.1091/mbc.E05-06-0508.

Mullins, R. Dyche, John A. Heuser, and Thomas D. Pollard. 1998. "The Interaction of Arp2/3 Complex with Actin: Nucleation, High Affinity Pointed End Capping, and Formation of Branching Networks of Filaments." *Proceedings of the National Academy of Sciences of the United States of America* 95(11):6181–86. doi: 10.1073/PNAS.95.11.6181.

Munro, Edwin, Jeremy Nance, and James R. Priess. 2004. "Cortical Flows Powered by Asymmetrical Contraction Transport PAR Proteins to Establish and Maintain Anterior-Posterior Polarity in the Early C. Elegans Embryo." *Developmental Cell* 7(3):413–24. doi: 10.1016/j.devcel.2004.08.001.

Muresan, Camelia G., Zachary Gao Sun, Vikrant Yadav, A. Pasha Tabatabai, Laura Lanier, June Hyung Kim, Taeyoon Kim, and Michael P. Murrell. 2022. "F-Actin Architecture Determines Constraints on Myosin Thick Filament Motion." *Nature Communications 2022 13:1* 13(1):1–16. doi: 10.1038/s41467-022-34715-6.

Musacchio, Andrea, and Edward D. Salmon. 2007. "The Spindle-Assembly Checkpoint in Space and Time." *Nature Reviews Molecular Cell Biology 2007 8:5* 8(5):379–93. doi: 10.1038/nrm2163.

Nagel, Benedikt M., Meike Bechtold, Luis Garcia Rodriguez, and Sven Bogdan. 2017. “Drosophila WASH Is Required for Integrin-Mediated Cell Adhesion, Cell Motility and Lysosomal Neutralization.” *Journal of Cell Science* 130(2):344–59. doi: 10.1242/jcs.193086.

Nikon. n.d. “CSU-W1 SoRa | CSU Series | Confocal Microscopes | Nikon Microscope Products | Nikon Europe B.V.” Retrieved September 1, 2022 (https://www.microscope.healthcare.nikon.com/en_EU/products/confocal-microscopes/csu-series/csu-w1-sora).

Nipper, Rick W., Karsten H. Siller, Nicholas R. Smith, Chris Q. Doe, and Kenneth E. Prehoda. 2007. “Gαi Generates Multiple Pins Activation States to Link Cortical Polarity and Spindle Orientation in Drosophila Neuroblasts.” *Proceedings of the National Academy of Sciences of the United States of America* 104(36):14306–11. doi: 10.1073/PNAS.0701812104/SUPPL_FILE/01812MOVIE2.MOV.

Nolen, B. J., N. Tomasevic, A. Russell, D. W. Pierce, Z. Jia, C. D. McCormick, J. Hartman, R. Sakowicz, and T. D. Pollard. 2009. “Characterization of Two Classes of Small Molecule Inhibitors of Arp2/3 Complex.” *Nature 2009 460:7258* 460(7258):1031–34. doi: 10.1038/nature08231.

Oon, Chet Huan, and Kenneth E. Prehoda. 2019. “Asymmetric Recruitment and Actin- Dependent Cortical Flows Drive the Neuroblast Polarity Cycle.” *ELife* 8:1–15. doi: 10.7554/eLife.45815.

Oon, Chet Huan, and Kenneth E. Prehoda. 2021. “Phases of Cortical Actomyosin Dynamics Coupled to the Neuroblast Polarity Cycle.” *ELife* 10. doi: 10.7554/eLife.66574.

Ou, Guangshuo, Nico Stuurman, Michael D’Ambrosio, and Ronald D. Vale. 2010. “Polarized Myosin Produces Unequal-Size Daughters during Asymmetric Cell Division.” *Science* 330(6004):677–80. doi: 10.1126/SCIENCE.1196112/SUPPL_FILE/OU.SOM.PDF.

Panchal, Sanjay C., Donald A. Kaiser, Eduardo Torres, Thomas D. Pollard, and Michael K. Rosen. 2003. “A Conserved Amphipathic Helix in WASP/Scar Proteins Is Essential for Activation of Arp2/3 Complex.” *Nature Structural & Molecular Biology 2003 10:8* 10(8):591–98. doi: 10.1038/nsb952.

Parmentier, Marie-Laure, Daniel Woods, Steve Greig, Phu G. Phan, Anna Radovic, Peter Bryant, and Cahir J. O’kane. 2000. “Rapsynoid/Partner of Inscuteable Controls Asymmetric Division of Larval Neuroblasts in Drosophila.”

Petronczki, M., and J. A. Knoblich. 2000. “DmPAR-6 Directs Epithelial Polarity and Asymmetric Cell Division of Neuroblasts in Drosophila.” *Nature Cell Biology 2001 3:1* 3(1):43–49. doi: 10.1038/35050550.

Pham, Tri Thanh, Arnaud Monnard, Jonne Helenius, Erik Lund, Nicole Lee, Daniel J. Müller, and Clemens Cabernard. 2019. “Spatiotemporally Controlled Myosin Relocalization and Internal Pressure Generate Sibling Cell Size Asymmetry.” *IScience* 13:9–19.

Piekny, Alisa J., and Michael Glotzer. 2008. “Anillin Is a Scaffold Protein That Links RhoA, Actin, and Myosin during Cytokinesis.” *Current Biology* 18(1):30–36. doi: 10.1016/J.CUB.2007.11.068.

Pollard, Thomas D., and John A. Cooper. 2009. “Actin, a Central Player in Cell Shape and Movement.” *Science* 326(5957):1208–12. doi: 10.1126/science.1175862.

Pring, Martin, Marie Evangelista, Charles Boone, Changsong Yang, and Sally H. Zigmond. 2003. “Mechanism of Formin-Induced Nucleation of Actin Filaments.” *Biochemistry* 42(2):486–96. doi: 10.1021/bi026520j.

Qualmann, B., and R. B. Kelly. 2000. “Syndapin Isoforms Participate in Receptor-Mediated Endocytosis and Actin Organization.” *The Journal of Cell Biology* 148(5):1047. doi: 10.1083/JCB.148.5.1047.

Rajan, Akhila, An Chi Tien, Claire M. Haueter, Karen L. Schulze, and Hugo J. Bellen. 2009. “The Arp2/3 Complex and WASp Are Required for Apical

Trafficking of Delta into Microvilli during Cell Fate Specification of Sensory Organ Precursors." *Nature Cell Biology* 11(7):815–24. doi: 10.1038/ncb1888.

Ramkumar, Nitya, and Buzz Baum. 2016. "Coupling Changes in Cell Shape to Chromosome Segregation." *Nature Reviews Molecular Cell Biology* 17(8):511–21. doi: 10.1038/nrm.2016.75.

Rebollo, Elena, Mónica Roldán, and Cayetano Gonzalez. 2009. "Spindle Alignment Is Achieved without Rotation after the First Cell Cycle in Drosophila Embryonic Neuroblasts." *Development* 136(20):3393–97. doi: 10.1242/DEV.041822.

Rebollo, Elena, Paula Sampaio, Jens Januschke, Salud Llamazares, Hanne Varmark, and Cayetano González. 2007. "Functionally Unequal Centrosomes Drive Spindle Orientation in Asymmetrically Dividing Drosophila Neural Stem Cells." *Developmental Cell* 12(3):467–74. doi: 10.1016/j.devcel.2007.01.021.

Rhyu, Michelle S., Lily Yeh Jan, and Yuh Nung Jan. 1994. "Asymmetric Distribution of Numb Protein during Division of the Sensory Organ Precursor Cell Confers Distinct Fates to Daughter Cells." *Cell* 76(3):477–91. doi: 10.1016/0092-8674(94)90112-0.

Ridley, Anne J., Hugh F. Paterson, Caroline L. Johnston, Dagmar Diekmann, and Alan Hall. 1992. "The Small GTP-Binding Protein Rac Regulates Growth Factor-Induced Membrane Ruffling." *Cell* 70(3):401–10. doi: 10.1016/0092-8674(92)90164-8.

Riedl, Julia, Alvaro H. Crevenna, Kai Kessenbrock, Jerry Haochen Yu, Dorothee Neukirchen, Michal Bista, Frank Bradke, Dieter Jenne, Tad A. Holak, Zena Werb, Michael Sixt, and Roland Wedlich-Soldner. 2008. "Lifeact: A Versatile Marker to Visualize F-Actin." doi: 10.1038/NMETH.1220.

Rodriguez, Josana, Florent Peglion, Jack Martin, Lars Hubatsch, Jacob Reich, Nisha Hirani, Alicia G. Gubieda, Jon Roffey, Artur Ribeiro Fernandes, Daniel

St Johnston, Julie Ahringer, and Nathan W. Goehring. 2017. “APKC Cycles between Functionally Distinct PAR Protein Assemblies to Drive Cell Polarity.” *Developmental Cell* 42(4):400-415.e9. doi: 10.1016/J.DEVCEL.2017.07.007.

Rodriguez-Mesa, Evelyn, Maria Teresa Abreu-Blanco, Alicia E. Rosales-Nieves, and Susan M. Parkhurst. 2012. “Developmental Expression of Drosophila Wiskott-Aldrich Syndrome Family Proteins.” *Developmental Dynamics* 241(3):608–26. doi: 10.1002/dvdy.23742.

Rolls, Melissa M., Roger Albertson, Hsin Pei Shih, Cheng Yu Lee, and Chris Q. Doe. 2003. “Drosophila APKC Regulates Cell Polarity and Cell Proliferation in Neuroblasts and Epithelia.” *Journal of Cell Biology* 163(5):1089–98. doi: 10.1083/JCB.200306079.

Rørth, Pernille. 1996. “A Modular Misexpression Screen in Drosophila Detecting Tissue-Specific Phenotypes.” *Proceedings of the National Academy of Sciences of the United States of America* 93(22):12418–22. doi: 10.1073/PNAS.93.22.12418.

Rosa, André, Evi Vlassaks, Franck Pichaud, Buzz Baum, Evi Vlassaks, Franck Pichaud, Buzz Baum, André Rosa, Evi Vlassaks, Franck Pichaud, Buzz Baum, Evi Vlassaks, Franck Pichaud, and Buzz Baum. 2015. “Ect2/Pbl Acts via Rho and Polarity Proteins to Direct the Assembly of an Isotropic Actomyosin Cortex upon Mitotic Entry.” *Developmental Cell* 32(5):604–16. doi: 10.1016/j.devcel.2015.01.012.

Roubinet, Chantal, Anna Tsankova, Tri Thanh Pham, Arnaud Monnard, Emmanuel Caussinus, Markus Affolter, and Clemens Cabernard. 2017. “Spatio-Temporally Separated Cortical Flows and Spindle Geometry Establish Physical Asymmetry in Fly Neural Stem Cells.” *Nature Communications* 1–15. doi: 10.1038/s41467-017-01391-w.

Rousso, Tal, Eyal D. Schejter, and Ben Zion Shilo. 2016. “Orchestrated Content Release from Drosophila Glue-Protein Vesicles by a Contractile Actomyosin Network.” *Nature Cell Biology* 18(2):181–90. doi: 10.1038/ncb3288.

Royou, Anne, William Sullivan, and Roger Karess. 2002. “Cortical Recruitment of Nonmuscle Myosin II in Early Syncytial Drosophila Embryos: Its Role in Nuclear Axial Expansion and Its Regulation by Cdc2 Activity.” *The Journal of Cell Biology* 158(1):127–37. doi: 10.1083/jcb.200203148.

Rusan, Nasser M., and Mark Peifer. 2007. “A Role for a Novel Centrosome Cycle in Asymmetric Cell Division.” *Journal of Cell Biology* 177(1):13–20. doi: 10.1083/JCB.200612140.

Schaefer, Matthias, Mark Petronczki, Daniela Dorner, Michael Forte, and Juergen A. Knoblich. 2001. “Heterotrimeric G Proteins Direct Two Modes of Asymmetric Cell Division in the Drosophila Nervous System.” *Cell* 107(2):183–94. doi: 10.1016/S0092-8674(01)00521-9.

Schaefer, Matthias, Anna Andrej Shevchenko, Anna Andrej Shevchenko, and Juergen A. Knoblich. 2000. “A Protein Complex Containing Inscuteable and the Galpha-Binding Protein Pins Orients Asymmetric Cell Divisions in Drosophila.” *Current Biology : CB* 10(7):353–62. doi: 10.1016/s0960-9822(00)00401-2.

Schaefer, Matthias, Anna Shevchenko, Andrej Shevchenko, and Juergen A. Knoblich. 2000a. “A Protein Complex Containing Inscuteable and the Gα-Binding Protein Pins Orients Asymmetric Cell Divisions in Drosophila.” *Current Biology* 10(7):353–62. doi: 10.1016/S0960-9822(00)00401-2.

Schaefer, Matthias, Anna Shevchenko, Andrej Shevchenko, and Juergen A. Knoblich. 2000b. “A Protein Complex Containing Inscuteable and the Gα-Binding Protein Pins Orients Asymmetric Cell Divisions in Drosophila.” *Current Biology* 10(7):353–62. doi: 10.1016/S0960-9822(00)00401-2.

Schäfer, Gritt, Susanne Weber, Anne Holz, Sven Bogdan, Sabine Schumacher, Arno Müller, Renate Renkawitz-Pohl, and Susanne Filiz Önel. 2007. “The Wiskott–Aldrich Syndrome Protein (WASP) Is Essential for Myoblast Fusion in Drosophila.” *Developmental Biology* 304(2):664–74. doi: 10.1016/J.YDBIO.2007.01.015.

Schindelin, Johannes, Ignacio Arganda-Carreras, Erwin Frise, Verena Kaynig, Mark Longair, Tobias Pietzsch, Stephan Preibisch, Curtis Rueden, Stephan Saalfeld, Benjamin Schmid, Jean Yves Tinevez, Daniel James White, Volker Hartenstein, Kevin Eliceiri, Pavel Tomancak, and Albert Cardona. 2012. “Fiji: An Open-Source Platform for Biological-Image Analysis.” *Nature Methods 2012 9:7* 9(7):676–82. doi: 10.1038/nmeth.2019.

Schirenbeck, Antje, Till Bretschneider, Rajesh Arasada, Michael Schleicher, and Jan Faix. 2005. “The Diaphanous-Related Formin DDia2 Is Required for the Formation and Maintenance of Filopodia.” *Nature Cell Biology* 7(6):619–25. doi: 10.1038/NCB1266.

Schneider, Stephan Q., and Bruce Bowerman. 2003. “Cell Polarity and the Cytoskeleton in the Caenorhabditis Elegans Zygote.” *Annual Review of Genetics* 37:221–49. doi: 10.1146/ANNUREV.GENET.37.110801.142443.

Schober, Markus, Matthias Schaefer, and Juergen A. Knoblich. 1999a. “Bazooka Recruits Inscuteable to Orient Asymmetric Cell Divisions in Drosophila Neuroblasts.” *Nature 1999 402:6761* 402(6761):548–51. doi: 10.1038/990135.

Schober, Markus, Matthias Schaefer, and Juergen A. Knoblich. 1999b. “Bazooka Recruits Inscuteable to Orient Asymmetric Cell Divisions in Drosophila Neuroblasts.” *Nature* 402(6761):548–51. doi: 10.1038/990135.

Scholze, Melina J., Kévin S. Barbieux, Alessandro de Simone, Mathilde Boumasmoud, Camille C. N. Süess, Ruijia Wang, and Pierre Gönczy. 2018. “PI(4,5)P2 Forms Dynamic Cortical Structures and Directs Actin Distribution as Well as Polarity in Caenorhabditis Elegans Embryos.” *Development (Cambridge)* 145(11):169144. doi: 10.1242/dev.164988.

Schweisguth, François. 2004. “Regulation of Notch Signaling Activity.” *Current Biology* 14(3):R129–38. doi: 10.1016/J.CUB.2004.01.023.

Sept, David, and J. Andrew McCammon. 2001. “Thermodynamics and Kinetics of Actin Filament Nucleation.” *Biophysical Journal* 81(2):667–74. doi: 10.1016/S0006-3495(01)75731-1.

Shen, Chun Pyn, Lily Y. Jan, and Yuh Nung Jan. 1997. “Miranda Is Required for the Asymmetric Localization of Prospero during Mitosis in Drosophila.” *Cell* 90(3):449–58. doi: 10.1016/S0092-8674(00)80505-X.

Siegrist, Sarah E., and Chris Q. Doe. 2005. “Microtubule-Induced Pins/Galphai Cortical Polarity in Drosophila Neuroblasts.” *Cell* 123(7):1323–35. doi: 10.1016/J.CELL.2005.09.043.

Siller, Karsten H., Clemens Cabernard, and Chris Q. Doe. 2006. “The NuMA-Related Mud Protein Binds Pins and Regulates Spindle Orientation in Drosophila Neuroblasts.” *Nature Cell Biology* 8(6):594–600. doi: 10.1038/ncb1412.

Skau, Colleen T., Erin M. Neidt, and David R. Kovar. 2009. “Role of Tropomyosin in Formin-Mediated Contractile Ring Assembly in Fission Yeast.” *Molecular Biology of the Cell* 20(8):2160–73. doi: 10.1091/MBC.E08-12-1201.

Skeath, J. B., and S. B. Carroll. 1992. “Regulation of Proneural Gene Expression and Cell Fate during Neuroblast Segregation in the Drosophila Embryo.” *Development (Cambridge, England)* 114(4):939–46. doi: 10.1242/DEV.114.4.939.

Snapper, Scott B., Fuminao Takeshima, Inés Antón, Ching Hui Liu, Sheila M. Thomas, Deanna Nguyen, Darryll Dudley, Hunter Fraser, Daniel Purich, Marco Lopez-Ilasaca, Christoph Klein, Laurie Davidson, Roderick Bronson, Richard C. Mulligan, Fred Southwick, Raif Geha, Marcia B. Goldberg, Fred S. Rosen, John H. Hartwig, and Frederick W. Alt. 2001. “N-WASP Deficiency Reveals Distinct Pathways for Cell Surface Projections and Microbial Actin-Based Motility.” *Nature Cell Biology* 3(10):897–904. doi: 10.1038/NCB1001-897.

Soderling, Scott H., Lorene K. Langeberg, Jacquelyn A. Soderling, Stephen M. Davee, Richard Simerly, Jacob Raber, and John D. Scott. 2003. “Loss of WAVE-1 Causes Sensorimotor Retardation and Reduced Learning and Memory in Mice.” *Proc. Natl Acad. Sci. USA* 100(4):1723–28. doi: 10.1073/pnas.0438033100.

Steffen, Anika, Jan Faix, Guenter P. Resch, Joern Linkner, Juergen Wehland, J. Victor Small, Klemens Rottner, and Theresia E. B. Stradal. 2006. “Filopodia Formation in the Absence of Functional WAVE- and Arp2/3-Complexes.” *Mol. Biol. Cell* 17(6):2581–91. doi: 10.1091/mbc.e05-11-1088.

Stevens, Joanne M., Edouard E. Galyov, and Mark P. Stevens. 2006. “Actin-Dependent Movement of Bacterial Pathogens.” *Nature Reviews Microbiology 2006 4:2* 4(2):91–101. doi: 10.1038/nrmicro1320.

Stewart, Martin P., Jonne Helenius, Yusuke Toyoda, Subramanian P. Ramanathan, Daniel J. Muller, and Anthony A. Hyman. 2011. “Hydrostatic Pressure and the Actomyosin Cortex Drive Mitotic Cell Rounding.” *Nature 2010 469:7329* 469(7329):226–30. doi: 10.1038/nature09642.

Suetsugu, Shiro, Daisuke Yamazaki, Shusaku Kurisu, and Tadaomi Takenawa. 2003. “Differential Roles of WAVE1 and WAVE2 in Dorsal and Peripheral Ruffle Formation for Fibroblast Cell Migration.” *Dev. Cell* 5(4):595–609. doi: 10.1016/s1534-5807(03)00297-1.

Sun, Shao Chen, Zhen Bo Wang, Yong Nan Xu, Seung Eun Lee, Xiang Shun Cui, and Nam Hyung Kim. 2011. “Arp2/3 Complex Regulates Asymmetric Division and Cytokinesis in Mouse Oocytes.” *PLOS ONE* 6(4):e18392. doi: 10.1371/JOURNAL.PONE.0018392.

Truman, James W., and Michael Bate. 1988. “Spatial and Temporal Patterns of Neurogenesis in the Central Nervous System of Drosophila Melanogaster.” *Developmental Biology* 125(1):145–57. doi: 10.1016/0012-1606(88)90067-X.

Trylinski, Mateusz, Khalil Mazouni, and François Schweisguth. 2017. “Intra-Lineage Fate Decisions Involve Activation of Notch Receptors Basal to the Midbody in Drosophila Sensory Organ Precursor Cells.” *Current Biology* 27(15):2239-2247.e3. doi: 10.1016/j.cub.2017.06.030.

Trylinski, Mateusz, and François Schweisguth. 2019. “Activation of Arp2/3 by WASp Is Essential for the Endocytosis of Delta Only during Cytokinesis in Drosophila.” *Cell Reports* 28(1):1-10.e3. doi: 10.1016/j.celrep.2019.06.012.

Tsankova, Anna, Tri Thanh Pham, David Salvador Garcia, Fabian Otte, and Clemens Cabernard. 2017. “Cell Polarity Regulates Biased Myosin Activity and Dynamics during Asymmetric Cell Division via Drosophila Rho Kinase and Protein Kinase N.” *Developmental Cell* 42(2):143-155.e5. doi: 10.1016/j.devcel.2017.06.012.

Tsarouhas, Vasilios, Dan Liu, Georgia Tsikala, Alina Fedoseienko, Kai Zinn, Ryo Matsuda, Daniel D. Billadeau, and Christos Samakovlis. 2019. “WASH Phosphorylation Balances Endosomal versus Cortical Actin Network Integrities during Epithelial Morphogenesis.” *Nature Communications 2019 10:1* 10(1):1–16. doi: 10.1038/s41467-019-10229-6.

Tsuji, Takuya, Eri Hasegawa, and Takako Isshiki. 2008. “Neuroblast Entry into Quiescence Is Regulated Intrinsically by the Combined Action of Spatial Hox Proteins and Temporal Identity Factors.” *Development (Cambridge, England)* 135(23):3859–69. doi: 10.1242/DEV.025189.

Udolph, Gerald, Karin Lüer, Torsten Bossing, and Gerhard M. Technau. 1995. “Commitment of CNS Progenitors along the Dorsoventral Axis of Drosophila Neuroectoderm.” *Science (New York, N.Y.)* 269(5228):1278–81. doi: 10.1126/SCIENCE.7652576.

Velarde, Nathalie, Kristin C. Gunsalus, and Fabio Piano. 2007. “Diverse Roles of Actin in C. Elegans Early Embryogenesis.” *BMC Developmental Biology* 7(1):1–16. doi: 10.1186/1471-213X-7-142/FIGURES/4.

Verboon, Jeffrey M., Hector Rincon-Arano, Timothy R. Werwie, Jeffrey J. Delrow, David Scalzo, Vivek Nandakumar, Mark Groudine, and Susan M. Parkhurst. 2015. “Wash Interacts with Lamin and Affects Global Nuclear Organization.” *Current Biology* 25(6):804–10. doi: 10.1016/j.cub.2015.01.052.

Verstreken, Patrik, Tomoko Ohyama, Claire Haueter, Ron L. P. Habets, Yong Q. Lin, Laura E. Swan, Cindy V. Ly, Koen J. T. Venken, Pietro De Camilli, and Hugo J. Bellen. 2009. “Tweek, an Evolutionarily Conserved Protein, Is Required for Synaptic Vesicle Recycling.” *Neuron* 63(2):203–15. doi: 10.1016/J.NEURON.2009.06.017.

Wakatsuki, Tetsuro, Bill Schwab, Nathan C. Thompson, and Elliot L. Elson. 2001. “Effects of Cytochalasin D and Latrunculin B on Mechanical Properties of Cells.” *Journal of Cell Science* 114(Pt 5):1025–36. doi: 10.1242/JCS.114.5.1025.

Wang, Cheng, Song Li, Jens Januschke, Fabrizio Rossi, Yasushi Izumi, Gisela Garcia-Alvarez, Serene Sze Ling Gwee, Swee Beng Soon, Harpreet Kaur Sidhu, Fengwei Yu, Fumio Matsuzaki, Cayetano Gonzalez, and Hongyan Wang. 2011. “An Ana2/Ctp/Mud Complex Regulates Spindle Orientation in Drosophila Neuroblasts.” *Developmental Cell* 21(3):520–33. doi: 10.1016/J.DEVCEL.2011.08.002.

Wang, Hongyan, Yingshi Ouyang, W. Gregory Somers, William Chia, and Bingwei Lu. 2007. “Polo Inhibits Progenitor Self-Renewal and Regulates Numb Asymmetry by Phosphorylating Pon.” *Nature* 449(7158):96–100. doi: 10.1038/NATURE06056.

Weed, Scott A., Andrei V. Karginov, Dorothy A. Schafer, Alissa M. Weaver, Andrew W. Kinley, John A. Cooper, and J. Thomas Parsons. 2000. “Cortactin Localization to Sites of Actin Assembly in Lamellipodia Requires Interactions with F-Actin and the Arp2/3 Complex.” *J. Cell Biol.* 151(1):29–40. doi: 10.1083/jcb.151.1.29.

Wegner, A., and G. Isenberg. 1983. “12-Fold Difference between the Critical Monomer Concentrations of the Two Ends of Actin Filaments in Physiological

Salt Conditions." *Proceedings of the National Academy of Sciences of the United States of America* 80(16):4922. doi: 10.1073/PNAS.80.16.4922.

Winter, Dirk, Alexandre v. Podtelejnikov, Matthias Mann, and Rong Li. 1997. "The Complex Containing Actin-Related Proteins Arp2 and Arp3 Is Required for the Motility and Integrity of Yeast Actin Patches." *Curr. Biol.* 7(7):519–29. doi: 10.1016/s0960-9822(06)00223-5.

Wodarz, Andreas, Andreas Ramrath, Alexandra Grimm, and Elisabeth Knust. 2000. "Drosophila Atypical Protein Kinase C Associates with Bazooka and Controls Polarity of Epithelia and Neuroblasts." *Journal of Cell Biology* 150(6):1361–74. doi: 10.1083/JCB.150.6.1361.

Wodarz, Andreas, Andreas Ramrath, Ute Kuchinke, and Elisabeth Knust. 1999a. "Bazooka Provides an Apical Cue for Inscuteable Localization in Drosophila Neuroblasts." *Nature 1999 402:6761* 402(6761):544–47. doi: 10.1038/990128.

Wodarz, Andreas, Andreas Ramrath, Ute Kuchinke, and Elisabeth Knust. 1999b. "Bazooka Provides an Apical Cue for Inscuteable Localization in Drosophila Neuroblasts." *Nature* 402(6761):544–47. doi: 10.1038/990128.

Xu, T., and G. M. Rubin. 1993. "Analysis of Genetic Mosaics in Developing and Adult Drosophila Tissues." *Development* 117(4):1223–37. doi: 10.1242/dev.117.4.1223.

Yamazaki, Daisuke, Tsukasa Oikawa, and Tadaomi Takenawa. 2007. "Rac-WAVE-Mediated Actin Reorganization Is Required for Organization and Maintenance of Cell-Cell Adhesion." *J. Cell Sci.* 120(1):86–100. doi: 10.1242/jcs.03311.

Yan, Catherine, Narcisa Martinez-Quiles, Sharon Eden, Tomoyuki Shibata, Fuminao Takeshima, Reiko Shinkura, Yuko Fujiwara, Roderick Bronson, Scott B. Snapper, Marc W. Kirschner, Raif Geha, Fred S. Rosen, and Frederick W. Alt. 2003. "WAVE2 Deficiency Reveals Distinct Roles in

Embryogenesis and Rac-Mediated Actin-Based Motility." *The EMBO Journal* 22(14):3602–12. doi: 10.1093/EMBOJ/CDG350.

Yi, Kexi, Jay R. Unruh, Manqi Deng, Brian D. Slaughter, Boris Rubinstein, and Rong Li. 2011. "Dynamic Maintenance of Asymmetric Meiotic Spindle Position through Arp2/3-Complex-Driven Cytoplasmic Streaming in Mouse Oocytes." *Nature Cell Biology* 13(10):1252–58. doi: 10.1038/ncb2320.

Yoshiura, Shigeki, Nao Ohta, and Fumio Matsuzaki. 2012. "Tre1 GPCR Signaling Orients Stem Cell Divisions in the Drosophila Central Nervous System." *Developmental Cell* 22(1):79–91. doi: 10.1016/J.DEVCEL.2011.10.027.

Yu, Fengwei, Xavier Morin, Yu Cai, Xiaohang Yang, and William Chia. 2000a. "Analysis of Partner of Inscuteable, a Novel Player of Drosophila Asymmetric Divisions, Reveals Two Distinct Steps in Inscuteable Apical Localization." *Cell* 100(4):399–409. doi: 10.1016/S0092-8674(00)80676-5.

Yu, Fengwei, Xavier Morin, Yu Cai, Xiaohang Yang, and William Chia. 2000b. "Analysis of Partner of Inscuteable, a Novel Player of Drosophila Asymmetric Divisions, Reveals Two Distinct Steps in Inscuteable Apical Localization." *Cell* 100(4):399–409. doi: 10.1016/S0092-8674(00)80676-5.

Yu, Fengwei, Xavier Morin, Yu Cai, Xiaohang Yang, and William Chia. 2000c. "Analysis of Partner of Inscuteable, a Novel Player of Drosophila Asymmetric Divisions, Reveals Two Distinct Steps in Inscuteable Apical Localization." *Cell* 100(4):399–409. doi: 10.1016/S0092-8674(00)80676-5.

Zallen, Jennifer A., Yehudit Cohen, Andrew M. Hudson, Lynn Cooley, Eric Wieschaus, and Eyal D. Schejter. 2002. "SCAR Is a Primary Regulator of Arp2/3-Dependent Morphological Events in Drosophila." *Journal of Cell Biology* 156(4):689–701. doi: 10.1083/jcb.200109057.

Zelhof, Andrew C., and Robert W. Hardy. 2004. "WASp Is Required for the Correct Temporal Morphogenesis of Rhabdomere Microvilli." *The Journal of Cell Biology* 164(3):417. doi: 10.1083/JCB.200307048.

Zhuang, Chunmei, Hongxing Tang, Sharmila Dissanaike, Everardo Cobos, Yunxia Tao, and Zonghan Dai. 2011. “CDK1-Mediated Phosphorylation of Abi1 Attenuates Bcr-Abl-Induced F-Actin Assembly and Tyrosine Phosphorylation of WAVE Complex during Mitosis.” *The Journal of Biological Chemistry* 286(44):38614–26. doi: 10.1074/JBC.M111.281139.